NASA Technical Memorandum 82939

Wind Tunnel Tests of a Zero-Length, Slotted-Lip Engine Air Inlet for a Fixed Nacelle V/STOL Aircraft

R. R. Woollett
Lewis Research Center
Cleveland, Ohio

and

W. E. Beck, Jr. and E. R. Glasgow
Lockheed-California Company
Burbank, California 91520

August 1982

NASA

TABLE OF CONTENTS

TABLE OF CONTENTS (Continued)

WIND TUNNEL TESTS OF A ZERO-LENGTH, SLOTTED-LIP ENGINE AIR INLET FOR A FIXED NACELLE V/STOL AIRCRAFT

R.R. Woollett
National Aeronautics and Space Administration
Lewis Research Center
Cleveland, Ohio 44135

and

W.E. Beck, Jr. and E.R. Glasgow
Lockheed-California Company
Burbank, California 91520

SUMMARY

Zero-length, slotted-lip inlet performance and associated fan blade stress levels were determined from model tests using a 20-inch diameter fan unit installed in the NASA-Lewis Research Center (LeRC) 9- by 15-foot low speed wind tunnel. The model is a half-scale axisymmetric representation of the inlet designed by the Lockheed-California Company for a horizontal fixed nacelle installation on a subsonic V/STOL aircraft. The model configuration variables included slat contraction ratios of 1.2 and 1.3, slot-gap widths ranging from zero to 0.65 inches, constant area sections between the inlet throat and fan face having lengths of 2 and 4 inches, and slot-gap fillers to simulate the zero gap configuration as well as 90 degree sectors over which the slot is ineffective for simulating a Siamese nacelle installation.

The model tests were conducted at tunnel speeds up to 105 knots (M_o = 0.16), at angles of attack up to 120 degrees at 35 knots and 70 degrees at 105 knots and at fan speeds up to 95 percent of the design speed, sufficient to cover most of the estimated operating envelope for the V/STOL application. Instrumentation was provided to measure the fan face total pressure recovery and distortion, the inlet surface static pressure distributions, and fan blade stress levels for all conditions tested.

The following results were obtained during the test.

- The zero-length, slotted-lip inlet operated completely satisfactorily over the V/STOL operating envelope, providing a flow to the fan having total pressure recoveries of no less than 0.995 and with distortion levels resulting in insignificant fan blade stress levels. This envelope includes crosswind velocities up to 35 knots at 120 degrees angle of attack and forward speeds of 105 knots at 30 degrees angle of attack. At the 105 knot forward speed, the 1.2 and 1.3 contraction ratio slats were capable of operating up to 57 and 66 degrees angle of attack, respectively, prior to producing a flow separation profile at the fan face.

- At high angle-of-attack conditions the total pressure recovery of the airflow through the slot is uniform across the slot width, due to area convergence through the slot, and also uniform circumferentially around the inlet due to compensating effects of reduced slot flow rate and increased pressure loss coefficients as the angular displacement from the windward side of the nacelle increased.

- For the zero-length configuration significant radial and circumferential flow velocity gradients existed at the inlet throat/fan face at high angles of attack but were shown to have little effect on the fan performance (i.e., fan pressure ratio at a given value of corrected airflow).

- A slot-gap width of 0.36 inches (width to throat diameter ratio of 0.018) provided the highest total pressure recovery at high angles of attack. This gap dimension resulted in slot flows whereby the external slat and cowl lip surfaces have an equal pressure loading. At the maximum crosswind design condition of 35 knots and 120 degrees angle of attack, the slot improved the total pressure recovery by almost 2 percent compared to the unslotted configuration for the 1.2 contraction ratio slot and almost 1 percent for the 1.3 contraction ratio slat.

- At the maximum fan airflow (fan face Mach number of 0.52 which corresponds to 95 percent of design speed) the throat/fan face spacer provides no benefit in performance, although the velocity distortions at the fan face are reduced with increasing spacer length. At lower airflows (part power operation) and high model angles-of-attack, the reduced pumping action of the fan slightly degrades the total pressure recovery with no spacer installed.

- Installation of the slot fillers to simulate an ineffective slot gap over a 90 degree circumferential sector due to the proximity of an adjacent nacelle has virtually no effect on inlet performance.

- Calculated inlet surface velocities from measured static pressures show good agreement with velocities predicted from potential flow analysis.

INTRODUCTION

A conventional inlet can be designed for a fixed horizontal nacelle V/STOL aircraft which has sufficient internal contraction for preventing internal flow separation at the low speed, high inlet angle-of-attack conditions. However, application of a conventional inlet to such a propulsion system often results in an inlet face location which tends to restrict the pilot's view during vertical flight operation. Attempts to alleviate this situation by reducing the inlet diffuser length requires that the maximum nacelle diameter be increased. The reason for this being that, for the same internal contraction ratio and the same conical diffusion angle, the highlight diameter increases as the diffuser length is decreased. Thus, in order to maintain sufficient forebody projected frontal area to achieve the required drag divergence Mach number, the maximum nacelle diameter must increase with a reduction in diffuser length.

A potential solution to this problem is to use a slotted-lip inlet. This inlet contains blow-in doors, located in the inlet forebody, which open during high mass-flow/angle-of-attack operating conditions, thus permitting airflow to enter the inlet just upstream of the inlet throat. This effectively increases the inlet aerodynamic contraction ratio and decreases the peak surface Mach number in the highlight region compared to that which would be obtained for a conventional inlet with the same geometric contraction ratio. Thus, the slot permits use of a lower geometric contraction ratio compared to that which would be required for a conventional inlet for the same peak surface Mach number. This reduction in geometric contraction ratio in turn permits a reduction in diffuser length while maintaining a maximum nacelle diameter which does not exceed that required based on engine/accessory envelope constraints.

Additional beneficial features associated with the reduced length of the slotted-lip inlet include reduced weight and a reduced moment arm for the crosswind lip forces. The latter feature reduces the amount of thrust vectoring required to achieve required yaw acceleration rates. However, reducing the diffuser length may produce increased fan blade stresses due to fan face flow velocity gradients at the high angle-of-attack operation.

A test program was conducted in the NASA-LeRC 9- by 15-foot low speed wind tunnel to evaluate the overall performance of a zero-length, slotted-lip inlet concept and to establish operating limits of the inlet relative to the estimated velocity/angle-of-attack envelope for the fixed nacelle V/STOL aircraft. The aerodynamic design of the model is representative of the nacelle inlet resulting from configuration studies conducted by the Lockheed-California Company for the NAVY Type A V/STOL aircraft, and was sized for installation on the NASA-LeRC 20-inch diameter fan unit. The test was conducted by NASA-LeRC personnel in August 1980.

This report presents a detailed description of the wind tunnel model test program. The test facility and procedures are discussed first followed by a description of the model and associated instrumentation. The test results are presented and discussed for a baseline configuration and then relative to the effects on performance of each of the configuration changes. Conclusions regarding the angle-to-attack capability of the inlet and the application of this concept to subsonic aircraft are made.

SYMBOLS

A_{HL} - highlight area

A_{TH} - inlet throat area

CR - Slat contraction ratio, A_{HL}/A_{TH}

h - slot rake probe location, measured from cowl lip surface

KD2 - flow total pressure distortion parameter

KD - flow total pressure distortion parameter

M_F - fan face Mach number

M_o - tunnel Mach number

ND1 - flow total pressure distortion parameter

N - fan speed, rpm

P - static pressure

P_t - total pressure

R - duct radius measured from fan centerline

R_{MAX} - maximum duct radius at fan face

T - static temperature

T_t - total temperature

V - flow velocity

W - fan airflow

X - coordinate in axial direction

Y - coordinate normal to fan centerline

α - model angle of attack

θ - angle measured circumferentially in plane normal to fan centerline

Θ - corrected total temperature

ω - corrected airflow

SYMBOLS (Continued)

SUBSCRIPTS

$_0$	-	tunnel (freestream) conditions
2	-	fan face station
3	-	fan stator exit station
HL	-	inlet highlight station
TH	-	inlet throat station

SUPERSCRIPT

*	-	Mach 1 condition

TEST FACILITY AND PROCEDURES

Test Facility

The inlet test discussed herein was conducted in the NASA-LeRC 9- by 15-foot low speed wind tunnel. This facility operates at atmospheric total pressure with a test section Mach number range of zero to 0.22. A 20-inch diameter, turbine-driven, single-stage fan was used to produce the inlet mass flow.

A photograph of the inlet/fan installation in the test section is shown in figure 1. The model rotates in a horizontal plane about a vertical support post which also provides a passage for the heated, high-pressure, turbine drive air. A portion of the wind tunnel vertical wall adjacent to the model was removed to allow the fan and turbine exhaust flows to pass through the wind tunnel during high angle-of-attack conditions.

The turbine-driven fan was designed to simulate the relatively low pressure ratios representative of subsonic V/STOL aircraft having shaft-coupled engines. At the maximum tested fan speed of 7800 rpm, the fan pressure ratio is approximately 1.15 and the associated fan tip Mach number is 0.6. The fan has 15 rotor blades and 25 stator blades with a rotor-stator spacing of approximately one rotor tip chord length. The rotor blades have circular arc airfoil sections with no midspan dampers and were tested with the blade pitch set at the design angle. The rotor blades were fabricated from a titanium alloy.

More detailed information regarding the aerodynamic characteristics of the fan can be found in reference 1.

Test Procedures

The tunnel velocity/angle-of-attack test matrix originally scheduled for each model configuration was representative of the operational envelope for a fixed horizontal nacelle V/STOL aircraft application. Since the performance capability of the inlet was unknown, and the primary concern was to not exceed the fan blade stress limits, a zero angle-of-attack setting was tested first, followed by incremental increases until the envelope was covered. For each test point, (tunnel speed and angle of attack), the engine speed was increased

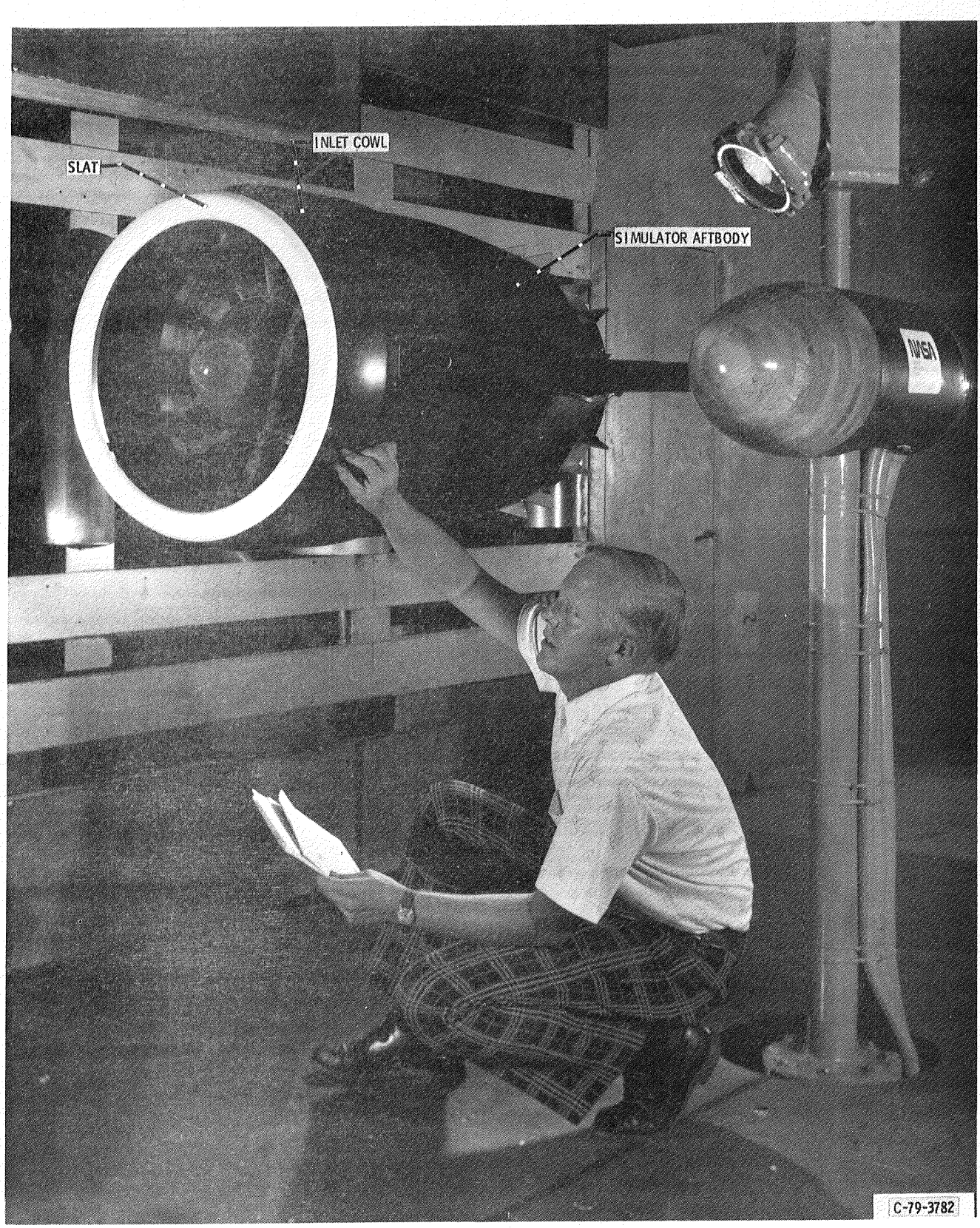

Figure 1. - Zero-length, slotted-lip inlet installed in NASA LeRC 9x15 foot low speed wind tunnel.

from idle to maximum rpm (approximately 2000-7800) and then returned to idle. At selected rpm levels all model pressure and tunnel data were recorded.

During each rpm excursion, measured fan blade stresses and three selected model pressures were visually monitored through use of X-Y plotters to determine when flow separation from the inlet surface occurred and to ensure that the fan stress limits were not exceeded. To recognize flow separation effects, two fan face total pressure probes referenced to the wall static, were recorded on the plotter. These probes were located 0.03 and 0.36 inches from the duct wall at the critical zero degree circumferential location. As the rpm increased the resulting dynamic pressure (P_t-P) measurement increased until separation occurred, as observed by a dramatic loss in dynamic pressure and movement of the stylus on the X-Y plotter. A typical plot is shown in figure 2. Upon realization that no flow separation was observed for the angles of attack associated with the V/STOL envelope, the test matrix was expanded to include higher angles. Once separation occurred, the angle was not increased further.

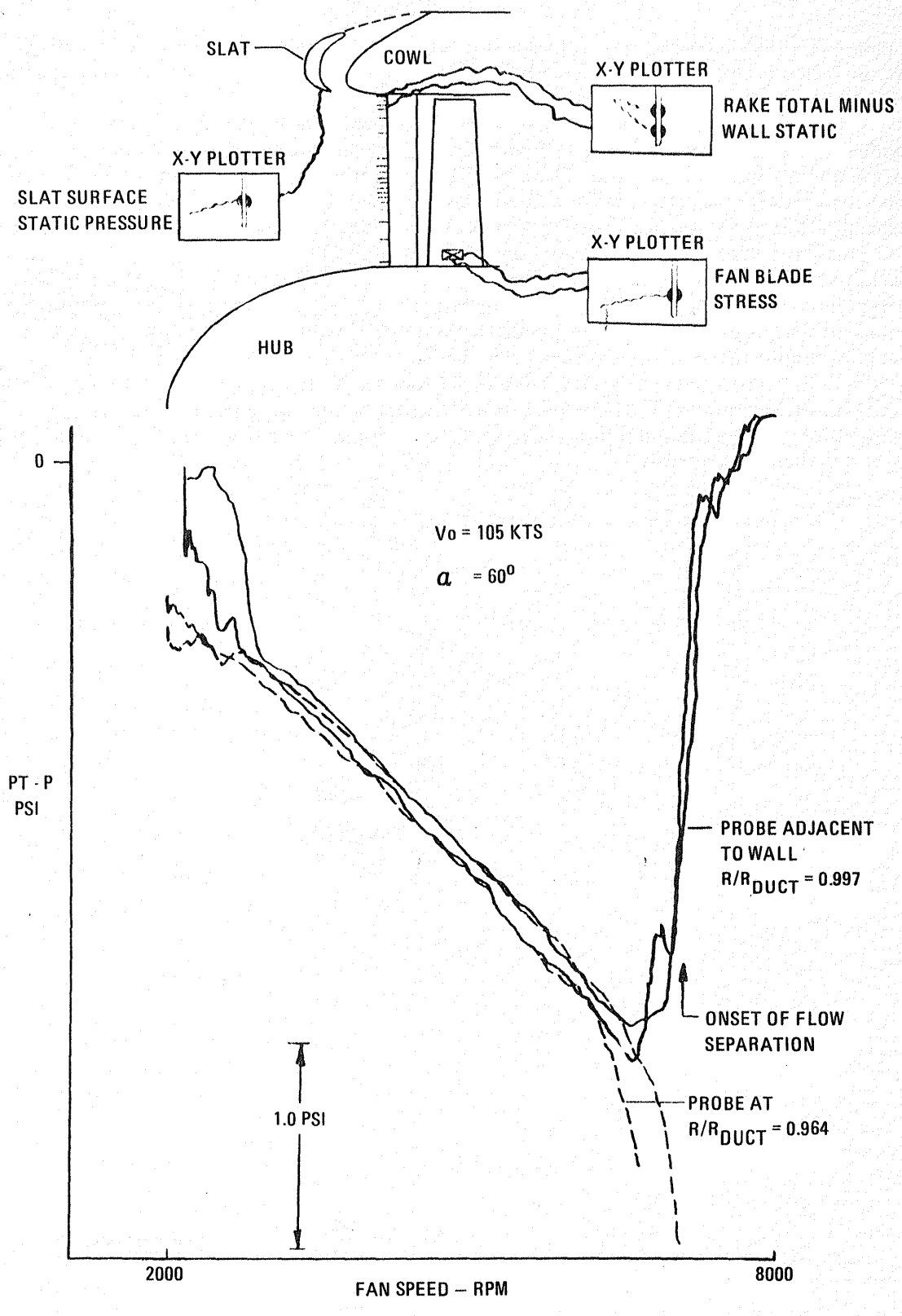

Figure 2. - Typical fan face total pressure trace during test run.

MODEL DESCRIPTION

The aerodynamic design of the axisymmetric zero-length, slotted-lip inlet model is representative of the inlet configured by the Lockheed-California Company for a subsonic V/STOL aircraft. The inlet throat coincides with the fan face (zero length). Hinged spring loaded blow-in doors are located in the external forebody surface and extend around the inlet periphery. At static and low speed operating conditions, the reduced internal static pressure sucks these doors open, providing an auxillary flow path (slot) for the engine airflow. At higher forward speeds (approximately greater than 0.2 Mach number) the static pressure differential (external surface minus internal throat) becomes positive and the doors close for normal flight operation.

Since the tests were designed to obtain low-speed performance data (up to 105 knots), the model configuration simulated the full scale design with the doors in the open position. In this open position a secondary (cowl) lip is exposed and a forward slat section is formed around the inlet circumference. Six circumferential struts were provided to attach and support the slat to the cowl. These struts are circular to allow fore and aft movement of the slat to vary the slot width. The support struts can be seen in the photograph of the model installed in the wind tunnel, figure 3.

The overall dimensions of the inlet model are defined in figure 4 for a selected baseline configuration. The throat diameter of 20.008 inches matches the existing LeRC fan tip dimension and represents a half-scale model of the V/STOL aircraft. The internal area contraction ratio (A_{HL}/A_T) of the two slats tested are 1.2 and 1.3, while for the secondary cowl lip this value is 1.12. The hub diameter of 9.20 inches results in a fan hub/tip diameter ratio of 0.46. The dashed line in the figure represents the external contour of the blow-in door and this same contour is used for the cowl forebody surface representing the door in the open position.

The configurations tested during the program are identified schematically in figure 5 and include primarily variations in slat contraction ratio and slot gap width. In addition, constant area duct spacers, shown in the photograph of figure 6, having lengths of 2 and 4 inches were installed to investigate the effect on performance of moving the inlet throat forward of the fan face. Furthermore, slot gap "fillers" were fabricated such that either the entire slot (360 degrees circumferentially) or only a 90 degree sector could be eliminated. The photograph in figure 7 shows the 90 degree filler installed.

The baseline design configuration was selected based on analytically predicted pressure distributions on the inlet surface. Using these data and

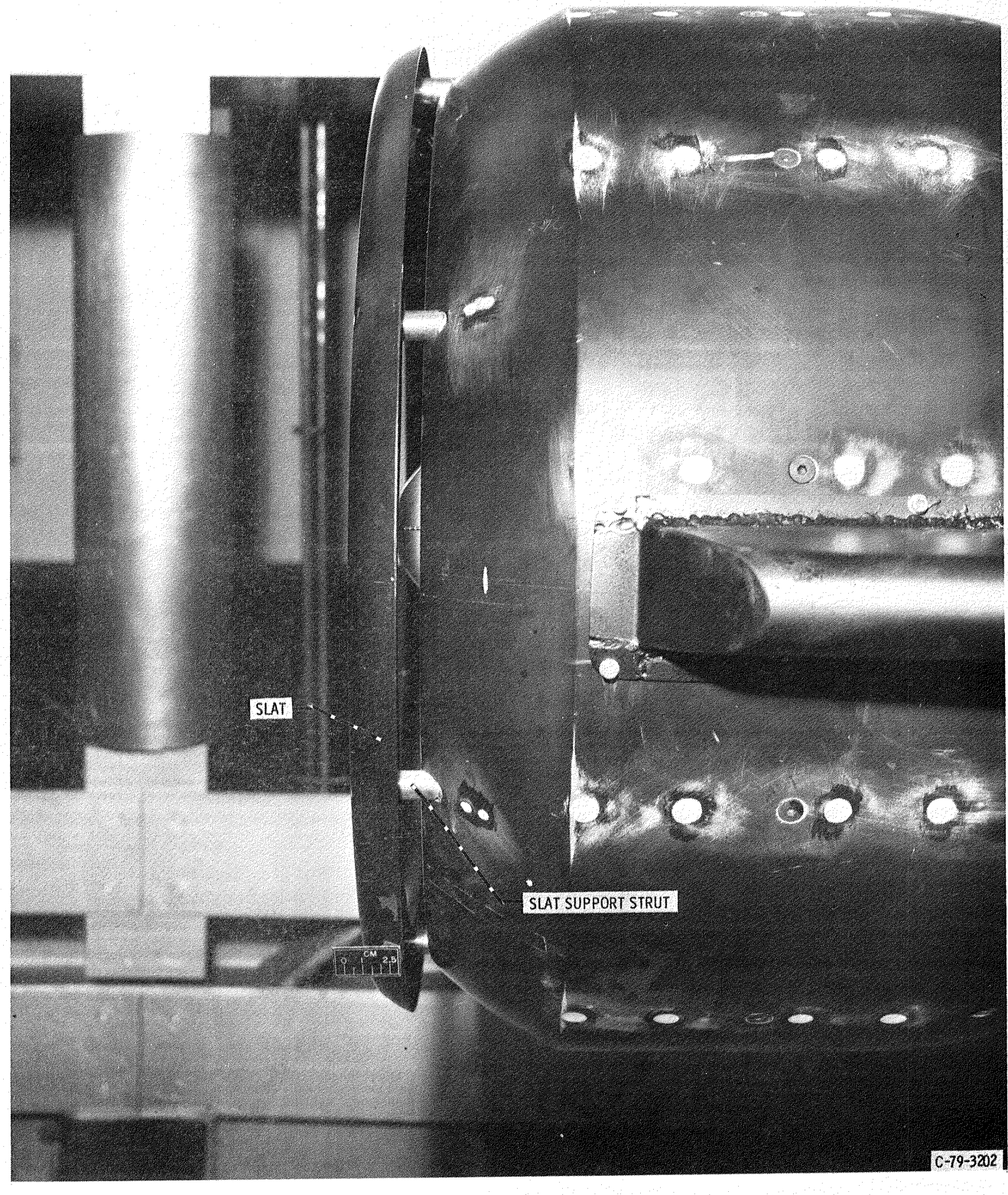

Figure 3. - Photograph of inlet model - side view.

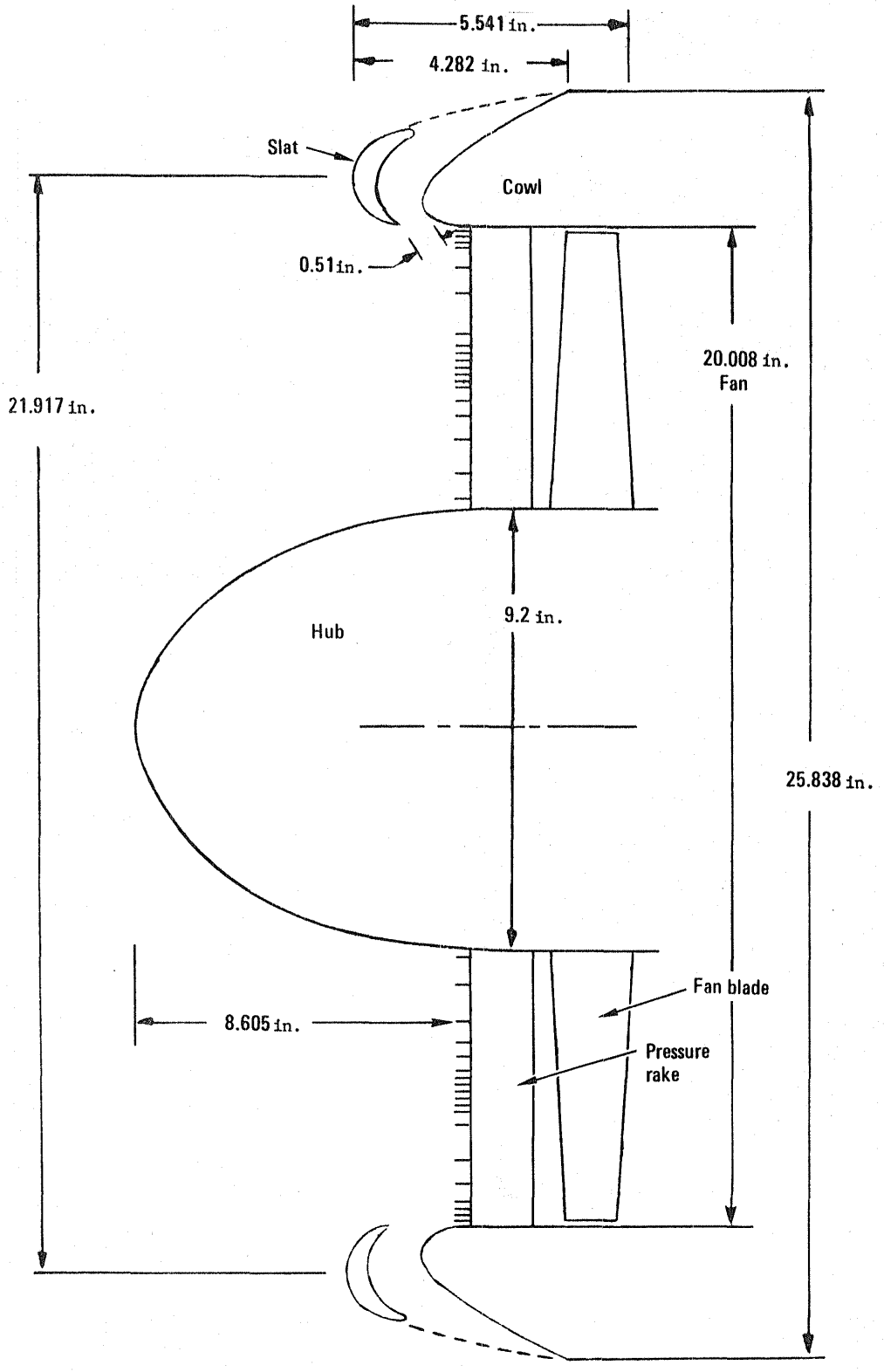

Figure 4. - Zero length inlet model basic dimensions baseline configuration.

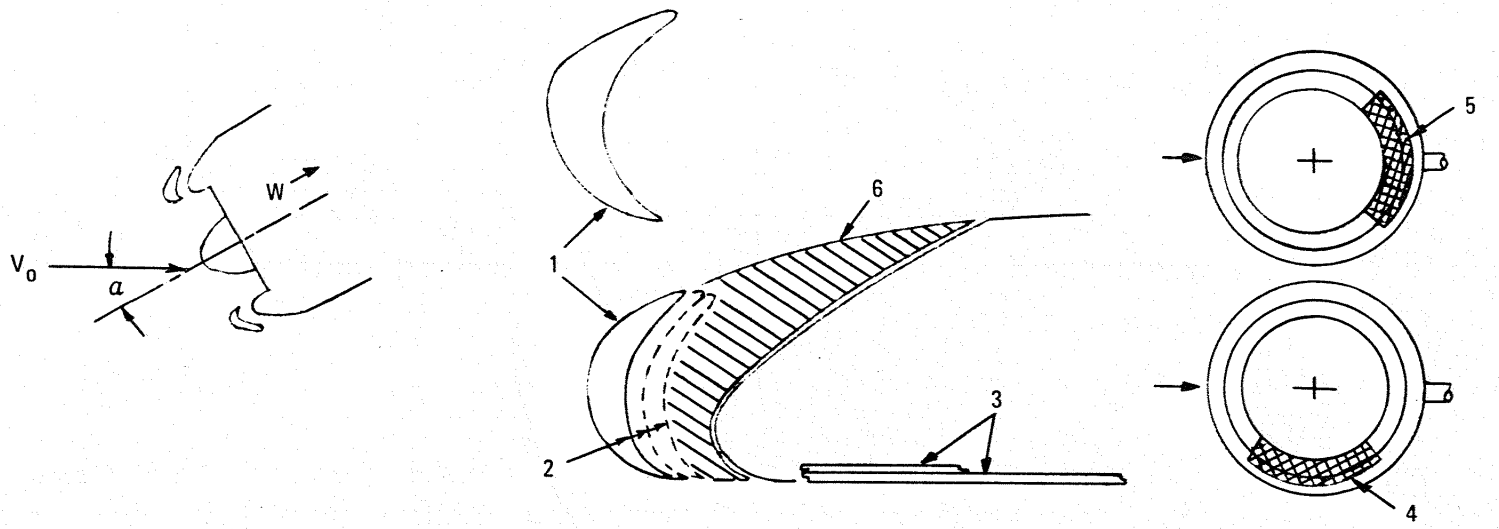

Operating variables

V_o – Tunnel velocity
a – Inlet angle of attack
W – Fan airflow

Configuration variables

1 Slat type, contraction ratio 1.2, 1.3
2 Slat position, slot gap width zero, 0.25 to 0.65 inches
3 Inlet spacer, zero, 2 in., 4 in.
4 90 Degree filler, angle of attack simulation 45–135°
5 90 Degree filler, crosswind simulation 135–225°
6 360 Degree filler, zero slot simulation

Figure 5. - Inlet model test and configuration variables.

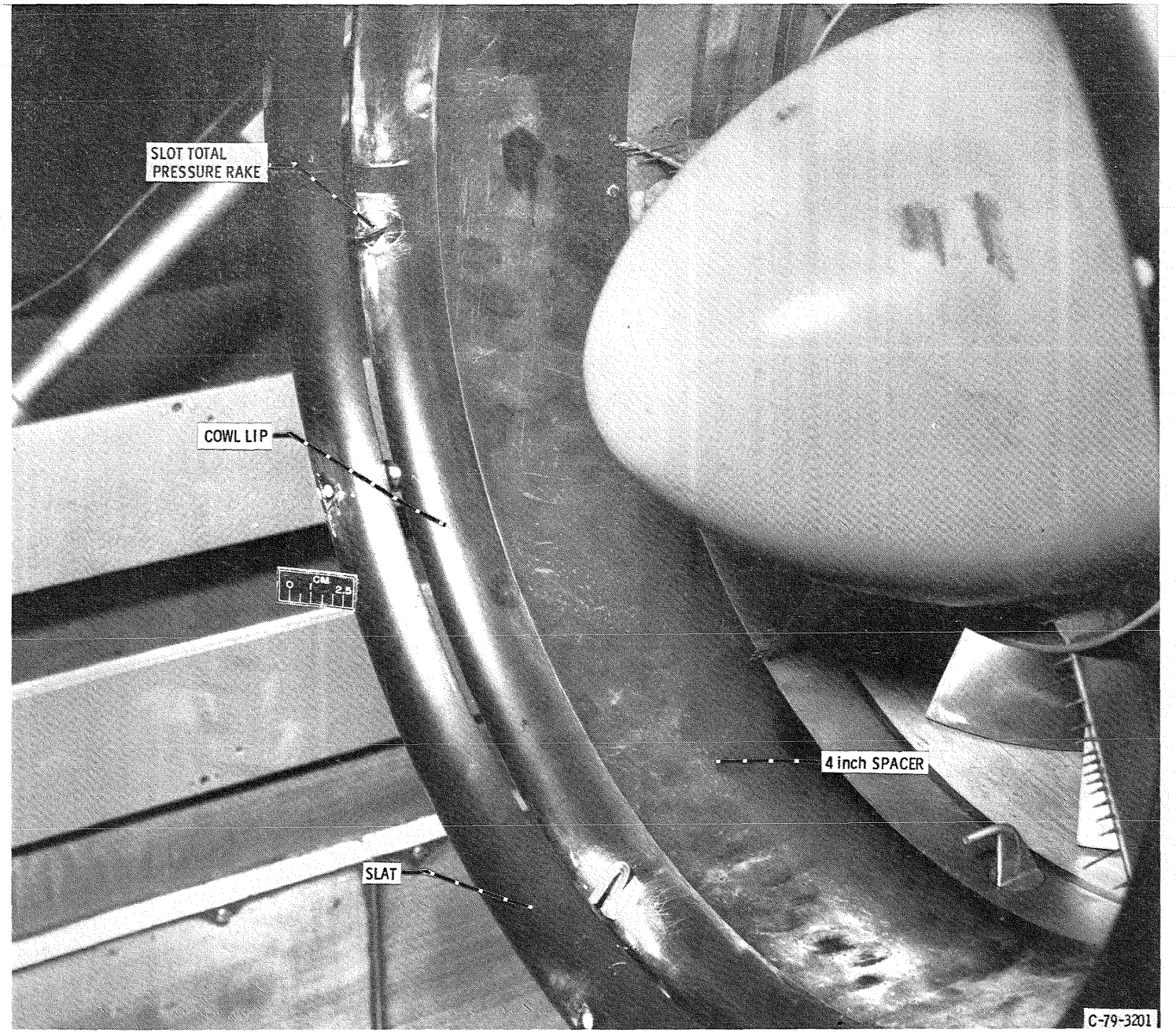

Figure 6. - Inlet model photograph showing spacer and slot rake.

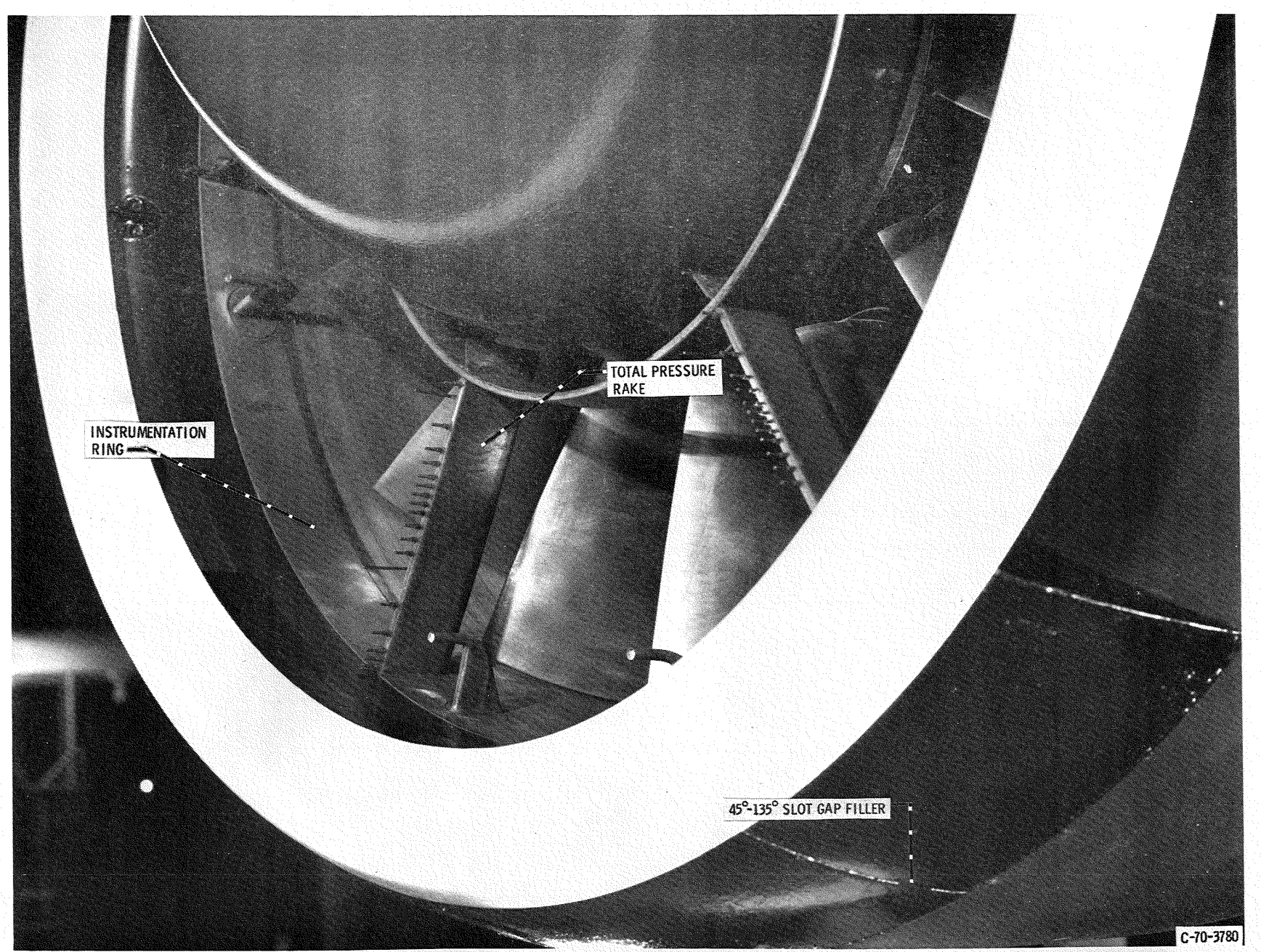

Figure 7. - Inlet model photograph showing slot-gap filler and fan face total pressure rake.

a maximum allowable surface Mach number of 1.4 as suggested in reference 2, it was determined that a slat contraction ratio of 1.2 and slot gap width of 0.51 inches would satisfy the critical operating conditions for the inlet.

Coordinates describing the inlet forebody shape are presented in figure 8 for the 1.2 contraction ratio slat in the most forward position. Above the highlight and extending to the maximum diameter the external contour is basically a Lockheed developed LMSC-1 profile designed for high speed operation. Below the slat highlight the outside contour is circular. To avoid a discontinuity in slope at the intersection of these profiles the circular section of the lower contour was extended slightly above the highlight, intersecting the LMSC-1 contour at the same value of surface slope. The inside contour of the slat (slot side) is a parabolic section above the highlight and a double circular arc below the highlight. This contour was developed to provide a uniformly converging area distribution for the slot airflow. At the slat leading edge a radius of approximately 0.06 inches was used to accommodate changes in location of the stagnation point at the various operating conditions. The slat internal trailing edge surface was directed aft toward the fan to turn the slot flow toward the fan and provide a pressure gradient to keep the flow attached to the lip.

The cowl contour is in part identical to the external door profile, rotated approximately 21 degrees. A lemniscate shape is utilized from the end of the door to the inlet throat, matching slopes at all intersections.

The alternate slat has a contraction ratio of 1.3 and is also circular below the highlight. Above the highlight to the maximum diameter an LMSC-1 contour is used. To maintain the same maximum cowl diameter the contour at the highlight for the 1.3 contraction ratio slat results in a somewhat sharper turn compared to the 1.2 contraction ratio slat. The coordinates describing slat-2 are presented in figure 9 along with a graphic comparison with slat-1.

To vary the slot-gap width at discrete positions, with assurance of high accuracy when repeating the setting, grooves were provided in the slat struts at appropriate locations and set screws inserted into the grooves firmly anchored the strut/slat. These locations and the resultant slot gap widths are shown in figure 10. Also illustrated schematically in the figure is the installation of the filler sections. These blocks were sized to eliminate the slot for the gap width of 0.51 inches and were fabricated in separate inside and outside pieces for easy installation.

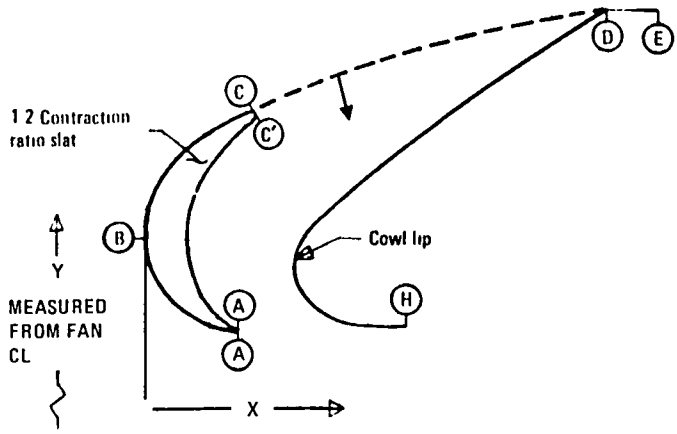

External contour A – E

X/R	Y/R	
0 0000	1 0954	B
0 0001	1 0911	
0 0002	1 0893	
0 0003	1 0879	
0 0006	1 0847	
0 0010	1 0817	
0 0015	1 0786	
0 0020	1 0760	
0 0040	1 0681	
0 0060	1 0621	
0 0080	1 0572	
0 0100	1 0529	
0 0150	1 0441	
0 0200	1 0370	
0 0250	1 0310	
0 0300	1 0260	
0 0350	1 0216	
0 0400	1 0178	
0 0450	1 0144	
0 0500	1 0115	
0 0550	1 0090	
0 0600	1 0068	
0 0650	1 0050	
0 0700	1 0035	
0 0750	1 0022	
0 0800	1 0013	
0 0850	1 0006	
0 0900	1 0002	
0 0950	1 0000	
0 0954	1 0000	A

X/R	Y/R	
0 0000	1 0954	B
0 0001	1 0998	
0 0002	1 1016	
0 0003	1 1030	
0 0006	1 1061	
0 0010	1 1092	
0 0015	1 1123	
0 0020	1 1149	
0 0040	1 1228	
0 0060	1 1287	
0 0080	1 1337	
0 0100	1 1380	
0 0150	1 1468	
0 0200	1 1539	
0 0250	1 1598	
0 0300	1 1649	
0 0350	1 1693	
0 0400	1 1731	
0 0450	1 1764	
0 0453	1 1767	
0 0485	1 1786	
0 0689	1 1900	
0 0798	1 1957	
0 0928	1 2019	
0 1045	1 2076	C
0 1198	1 2136	
0 1498	1 2252	
0 1798	1 2354	
0 2098	1 2445	
0 2398	1 2527	
0 2716	1 2605	
0 3057	1 2679	
0 3417	1 2746	
0 3777	1 2801	
0 4137	1 2836	
0 4438	1 2876	D
0 4857	1 2901	
0 5246	1 2911	
0 5696	1 2914	E

Cowl lip contour

X/R	Y/R	
0 2473	1 0000	H
0 2229	1 0004	
0 2128	1 0012	
0 2051	1 0022	
0 1987	1 0034	
0 1931	1 0047	
0 1881	1 0062	
0 1836	1 0078	
0 1794	1 0095	
0 1756	1 0113	
0 1721	1 0133	
0 1659	1 0173	
0 1605	1 0216	
0 1560	1 0262	
0 1521	1 0309	
0 1490	1 0358	
0 1464	1 0407	
0 1445	1 0458	
0 1432	1 0508	
0 1424	1 0558	
0 1421	1 0607	
0 1422	1 0631	
0 1423	1 0644	
0 1424	1 0655	
0 1425	1 0667	
0 1427	1 0679	
0 1431	1 0703	
0 1443	1 0748	
0 1460	1 0791	
0 1461	1 0832	
0 1493	1 0852	
0 1506	1 0871	
0 1520	1 0889	
0 1534	1 0906	
0 1550	1 0923	
0 1672	1 1034	
0 1912	1 1248	
0 2156	1 1450	
0 2404	1 1642	
0 2655	1 1825	
0 2924	1 2010	
0 3218	1 2201	
0 3530	1 2391	
0 3847	1 2571	
0 4167	1 2741	
0 4438	1 2876	D

Slat Internal contour

X/R	Y/R	
0 0956	1 0006	A'
0 0925	1 0010	
0 0900	1 0015	
0 0850	1 0028	
0 0800	1 0049	
0 0750	1 0076	
0 0700	1 0113	
0 0650	1 0161	
0 0600	1 0230	
0 0550	1 0321	
0 0500	1 0432	
0 0480	1 0486	
0 0460	1 0547	
0 0440	1 0621	
0 0420	1 0718	
0 0400	1 0954	
0 0420	1 1130	
0 0440	1 1203	
0 0460	1 1259	
0 0480	1 1306	
0 0500	1 1348	
0 0550	1 1436	
0 0600	1 1511	
0 0650	1 1577	
0 0700	1 1636	
0 0750	1 1691	
0 0800	1 1741	
0 0850	1 1789	
0 0900	1 1834	
0 0950	1 1877	
0 1000	1 1918	
0 1005	1 1984	C'

Figure 8. - Slat-1 and cowl lip coordinates.

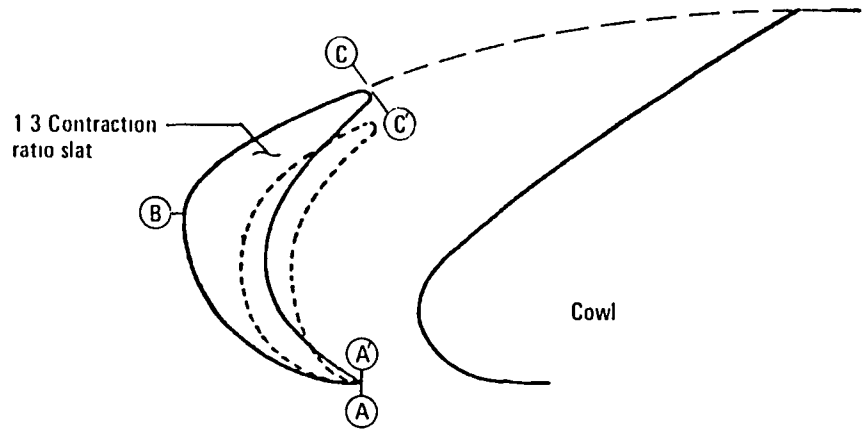

Slat
External Contour A-C

X/R	Y/R	X/R	Y/R
(B)–0 0000	1 1402	0 0000	1 1402–(B)
0 0001	1 1349	0 0001	1 1426
0 0002	1 1327	0 0003	1 1436
0 0003	1 1310	0 0006	1 1451
0 0006	1 1272	0 0011	1 1471
0 0010	1 1235	0 0023	1 1499
0 0015	1 1197	0 0034	1 1521
0 0020	1 1166	0 0046	1 1540
0 0040	1 1069	0 0057	1 1557
0 0060	1 0996	0 0085	1 1593
0 0080	1 0935	0 0114	1 1624
0 0100	1 0882	0 0142	1 1652
0 0150	1 0771	0 0171	1 1679
0 0200	1 0680	0 0228	1 1728
0 0250	1 0603	0 0285	1 1771
0 0300	1 0535	0 0342	1 1812
0 0350	1 0475	0 0399	1 1849
0 0400	1 0421	0 0456	1 1885
0 0450	1 0373	0 0570	1 1951
0 0500	1 0329	0 0854	1 2094
0 0550	1 0289	0 1139	1 2212
0 0600	1 0252	0 1447	1 2315–(C)
0 0650	1 0219		
0.0700	1 0188		
0 0750	1 0161		
0 0800	1 0136		
0 0850	1 0113		
0 0900	1 0093		
0 0950	1 0075		
0 1000	1 0059		
0 1050	1 0045		
0 1100	1 0033		
0 1150	1.0023		
0 1200	1 0015		
0 1250	1 0008		
0 1299	1 0004		
0 1349	1 0001		
0 1399	1 0001		
(A)–0 1402	1 0000		

Slat
Internal Contour

X/R	Y/R
0 1404	1 0006–(A')
0 1399	1 0009
0 1349	1 0042
0 1299	1 0077
0 1250	1 0113
0 1200	1 0150
0 1150	1 0189
0 1100	1 0230
0 1000	1 0320
0 0950	1 0370
0 0900	1 0424
0 0850	1 0484
0 0800	1 0551
0 0750	1 0632
0 0700	1 0735
0 0650	1 0940
0 0647	1 0996
0 0650	1 1060
0 0700	1 1299
0 0750	1 1420
0 0800	1 1513
0 0850	1 1592
0 0900	1 1661
0 0950	1 1724
0 1000	1 1782
0 1050	1 1836
0 1100	1 1887
0 1150	1 1935
0 1200	1 1980
0 1250	1 2024
0 1299	1 2066
0 1349	1 2106
0 1399	1 2145
0 1449	1 2182
0 1467	1 2195–(C')

Figure 9. - Slat-2 coordinates.

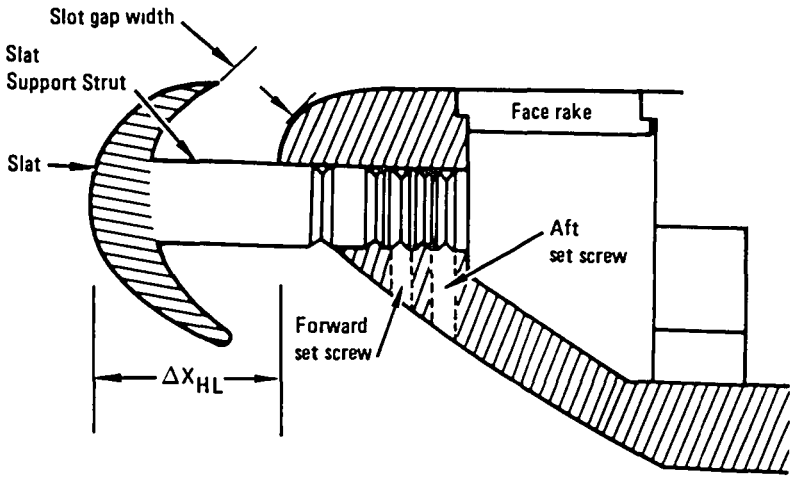

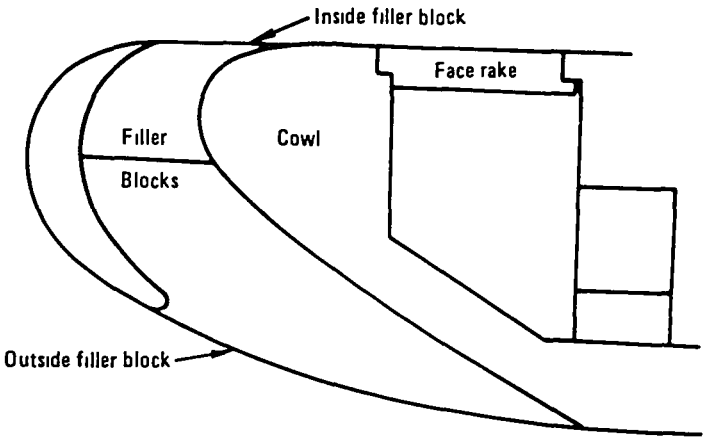

Slot gap width 0.51 in

Slat	ΔX_{HL} – in Distance From Slat HL to Cowl Lip HL	Slot Gap Width in
CR = 1 2	1 420	0 65
	1 264	0 51
	1 225	0 48
	1 070	0 36
	0 880	0 25
CR = 1 3	1 894	0 65
	1 739	0 51
	1 545	0 48
	1 356	0 36
	1 241	0 25

Figure 10. - Model details showing slot-gap settings and filler installation.

MODEL INSTRUMENTATION

Sufficient total and static pressure instrumentation was installed on the model to evaluate the inlet overall performance and to investigate the flow patterns into the inlet thereby gaining some insight as to the effects on performance of the various configurations changes and operating conditions. The measure of overall performance of the inlet was the total pressure recovery and distortion at the fan face - the recovery causing engine thrust losses and thus affecting the engine and aircraft sizing, and the total pressure distortion dictating the limits of safe operation of the fan relative to blade stress criteria.

To determine the fan face total pressure, six evenly spaced total pressure rakes having 19 probes each, were located immediately upstream of the fan face station. The 19 probes in each rake were distributed between the fan hub and tip (wall), as shown in figure 11 along with the appropriate dimensions. Also, a typical rake is shown in the photograph previously presented in figure 7. The outermost probes were sufficiently close to the wall to measure flow separation occurring on the slat and/or cowl lips. Also shown in figure 11 is the fraction of fan face cross-sectional area identified with each probe and subsequently used for calculating the area-weighted total pressure recovery. Furthermore, the radial location of the two stream statics installed in each rake and used to define the fan face flow static pressure profiles are shown.

To measure the fan blade stress levels resulting from the inlet flow, six strain gauges were mounted on three separate fan blades (two per blade) as shown in figure 12. During each test run the output from the root gauge at position 2 in figure 12 was continuously monitored as the fan speed was increased with an X-Y plotter to assure that the fan was not over-stressed.

To measure the slat/cowl surface pressures during each run, static pressures orifices were installed. The bulk of these taps were provided at the zero degree circumferential location which is critical relative to the tunnel flow at model angle of attack conditions. Figure 13 identifies the location of each tap. Also the taps were more heavily distributed in regions where flow separation is more likely to occur (i.e., below the highlight of the slat and cowl lip).

With the throat/fan face spacers installed, wall circumferential static pressures were measured by taps located as shown in figure 14. To measure the slot flow total pressures, three rakes were mounted from the cowl lip at the angular locations shown in figure 15. These rakes were displaced 5 degrees from the fan face total pressure rakes to avoid interference with the rake readings. Each rake consisted of five probes extending a distance from the

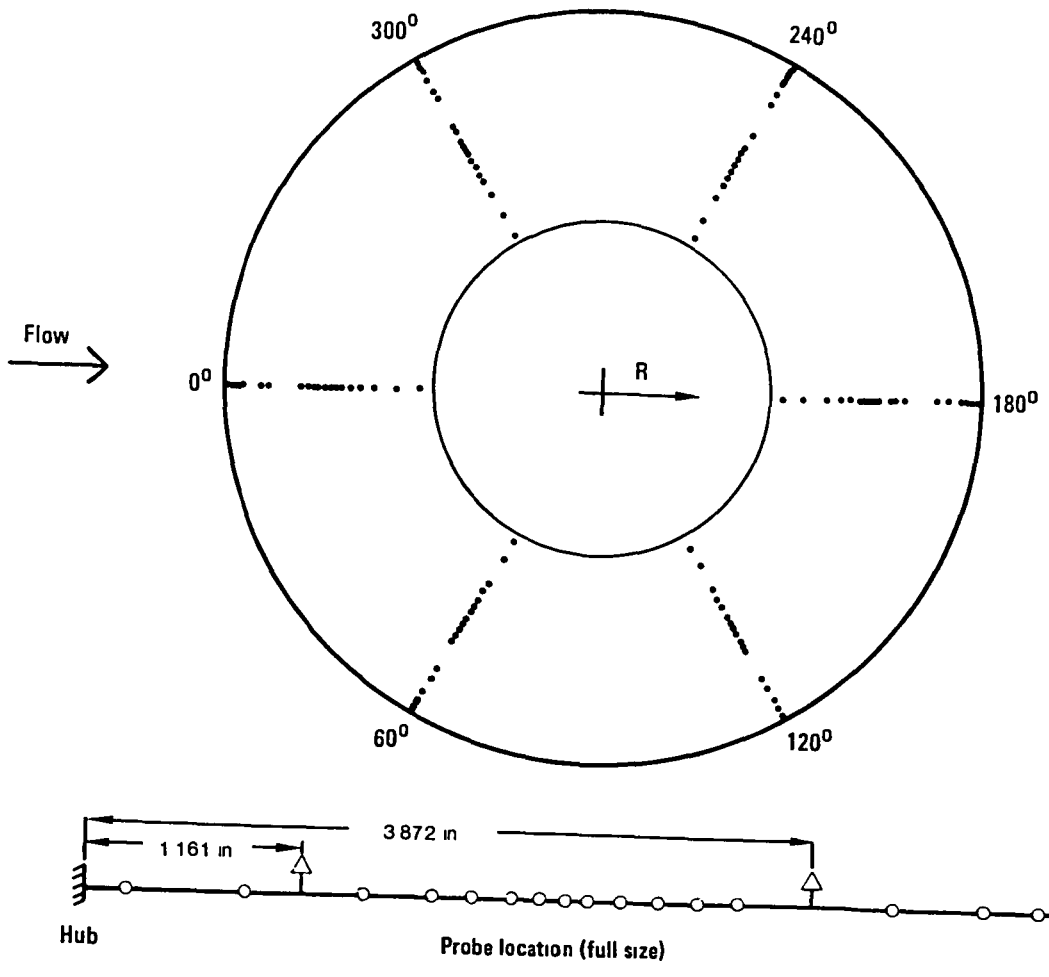

Probe Radius and Weighted Area
(Typical – Each Rake)

Ring No	Ring Rad., R (in.)	Probe Area, ΔA (in ^{2})	Probe Area, $\Delta A/A_{TH}$ (%)
Hub	4 60		
1	4 80	2 6465	1. 0685
2	5. 44	3. 6460	1. 4720
3	6 08	3 1468	1 2705
4	6 44	1 9108	0. 7715
5	6 65	1 4623	0 5903
6	6 86	1 2542	0 5063
7	7 00	1 0263	0 4143
8	7 14	1 0468	0 4227
9	7 28	1. 0673	0 4308
10	7 42	1 3630	0 5503
11	7 63	1 6780	0 6775
12	7 84	1. 7657	0 7128
13	8 06	4 5150	1 8228
14	8 89	5 9422	2. 3992
15	9 35	3 6550	1 4757
16	9 64	2. 1620	0 8728
17	9 78	1 3307	0 5372
18	9. 90	0. 9837	0 3972
19	9 97	0 6785	0 2740
Tip	10 004		

A_{TH} = 247 93 in ^{2}

O – Total pressure probe
Δ – Static pressure probe

Figure 11. - Fan face rake total and static pressure instrumentation.

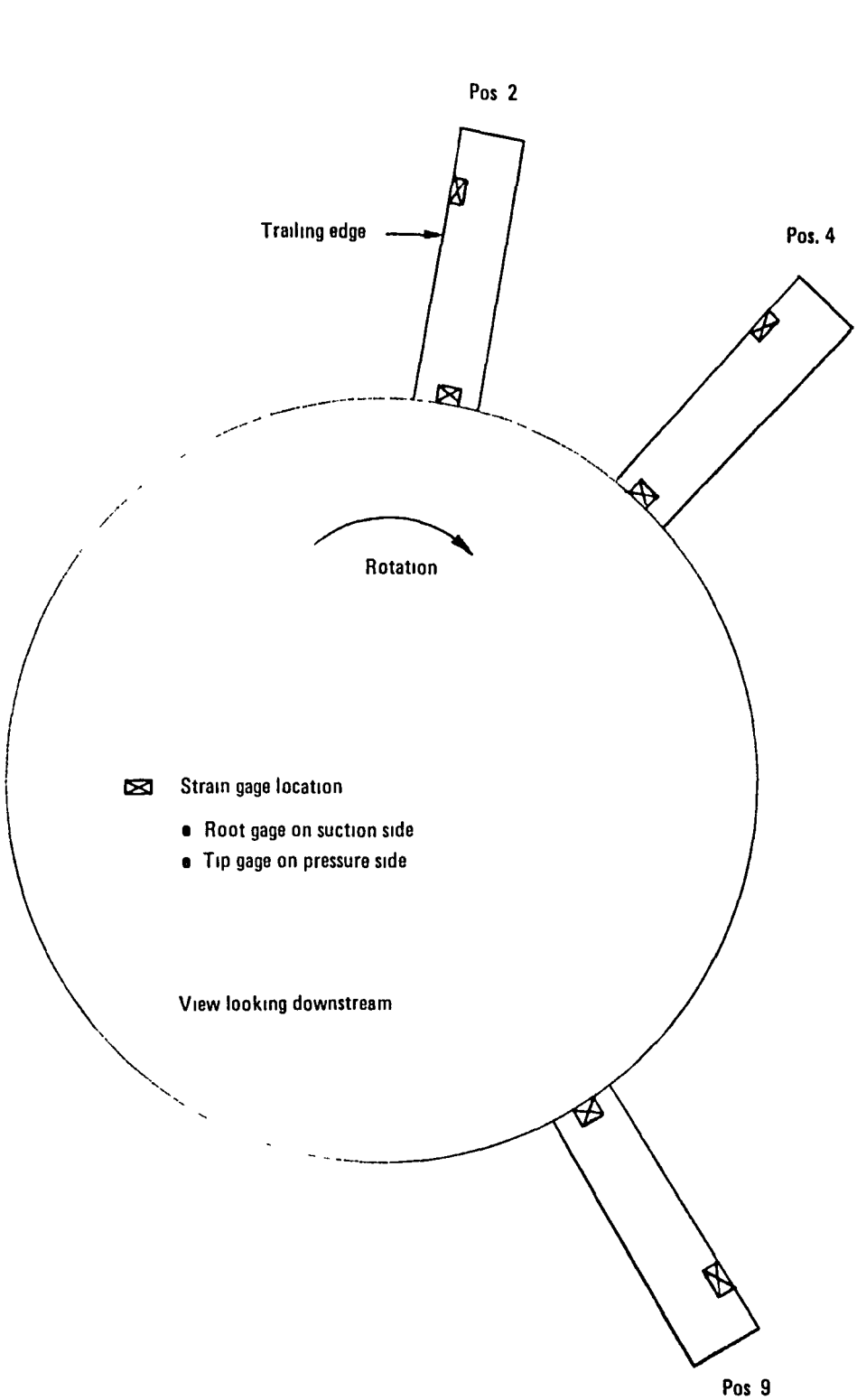

Figure 12. - Fan blade strain gage location.

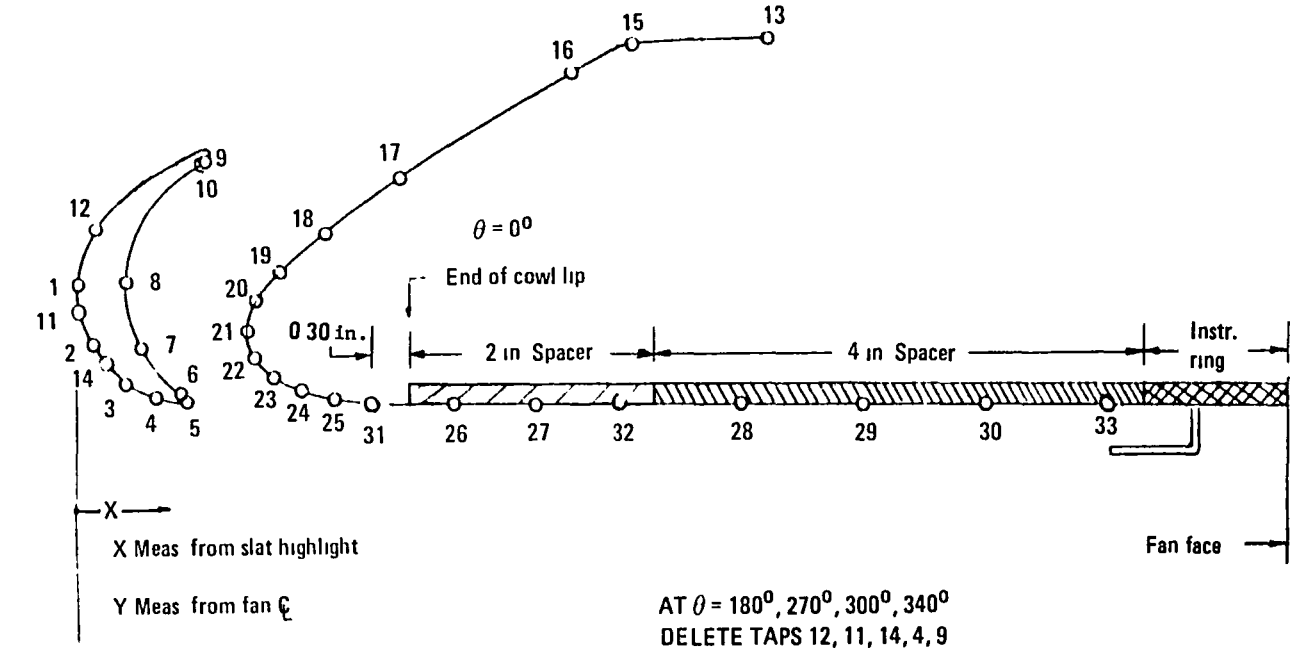

Slat-1 (CR = 1 2)

Tap	X(in)	Y(in.)
1	0	10 9587
2	0 0311	10 7171
3	0 1222	10 4913
11	0 2676	10 2959
14	0 4577	10 1436
4	0 6800	10 0440
5	0 9547	10 0040
6	0 6000	10 2340
7	0 5000	10 4370
8	0 4000	10 9587
9	1 0500	11 9650
10	1 0300	11 9500
12	0 5000	11 8000

Slat-2 (CR = 1 3)

Tap	X(in.)	Y(in.)
1	0	11 4063
2	0 0413	11 0684
3	0 1629	10 7504
11	0 3574	10 4710
14	0 6136	10 2468
4	0 9163	10 0909
5	1 2476	10 0125
6	1 2476	10 1183
7	0 8476	10 4910
8	0 6476	11 0000
9	1 4476	12 1873
10	1 4776	12 2100
12	0 1425	11 6570

Cowl Lip

Tap	X(in.)	Y(in.)
13	4 900	12 910
15	4 500	12 885
16	4 000	12 660
17	2 650	11 830
18	1 912	11 252
19	1 670	11 040
20	1 500	10 870
21	1 420	10 600
22	1 480	10 380
23	1 600	10 230
24	1 800	10 095
25	2 100	10 025
31	2 474	10 004

Figure 13. - Slat/cowl surface static pressure tap locations.

X ~IN	θ ~DEG	No Spacer	2 Inch Spacer	4 Inch Spacer
		Static tap number (see figure 13)		
1 054	0	31	31	31
	45	31	31	31
	80	31	31	31
	135	31	31	31
	180	31	31	31
	225	31	31	31
	270	31	31	31
	315	31	31	31
1 720	0		26	
2 050	0			28
	180			28
	270			28
	300			28
	340			28
2 390	0		27	
	180		27	
	270		27	
	300		27	
	340		27	
3 050	0			29
3 054	45		32	
	90		32	
	135		32	
	180		32	
	225		32	
	270		32	
	315		32	
4 050	0			30
	180			30
	270			30
	300			30
	340			30
5 054	45			33
	90			33
	135			33
	180			33
	225			33
	270			33
	315			33
X measured from cowl lip highlight				

Figure 14. - Location of internal wall static pressure taps mounted in throat and spacer.

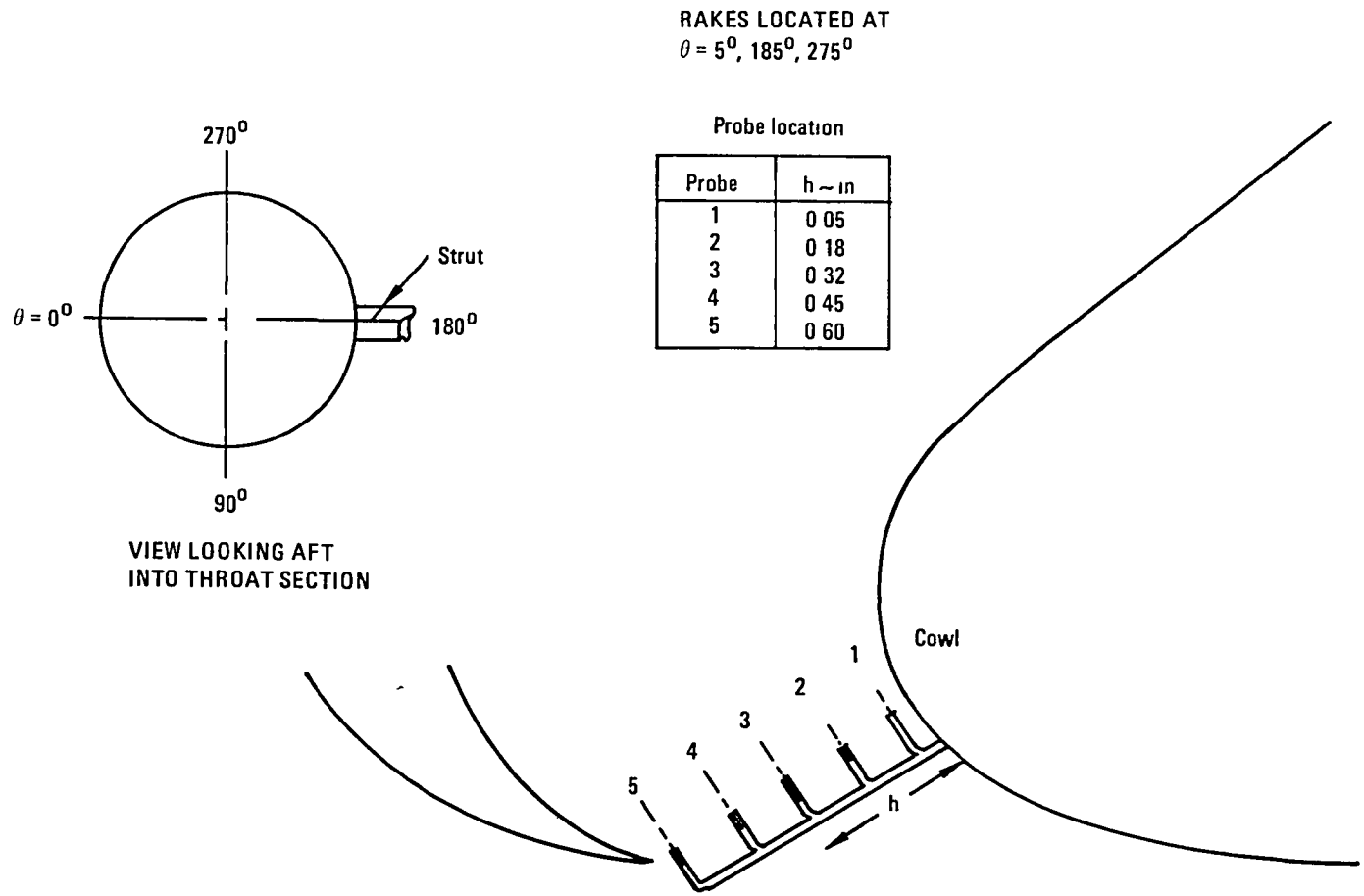

Figure 15. - Slot total pressure rake instrumentation.

wall sufficient to accommodate the largest slot width, i.e., with the slat in the most forward position. With the slat retracted, the outer probes that would be in the wake of the slat flow were cut off.

The fan exit total pressures were measured by five total pressure rakes as shown in figure 16. Each rake consisted of ten probes located radially as shown in the figure. These pressures were area weighted and the values ratioed to the fan inlet area weighted pressures to establish the fan pressure ratio.

All model and tunnel pressures were measured by a series of nine 48-channel scanivalves, each having a separate calibrated transducer. The fan face rake total pressures (114 measurements), from which the recovery and distortion levels are established, were divided between four of these scanivalves. To assure data accuracy and consistency, each of the calibrated transducers associated with these four scanivalves also measured the tunnel total pressure (from the same tunnel probe). These data were used to calculate the local to tunnel total pressure ratio (P_t/P_{to}) of each probe of the appropriate scanivalve.

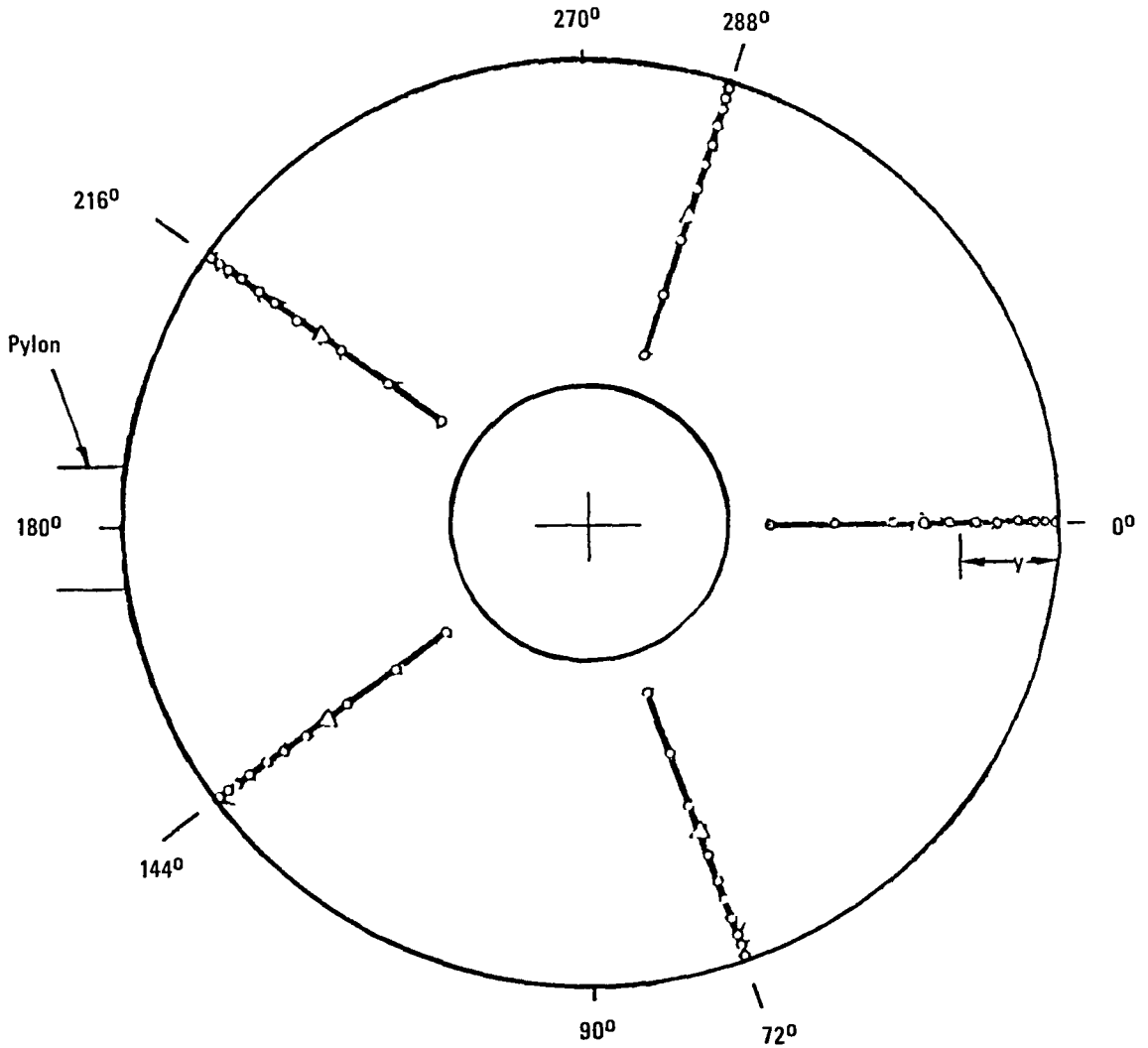

o Total pressure probe
△ Static pressure probe

Probe locations

y (in.)

0 030
0 100
0 220
0 318
0 650
0 986
1 708
2 094
2 501
3 386
4 410

Figure 16. - Fan stator exit total pressure instrumentation.

DATA REDUCTION PROCEDURES

A description of the methods used to calculate the performance data presented in this report is described below.

Inlet/Fan Airflow Rates

The fan airflow rates presented herein are based on correlations of the NASA-LeRC fan face rake against a calibrated bellmouth. The calibration reflects the true flow rate as a function of the rake integrated values from total and static pressure measurements, which is approximately 6 percent higher than the integrated value. To obtain corrected weight flows based on the total pressure and temperature at the fan face, the standard procedure is used, i.e.,

$$\frac{W\sqrt{\theta}}{\delta} = \frac{W\ (T_2/T_o)^{\frac{1}{2}}}{(P_{t2}/P_o)}$$

where T_o and P_o are the reference sea level values. Also, the inlet weight flow (or mass flow) ratioed to the choking value through the inlet net area is calculated by,

$$\frac{\omega}{\omega^*} = \frac{\frac{W\sqrt{\theta}}{\delta} \times \frac{1}{A}}{\left(\frac{W\sqrt{\theta}}{\delta A}\right)^*}$$

$$\left(\frac{W\sqrt{\theta}}{\delta A}\right)^* = 49.41 \text{ lb/sec/sq ft}$$

Fan Face Total Pressure Recovery

For comparison, several methods were used in the data reduction program at NASA-LeRC to calculate fan face total pressure recovery - including a mass-average, area-weighted average, equal area average, and a simple arithmetic average. The area-weighted method is considered to be the most correct (and also the lowest recovery) and was used in this report. It is defined as follows.

$$\frac{P_{t2}}{P_{to}} = \frac{\sum_{i=1 \text{ to } 6} \sum_{j=1 \text{ to } 19} P_{t_{ij}} \, dA_{ij}}{A_{net} \, P_{to}}$$

where $Pt_{i,j}$ are the individual probe measured total pressures and where $dA_{i,j}$ is the incremental area associated with each probe, as listed in figure 11.

Total Pressure Distortion

Three total pressure distortion parameters (i.e., NDI, KD2, and KΘ) that have been utilized for various production engines configurations in the past have been evaluated from the measured fan face total pressure. These parameters have been developed by the appropriate engine manufacturers and are intended to correlate resulting distortion patterns to allowable engine operation.

The General Electric procedure for calculating the NDI distortion parameter is as follows:

A_A = Total annulus area (1.5% outer diameter excluded)

$A_{outer} = A_A/2$

$\bar{P}_t$ = Area weighted P_t in A_A

$P_{T_{MAX}}$ = Maximum P_t in A_A

$P_{T_{MIN}}$ = Minimum P_t in A_A

A_L = Portion of A_A which is continuous where measured pressures are less than $\bar{P}_t$

A_{TL} = Portion of A_L in A_{outer}

$\bar{P}_{T_{MIN}}$ = Area weighted P_t in A_L

R_P = Radial profile index = $2 A_{TL}/A_L$

Procedure: Divide annulus into 180 equal area segments (10 rings, 18 sectors) interpolate rake data to obtain total pressure for each segment. Perform the following calculations for each continuous low pressure region.

$P_{T_{AV}}$ - Average P_t in A_L

$P_{T_{MIN}}$ - Minimum P_t in A_L

Shape Factor $$S = \frac{\pi}{2}\left[\frac{\overline{P}_T - P_{T_{AV}}}{\overline{P}_T - P_{T_{MIN}}}\right]$$

Extent factor $$E = 2\,A_L/A_A$$

Profile Factor $$Y = 1 + 2\,\mathrm{ABS}(2\,A_{T_L}/A_L - 1)$$

$$ND = \left[\frac{P_{T_{MAX}} - P_{T_{MIN}}}{\overline{P}_T}\right] \sqrt{SEY}$$

ND_{MAX} = maximum ND calculated for all low pressure regions

$$NDI = ND_{MAX}\left[\frac{ND_{MAX}}{ND_1 + ND_2 + \ldots ND_N}\right]^{\frac{1}{2}}$$

The Pratt and Whitney procedure in calculating the KD2 distortion parameter is outlined below:

For each instrumentation ring

$\overline{P}_T$ = Average over ring

θ_K = Angular extents where P_t is less than $\overline{P}_T$

$P_{T_{K,MIN}}$ = Minimum for each extent

$$\left(\frac{\Delta P\theta}{\overline{P}}\right)_K = \left[\frac{P_T - P_{T_{K,MIN}}}{\overline{P}_T}\right]\theta_K$$

$$\left(\frac{\Delta P\theta}{\overline{P}}\right)_{MAX} = 100 \times \mathrm{MAX}\left(\frac{\Delta P\theta}{\overline{P}}\right)\Bigg]_K \sim \mathrm{PERCENT}$$

Sum for each ring

$$KD2 = \frac{\sum_{i} \frac{1}{R_i} \left(\frac{\Delta P\Theta}{\overline{P}}\right)_{MAX,i}}{\sum_{i} \frac{1}{R_i}}$$

The Pratt and Whitney procedure for calculating the KΘ distortion parameter is outlined below:

$$K\Theta = \frac{\sum_{ring=1}^{J} \left[\left(\frac{A_n}{N^2}\right)_{max}\right]_{ring} \frac{W_{ring}}{D_{ring}}}{q/\overline{P}_T \sum_{ring=1}^{J} \frac{W_{ring}}{D_{ring}}} \qquad \text{(A-1)}$$

where

J = number of total rings which is equal to number of probes per rake

D_{ring} = diameter of the ring or radial probe

W_{ring} = ring area weighting factor

$\overline{P}_T$ = face average total pressure

$q/\overline{P}_T$ = dynamic head/average total pressure

To define the term $\left(\frac{A_n}{N^2}\right)_{max}$, a more detailed explanation is required.

In general, the circumferential distribution of total pressure at a given radius can be presented by a Fourier series. A particularly useful form of such an expression is:

$$\frac{P_T}{\overline{P}_T} = \frac{a_o}{2} + \sum_{n=1}^{\infty} (a_n \cos n\theta + b_n \sin n\theta)$$

where

$$a_n = \frac{1}{\pi} \int_{-\pi}^{\pi} \frac{P_T}{\overline{P}_T}(\theta) \cos n\theta \; d\theta$$

$$b_n = \frac{1}{\pi} \int_{-\pi}^{\pi} \frac{P_T}{\overline{P}_T}(\theta) \sin n\theta \; d\theta$$

If we define $A_n = \sqrt{a_n^2 + b_n^2}$ then the series can be written as:

$$\frac{P_T}{\overline{P}_T} = \frac{A_o}{2} + \sum_{n=1}^{\infty} A_n \sin (n\theta + \phi_n)$$

Thus defining $\left(\frac{A_n}{N^2}\right)_{max}$ as being the largest value of this expression for the sine series representation of the data.

Flow Velocity Distortion

At high inlet angles of attack a nonuniform static pressure profile exists at the throat/ fan face for a zero-length inlet. This distribution reults in a corresponding inlet flow velocity distortion (i.e., potential flow distortion) even though a uniform no loss total pressure profile may exist. The velocity is calculated at each probe from the measured total pressure and the static pressure profiles defined by a linear variation of the two stream static pressures measued in each rake, as follows;

$P_{t_{i,j}}$ = measured total pressure of each probe

$P_{1,j}$ = interpolated stream static at each probe location

$$M_{i,j} = \left[\left(\frac{2}{\gamma-1}\right) \left(\frac{P_{t_{i,j}}}{P_{i,j}} \right)^{\frac{\gamma-1}{\gamma}} - 1 \right]^{\frac{1}{2}}$$

$$V_{i,j}/V^* = M_{i,j} \left[\frac{\gamma+1}{2+(\gamma-1)\ M_{i,j}^2} \right]^{\frac{1}{2}}$$

$$V^* = \left[\gamma g\ R\ T_{to} / (1+\frac{\gamma-1}{2}) \right]^{\frac{1}{2}}$$

$$V_{i,j} = \frac{V_{i,j}}{V^*} \times V^*$$

Change in Blade Effective Angle of Attack

For each probe:

$V_{i,j}$ from above

$$V_{Tan} = \frac{\pi\ r_{i,j}\ N}{360}$$

$$\beta = \tan^{-1} \frac{V_{i,j}}{V_{Tan}}$$

$$\Delta\beta = [\text{MAX } \beta]_{j=1 \text{ to } 6}$$

Surface Pressures/Mach Number/Velocity

The measured surface static pressures presented in the report are normalized with freestream total pressure, i.e. P/P_{to}. From these data the local surface Mach number and velocity are calcuated from the compressible flow relationships previously used in calculating flow velocity distortion.

RESULTS AND DISCUSSION

General Discussion

This section presents the overall performance of the zero-length, slotted-lip inlet configuration and appropriate discussions of the test data. The section is structured, as outlined in figure 17, to present initially the performance of the design baseline configuration including effects of forward speed and model angle of attack. Subsequent to the discussion of these data, the effects on performance of each of the configuration variables tested are presented - slat contraction ratio, slot-gap width (slat fore and aft position), inlet throat/fan face spacer, and the 90 degree slot gap fillers. Finally, estimated angle-of-attack bounds based on flow separation are presented and slat/cowl surface velocities, calculated from measured static pressures, are compared to those predicted by potential flow analysis.

Baseline Configuration Performance

The baseline configuration, as described in the model description section, was selected as being the most likely to meet the design operating requirements of a subsonic V/STOL aircraft. This configuration has a slat contraction ratio of 1.2, a slot-gap width of 0.51 inches, and no inlet throat/fan face spacer. Within the limits of allowable flow distortion and fan blade stress levels, the measure of quality of the inlet flow is the total pressure recovery. Degradations in this parameter through friction and separation losses reduce the available engine net thrust. For the V/STOL aircraft, where lift at take-off is derived totally from engine thrust, this results in a direct increase in engine size and therefore, aircraft gross weight.

For the baseline configuration, the fan face total pressure recovery for all conditions tested is presented in figure 18 as a function of inlet airflow (or mass flow) ratio. This flow parameter is the ratio of the inlet airflow to the quantity necessary to choke the inlet area (i.e., maximum airflow) and is shown in relation to the throat Mach number and absolute corrected airflow in figure 19.

Figure 18 shows that except for the low airflows tested (representing engine idle operation), the lowest recovery measured was 0.988; this occurring at 105 knots tunnel speed and a model angle of attack of 60 degrees. Also shown in this figure are the flow total pressure distortion levels as calculated from the KD2 parameter. The distortion levels are consistent with the

BASELINE CONFIGURATION	
PERFORMANCE SUMMARY	FIGURES 18–22
EFFECT OF FORWARD SPEED	FIGURES 23–26
EFFECT OF ANGLE OF ATTACK	FIGURES 27–35
EFFECT OF FLOW VELOCITY DISTORTION ON FAN PERFORMANCE	FIGURES 36–39
EFFECT OF SLAT CONTRACTION RATIO	FIGURES 40–44
EFFECT OF SLOT GAP WIDTH	FIGURES 45–52
EFFECT OF THROAT/FAN SPACER	FIGURES 53–57
EFFECT OF 90^{0} SLOT FILLERS	FIGURES 58–65
FLOW SEPARATION AND INLET OPERATING ENVELOPES	FIGURES 66–69
COMPARISON WITH POTENTIAL FLOW PREDICTIONS	FIGURES 72–73

Figure 17. - Summary of performance curves.

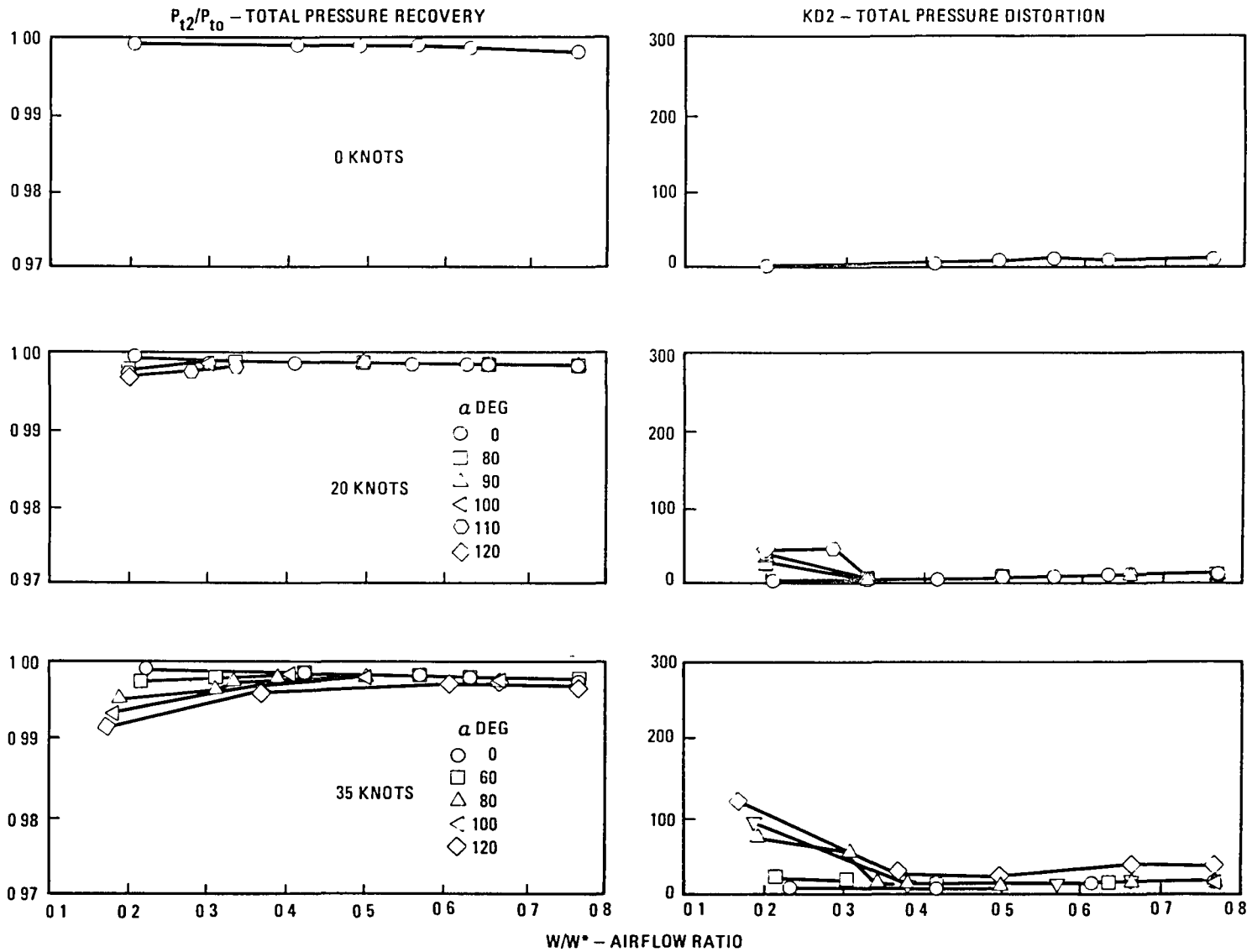

Figure 18. - Inlet total pressure recovery and flow distortion CR=1.2, 0.51 inch slot gap, no spacer.

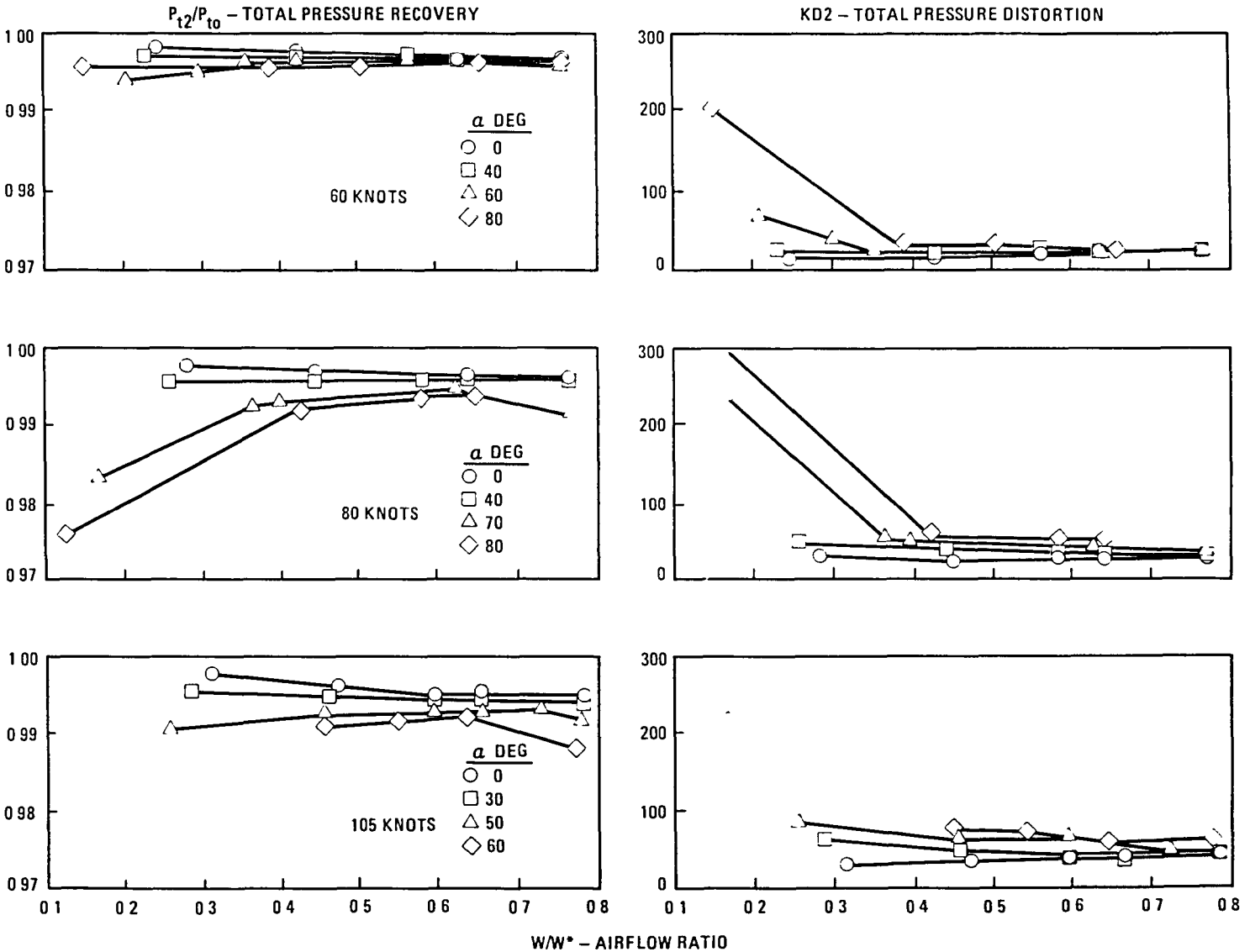

Figure 18. - Inlet total pressure recovery and flow distortion CR=1.2, 0.51 inch slot gap, no spacer. (Concluded.)

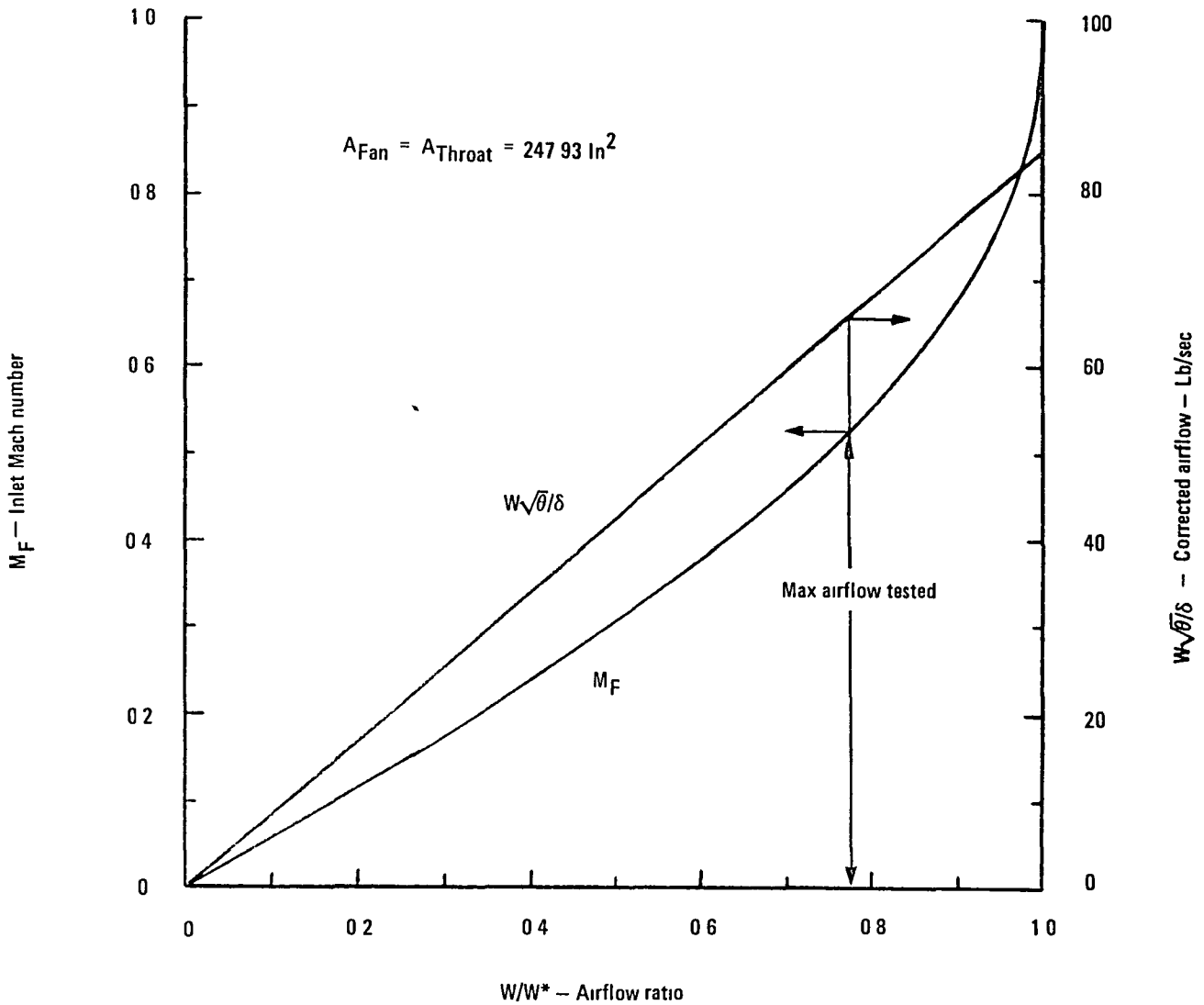

Figure 19. - Model airflow/inlet Mach number relationship.

high recoveries measured and are well below empirically derived criteria for acceptable fan operation, as will be discussed later.

Although the lowest recovery measured was 0.988, the associated model angle of attack (60 degrees) is outside the operating envelope for the V/STOL fixed nacelle application, as illustrated in figure 20. This figure presents the estimated V/STOL velocity/angle of attack envelope and lines of constant total pressure recovery based on measurements at the test data points shown. The V/STOL envelope is based on considerations of adverse crosswind velocity conditions during hover, as well as aircraft attitudes during transition and maneuvering flight modes. As can be noted on the figure, the fan face total pressure recovery is not less than 0.994 over the entire operating envelope. At hover, with a 35 knot crosswind at 120 degrees angle of attack, where engine sizing is influenced by inlet losses, the recovery is not less than 0.996.

The solid symbols in figure 20 represent test conditions at which inlet flow separation is indicated by the fan face rake. Occurrence of this separation is defined here as when any measured total pressure at the fan face approaches the measured static pressure. This first occurs adjacent to the duct wall at the zero degree rake location (critical at angle of attack). Since this separation is very localized at the conditions tested (as will be shown in subsequent total pressure profiles), the levels of average total pressure recovery are high and flow distortion low.

During each test run fan blade stress levels were continuously recorded as the fan speed was increased from idle to maximum. Since test procedures were such to limit the model angle of attack to the occurrence of separation, these stress levels did not exceed a low percentage of the safe operating value. Typical traces are shown in figure 21 at the maximum angle of attack tested for each tunnel speed. Also, for reference the zero degree angle-of-attack data are shown. As can be noted, the stress levels are very low; however at the maximum fan speed tested (maximum airflow) the levels are beginning to increase.

Since the measured stress levels are low, allowable inlet operating envelopes based on this parameter were not generated. These envelopes, however, would be peculiar to the specific fan tested and could not be readily generalized for fans having different structural integrities.

In addition to the KD2 flow distortion parameter presented in figure 18, two alternate parameters, $K\theta$ and NDI were calculated and are compared in figure 22, again for the maximum angles of attack tested. These parameters account for the magnitude and the radial and circumferential extent of the low total pressure regions at the fan face and are intended to correlate limits of operation with distortion for the fan. The NDI parameter, for example, has been employed by General Electric for the TF34 engine. The engine specification (reference 3) stipulates that no engine performance penalties result if the index (NDI) is below a value of 0.10, and fan operation is not restricted for values below 0.20 (i.e., a value of 0.20 would dictate the maximum allowable

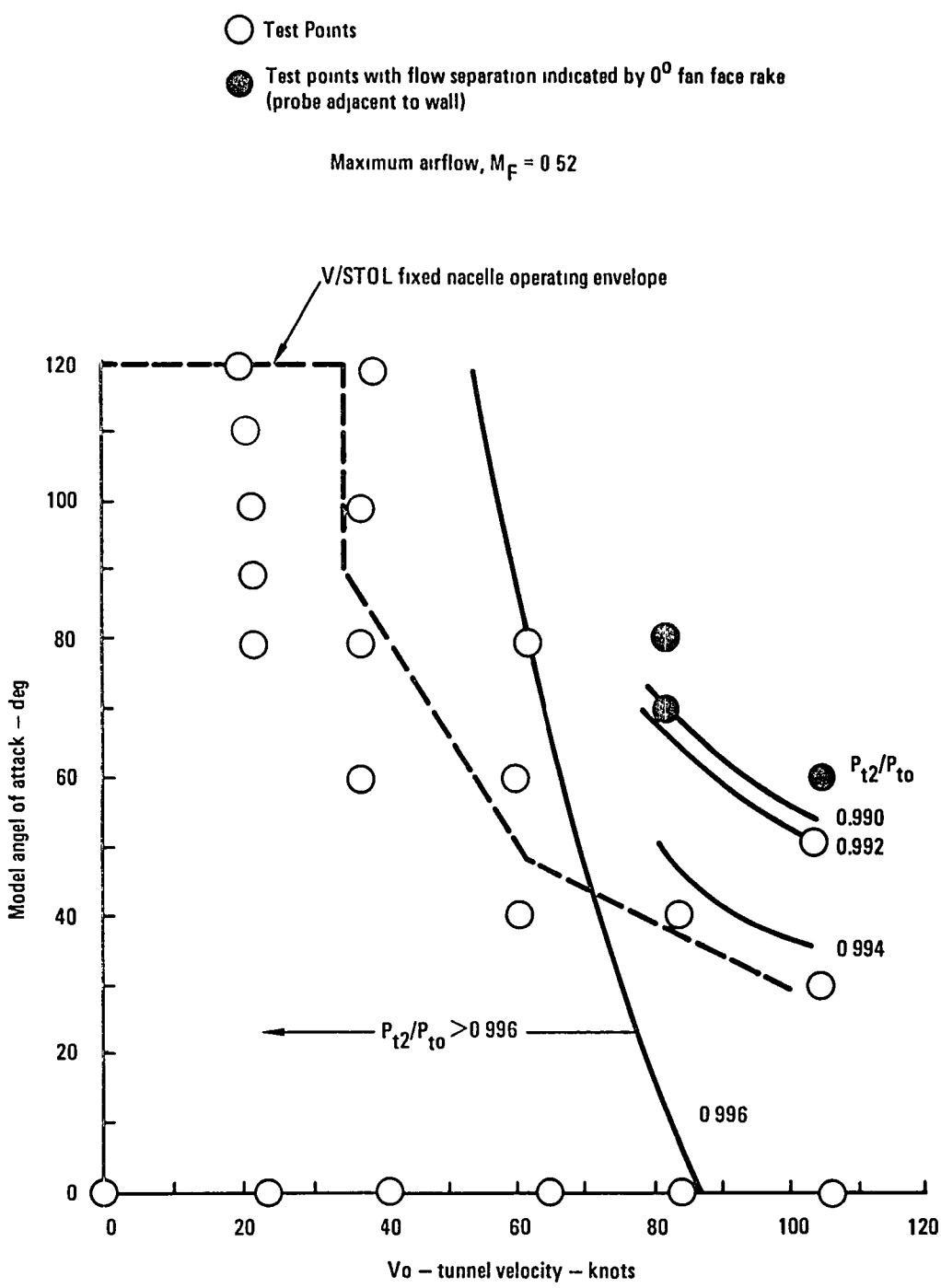

Figure 20. - Total pressure recovery summary over inlet operating envelope CR=1.2, 0.51 inch slot gap, no spacer.

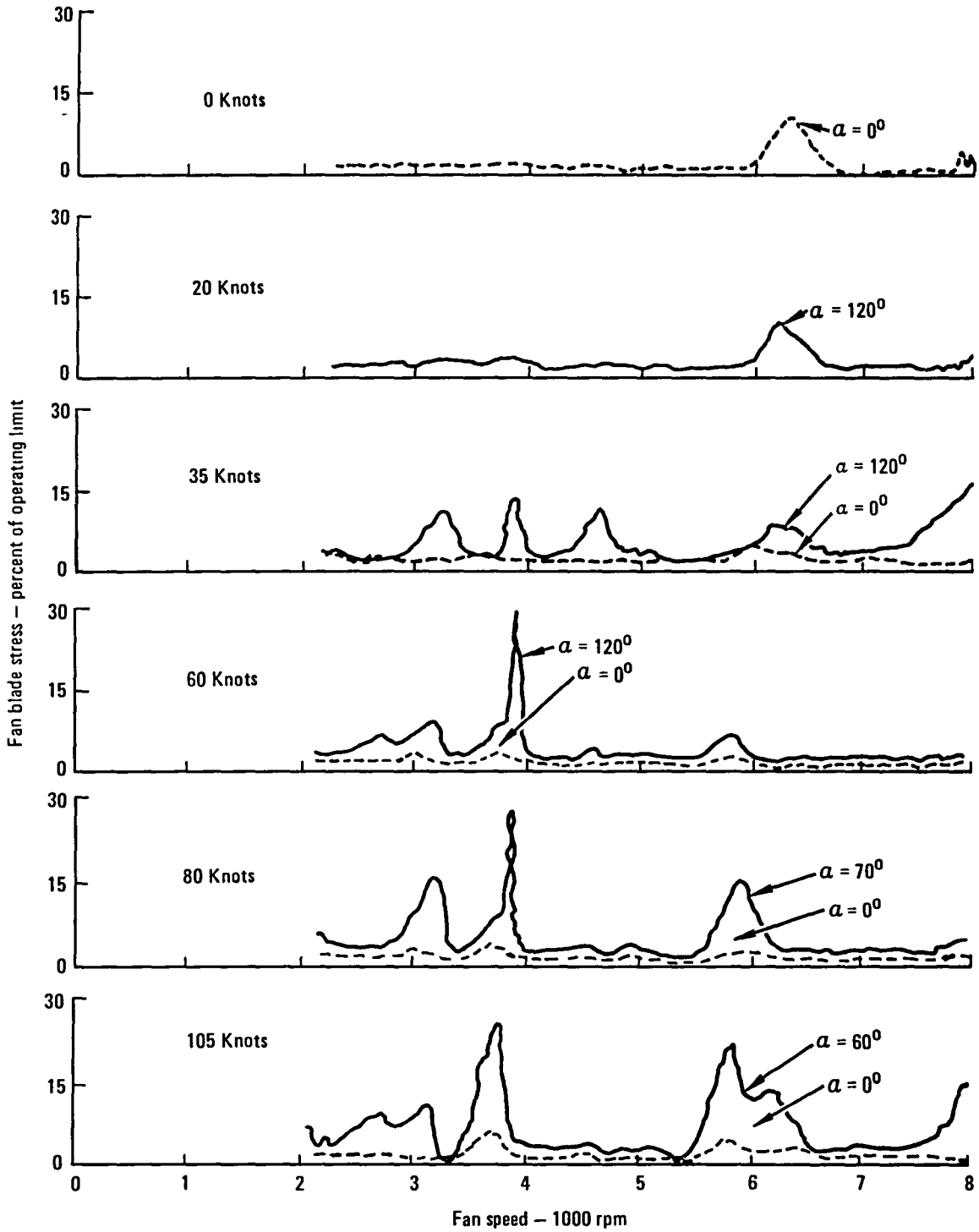

Figure 21. - Measured fan blade stress levels-baseline configuration CR=1.2, 0.51 inch slot gap, no spacer.

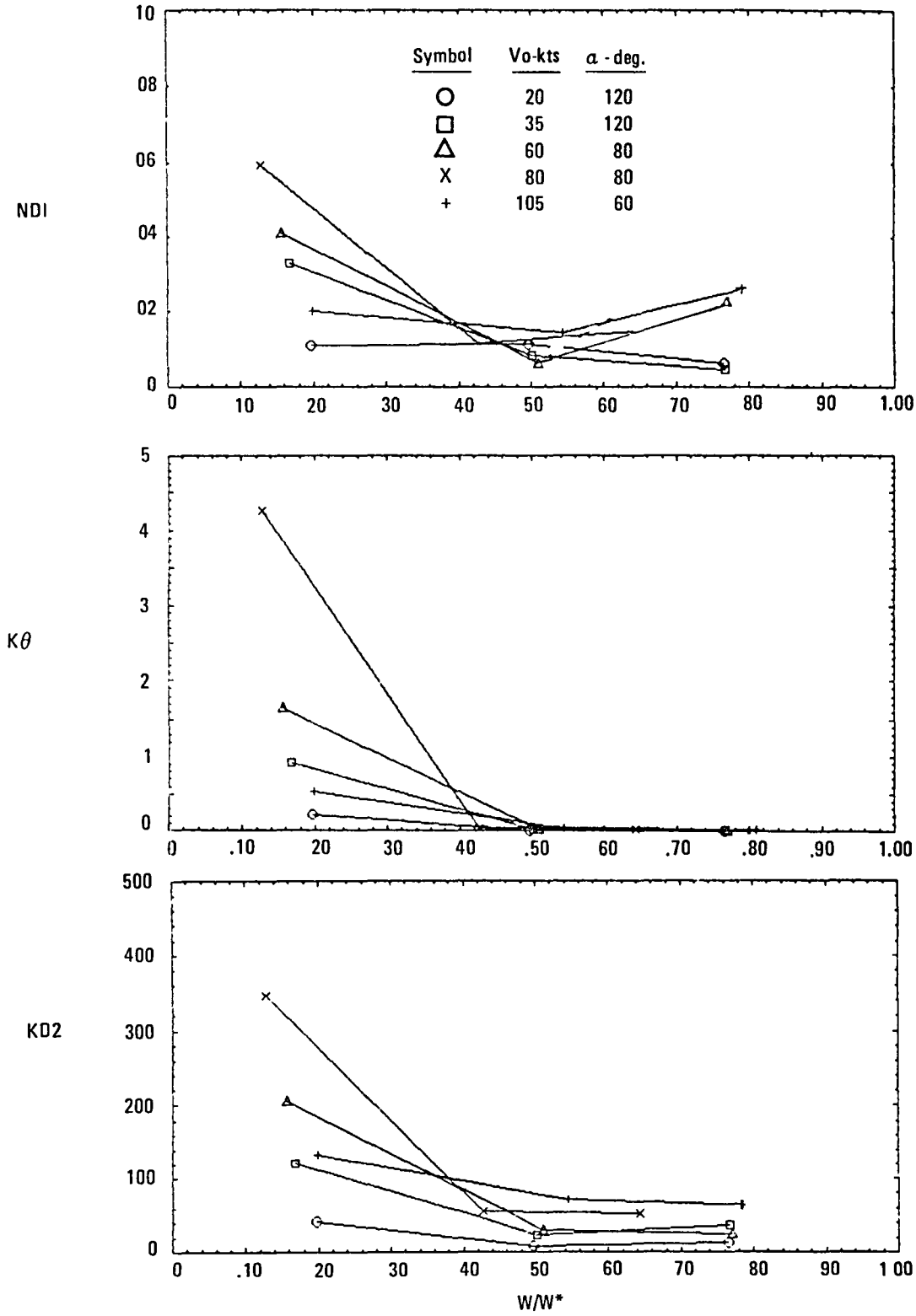

Figure 22. - Inlet flow total pressure distortion at maximum angles of attack tested, CR=1.2, 0.51 inch slot gap, no spacer.

fan speed). As can be noted for the baseline configuration, no values greater than 0.03 were calculated over the airflow range associated with high fan speeds.

For the KD2 parameter, data are available (reference 4) indicating the tolerance of the Pratt and Whitney TF30 engine. These data show allowable levels of distortion of 1240 at zero turbulence decreasing to 380 at a 3 percent turbulence level, well above the values calculated for the inlet model and shown in figure 22. The low levels of flow distortion calculated during the test preclude establishing an operating limit (angle of attack/forward speed) based on this parameter.

Effect of Forward Speed

For a conventional unslotted-lip inlet the effect of forward speed is to improve the total pressure recovery relative to the static condition (referred to as clean up). This results from a change in the pattern (direction) of the entering streamlines - the cowl surface stagnation point moving from infinity at static conditions to some forward location on the cowl depending on the forward speed.

For a slotted-lip inlet operating at a fan face Mach number of 0.52, the total pressure recovery is reduced with increasing forward speed, as shown in figure 23. This loss is also evidenced by the degradation in the fan face total pressure profiles shown in figure 24. As the speed increases, the flow enters the slot from a more forward direction, requiring greater turning around the slat leading edge and thereby incurring greater losses. The slat/cowl surface pressure distribution, also shown in figure 24, illustrates the shift in flow pattern with forward speed. This shift results in increasing pressures on the slat and decreasing pressures on the cowl as the speed increases. The reduction in slot flow recovery, as measured by the slot total pressure rakes, is shown in figure 25 and as can be noted the level of recovery is consistent with that measured by the fan face rake in the vicinity of the duct wall (figure 24). The change in the flow pattern into the inlet with forward speed is illustrated in figure 26 which compares the surface Mach number distribution at the zero and 105 knot tunnel speeds.

Effect of Angle of Attack

The effect of increasing model angle of attack is to ultimately cause the flow to separate from the slat/cowl surface with a corresponding reduction in total pressure recovery, as shown in figure 27. At tunnel speeds up to 35 knots the effective lip contraction ratio is sufficient to preclude flow separation up to a model angle of 120 degrees (noted by virtually no loss in recovery). At increasingly higher speeds the angle at which separation occurs is reduced, as indicated by the loss in total pressure. The dashed line on this figure indicates the maximum angles estimated for the V/STOL fixed nacelle operating envelope as previously shown in figure 20.

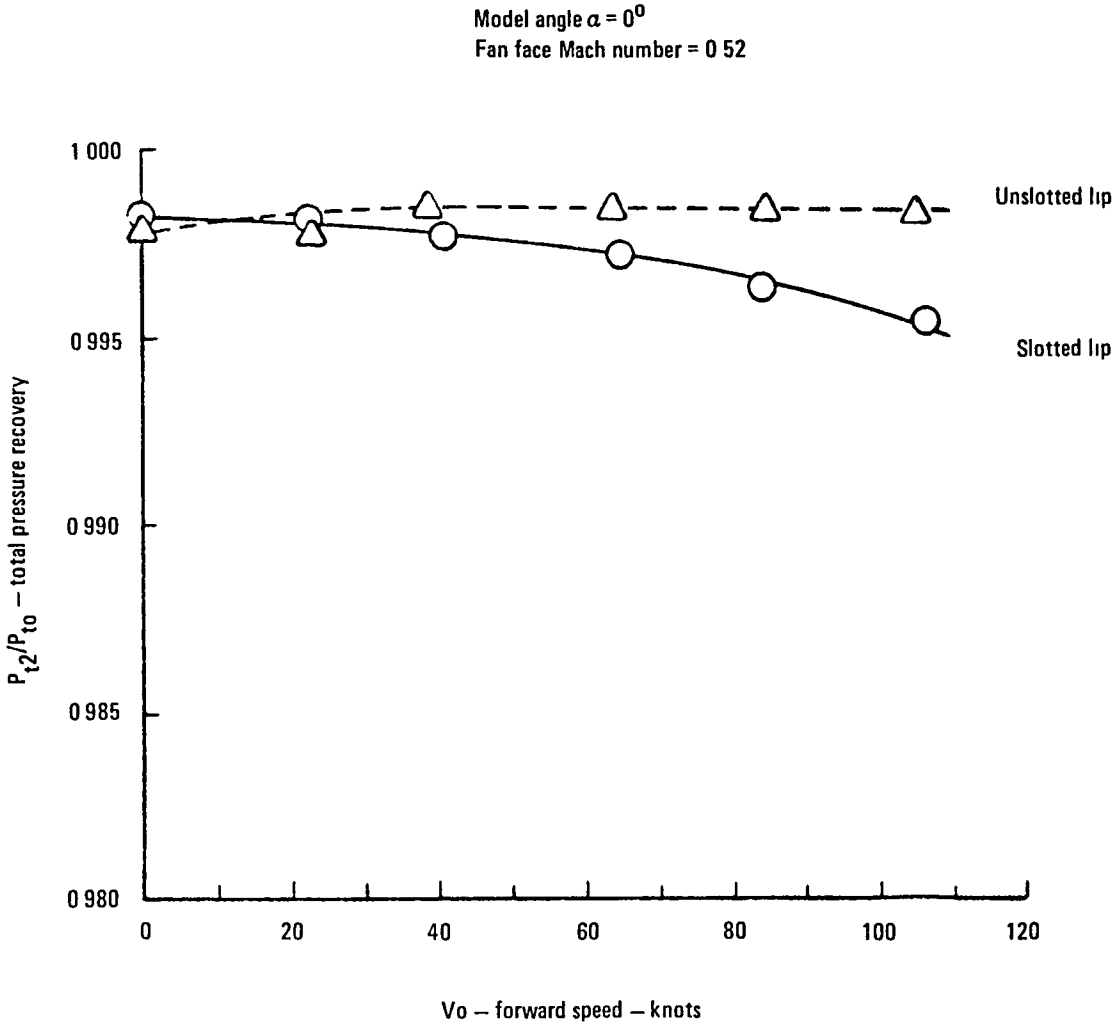

Figure 23. - Effect of forward speed on total pressure recovery of slotted lip inlet, CR=1.2, 0.51 inch slot gap, no spacer.

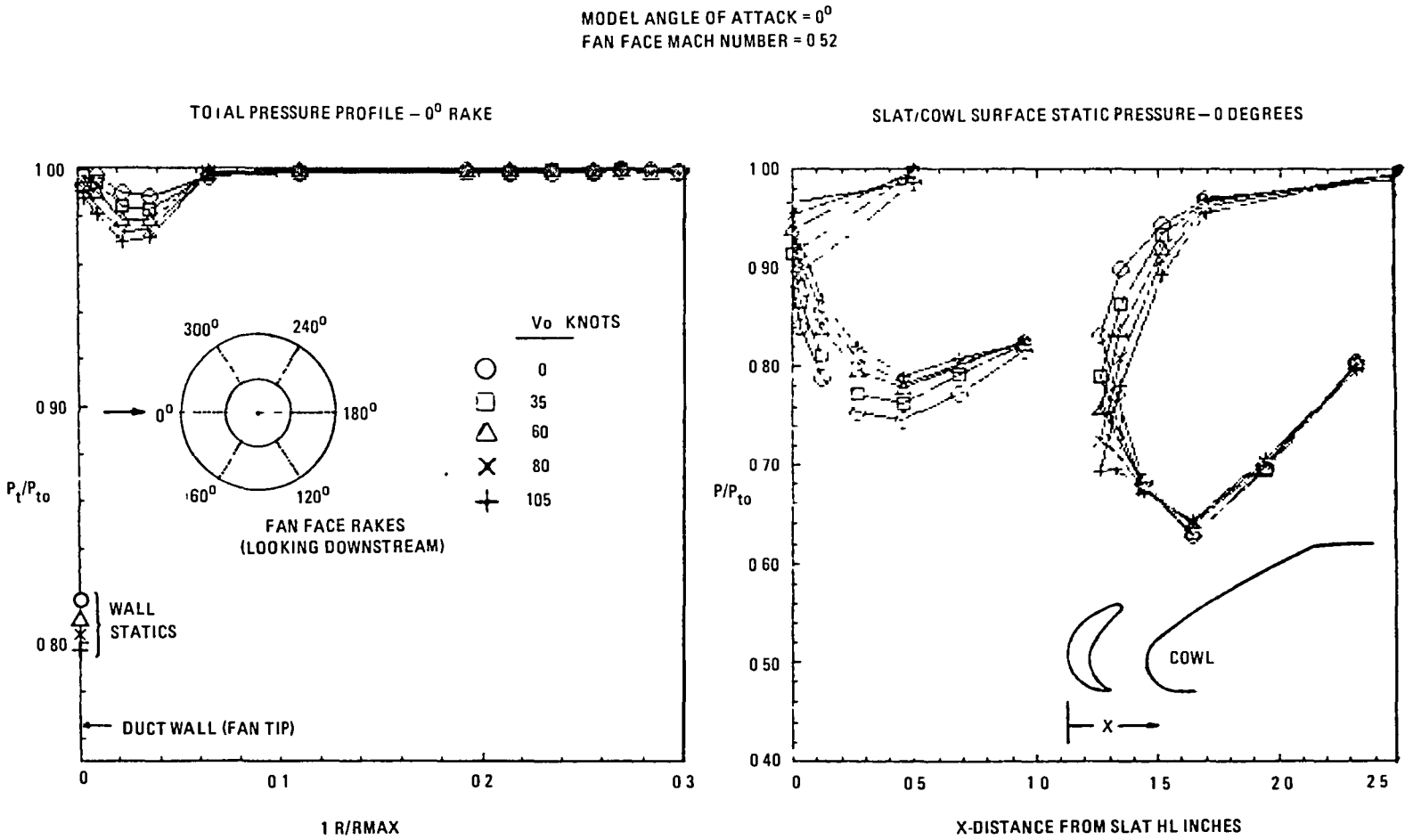

Figure 24. - Effect of forward speed on fan face total pressure profile and slat/cowl surface static pressures, CR=1.2, 0.51 inch slot gap, no spacer.

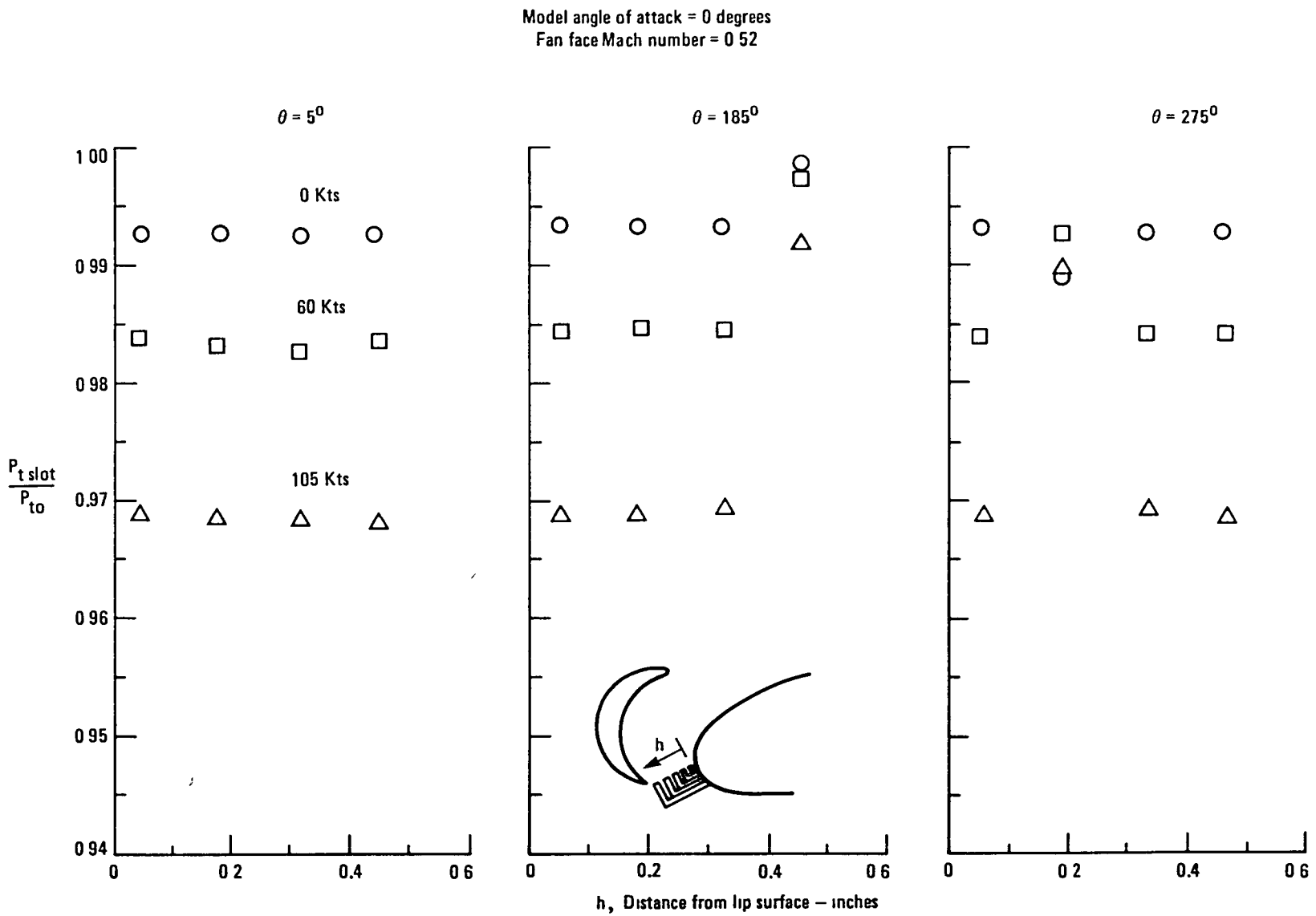

Figure 25. - Effect of forward velocity on slot flow total pressure recovery CR=1.2, 0.51 inch slot gap, no spacer.

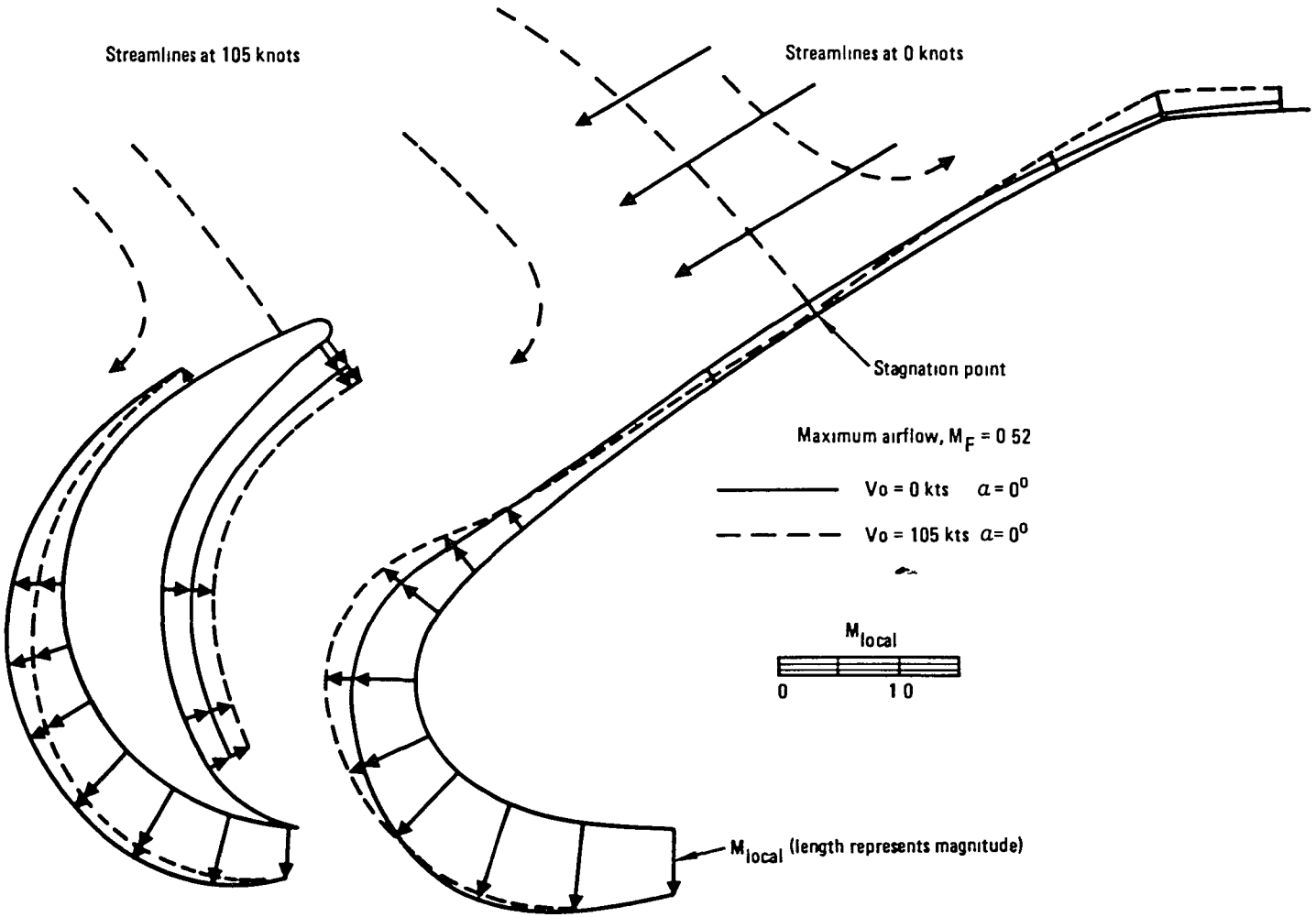

Figure 26. - Effect of forward speed on slat/cowl surface Mach number distribution.

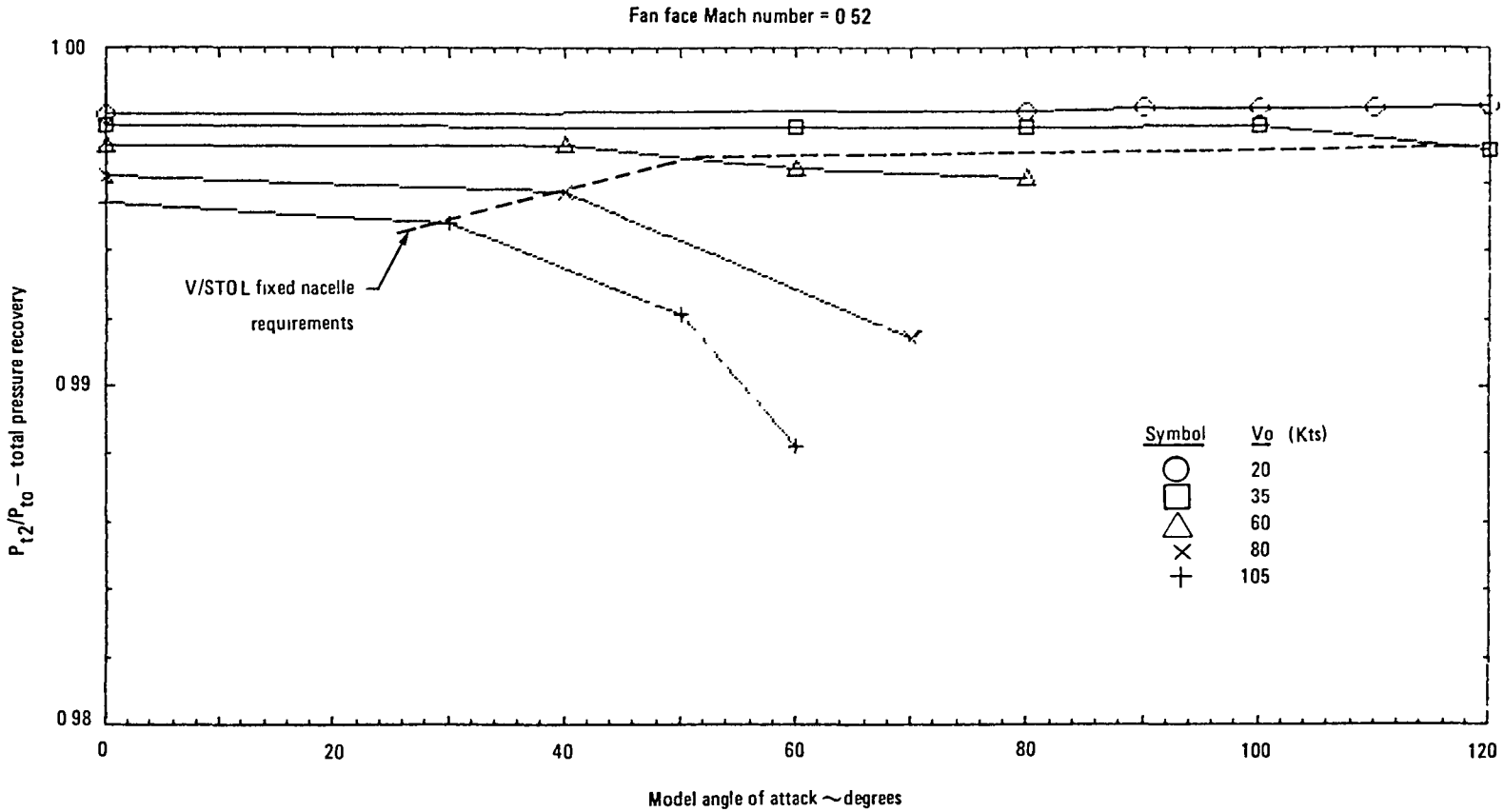

Figure 27. - Effect of model angle of attack on total pressure recovery, CR=1.2, 0.51 inch slot gap, no spacer.

The loss in inlet recovery with increasing angle of attack is illustrated by the fan face total pressure profiles shown in figure 28. As the model angle of attack is increased from zero degrees, the direction of the flow into the slot on the windward side of the nacelle becomes more aligned to the slot opening thus requiring less turning around the slat leading edge. This more favorable direction reduces the pressure loss through the slot as indicated by the improvement in the measured total pressure adjacent to the wall on the fan face rake, $(1-R/R_{max})<0.05$. Correspondingly, however, the flow direction associated with the higher angles of attack reduces the static pressures on the slat below the highlight, resulting in increased local flow separation on this surface. The separation is assumed from the loss in recovery as evidenced by the fan face rake measurements at a greater distance from the duct wall. This is more clearly illustrated in figure 29 at a tunnel speed of 60 knots and for a change in angle of attack from 0 to 80 degrees, a condition where the slot flow is not separated from the cowl lip. At sufficiently high combinations of speed and angle of attack (e.g. 80 knots/70 degrees) the slot flow does separate from the cowl lip as shown by the rake total pressure profile in figure 28.

The improvement in slot flow total pressure recovery with increasing angle of attack (until flow separation occurs from the cowl lip) alluded to above, was measured by the slot total pressure rake and is presented in figure 30. These data also indicate that the recovery is uniform across the slot exit width as well as circumferentially around the inlet. Since the area convergence through the slot is relatively large (approximately 2 to 1) the uniform profile across the slot appears reasonable. It was reasoned above, however, that at increasingly high angles of attack the alignment of the flow into the slot on the windward side of the nacelle was more favorable thereby improving the slot flow recovery. It might be expected, therefore, that on the leeward side of the nacelle the flow entering the slot must turn completely around the slat leading edge, thereby reducing the recovery compared to the windward side, a trend not supported by the uniform recovery data in figure 30. It must be considered, however, that at increasing angles of attack the static pressure across the slot exit on the leeward side becomes increasingly more positive thereby reducing the flow through the slot. This reduction in flow (and corresponding flow velocity) compensates for the increased turning loss around the slat to provide a uniform circumferential total pressure recovery through the slot. The increase in static pressure across the slot exit on the leeward side is evident from the surface Mach number distribution presented in figure 31.

The fan face total pressure profiles presented thus far are those measured by the zero degree rake (critical for separation at angle of attack). Figure 32 presents similar data for each of the six rakes installed for several test conditions at maximum fan airflow. These data illustrate the circumferential loss in freestream total pressure immediately adjacent to the duct wall (fan tip) as resulting from the slot and slat cowl surfaces, and the localization of high boundary layer loss at high angles of attack to the zero degree position (windward nacelle).

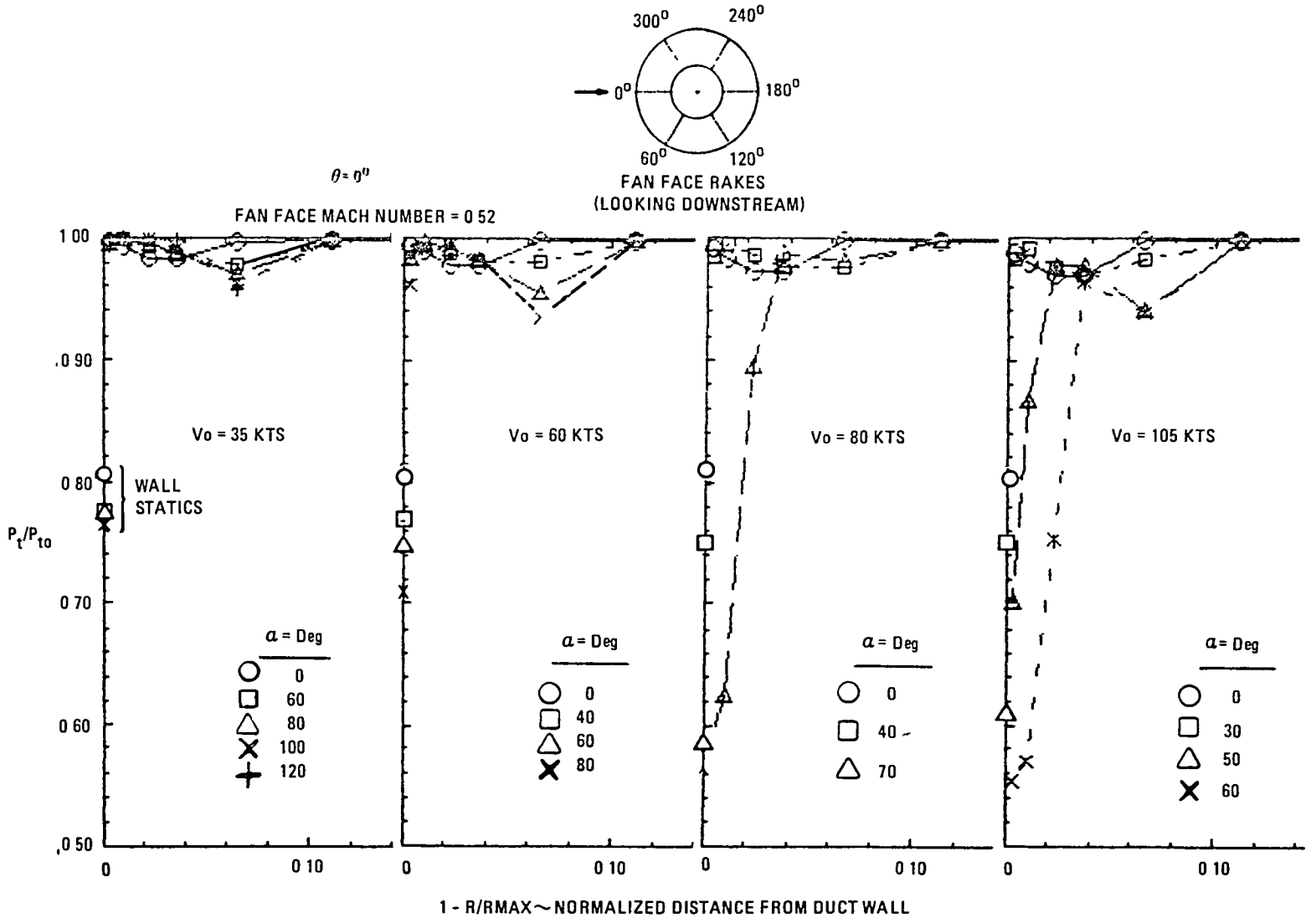

Figure 28. - Effect of model angle of attack on fan face total pressure profiles 0^{o} rake, CR=1.2, 0.51 inch slot gap, no spacer.

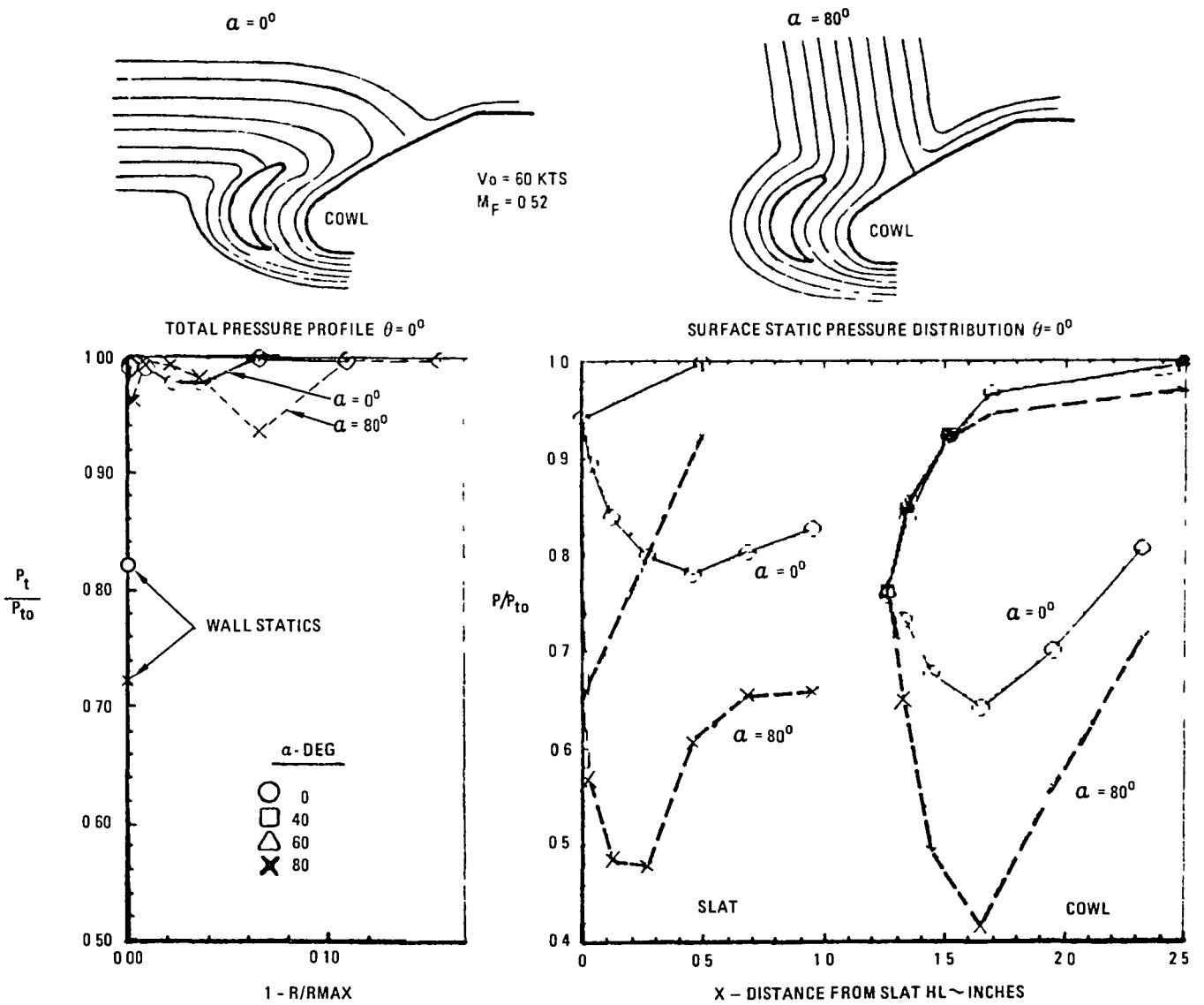

Figure 29. - Effect of angle of attack on slot inlet flow, CR= 1.2, 0.51 inch slot gap, no spacer.

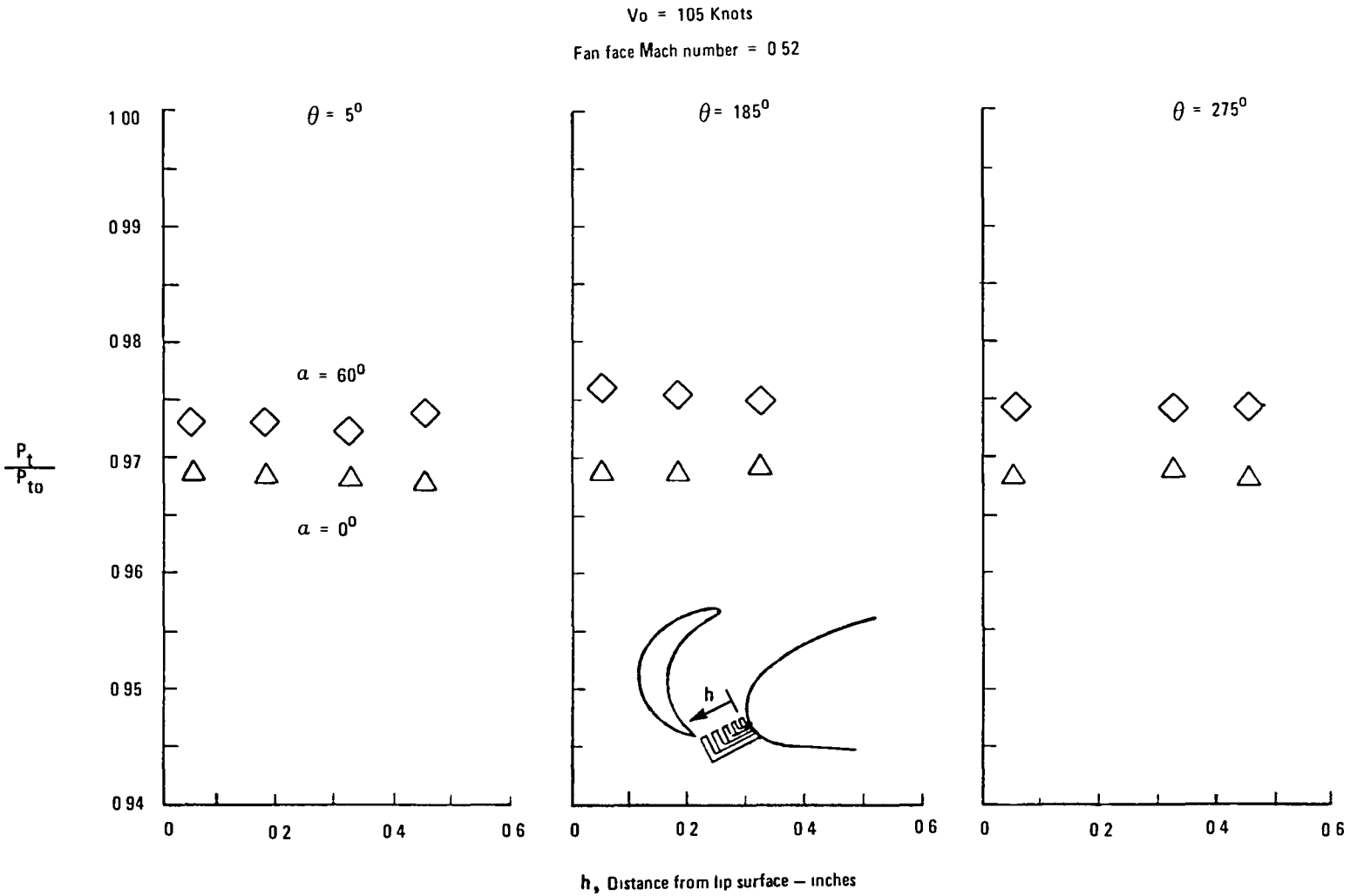

Figure 30. - Effect of model angle on slot flow total pressure recovery, CR=1.2, 0.51 inch slot gap, no spacer.

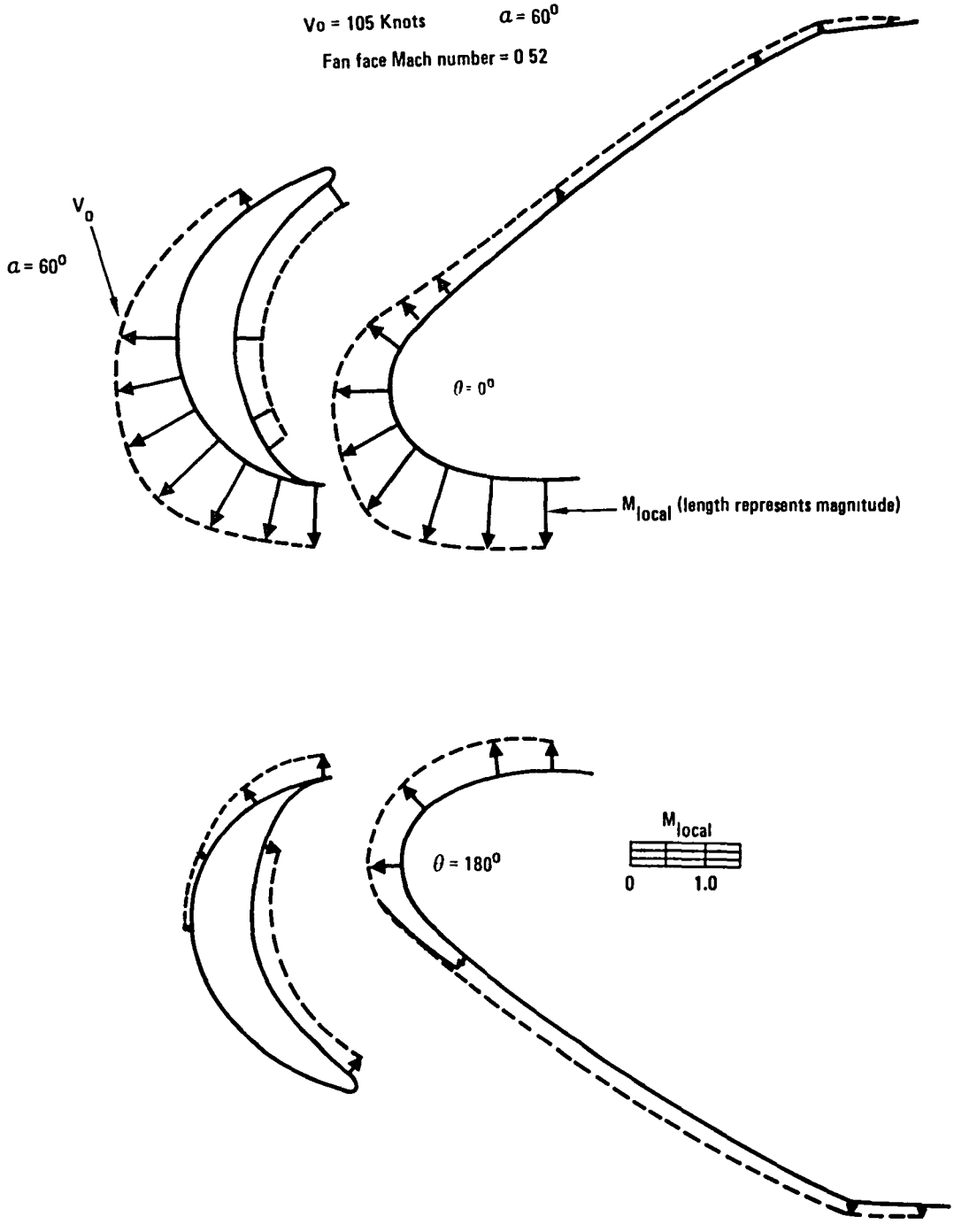

Figure 31. - Effect of model angle of attack on surface Mach number distribution, CR=1.2, 0.51 inch slot gap, no spacer.

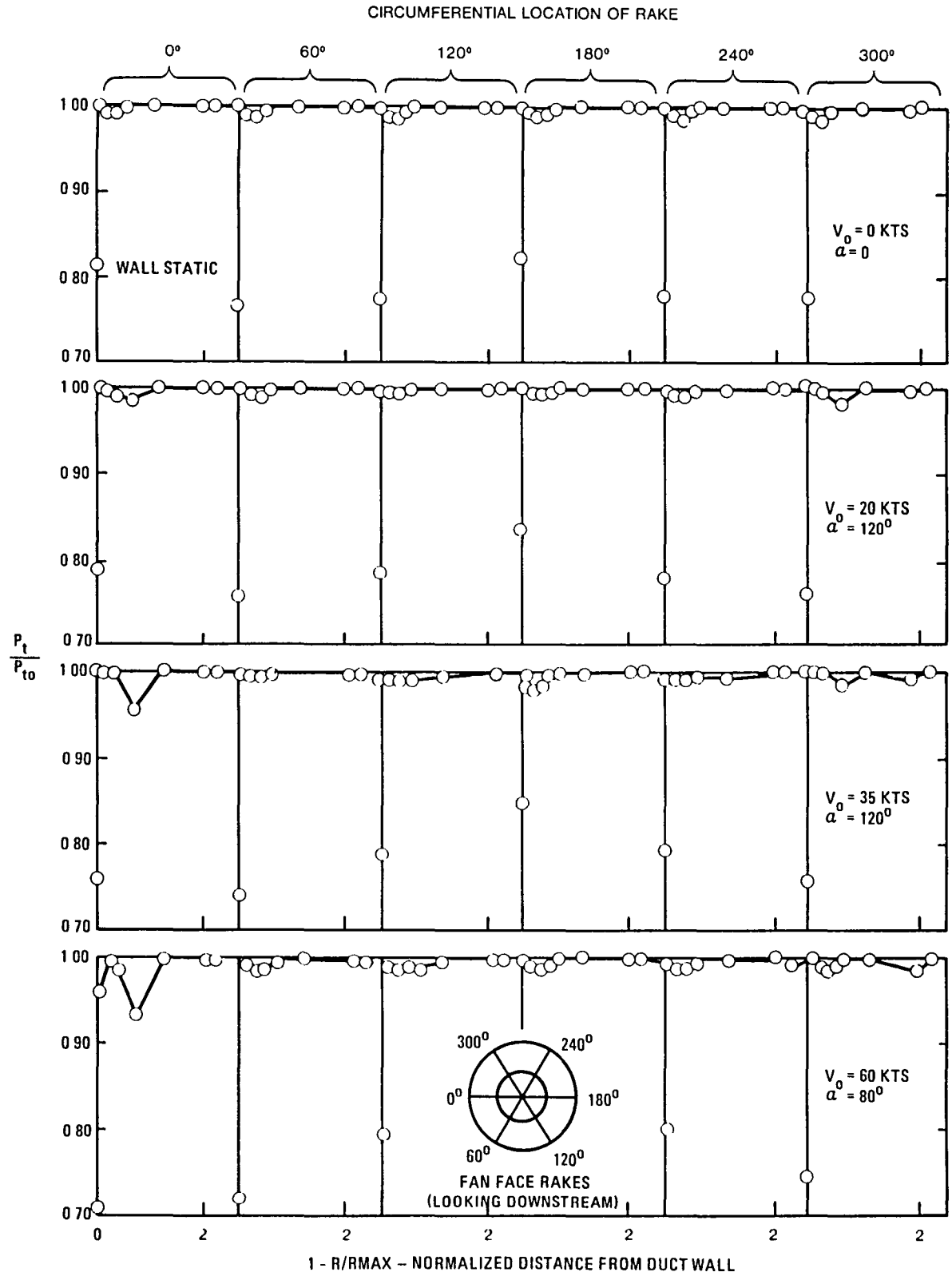

Figure 32. - Fan face total pressure profiles at maximum angles of attack tested, CR = 1.2, 0.51 inch slot gap, no spacer.

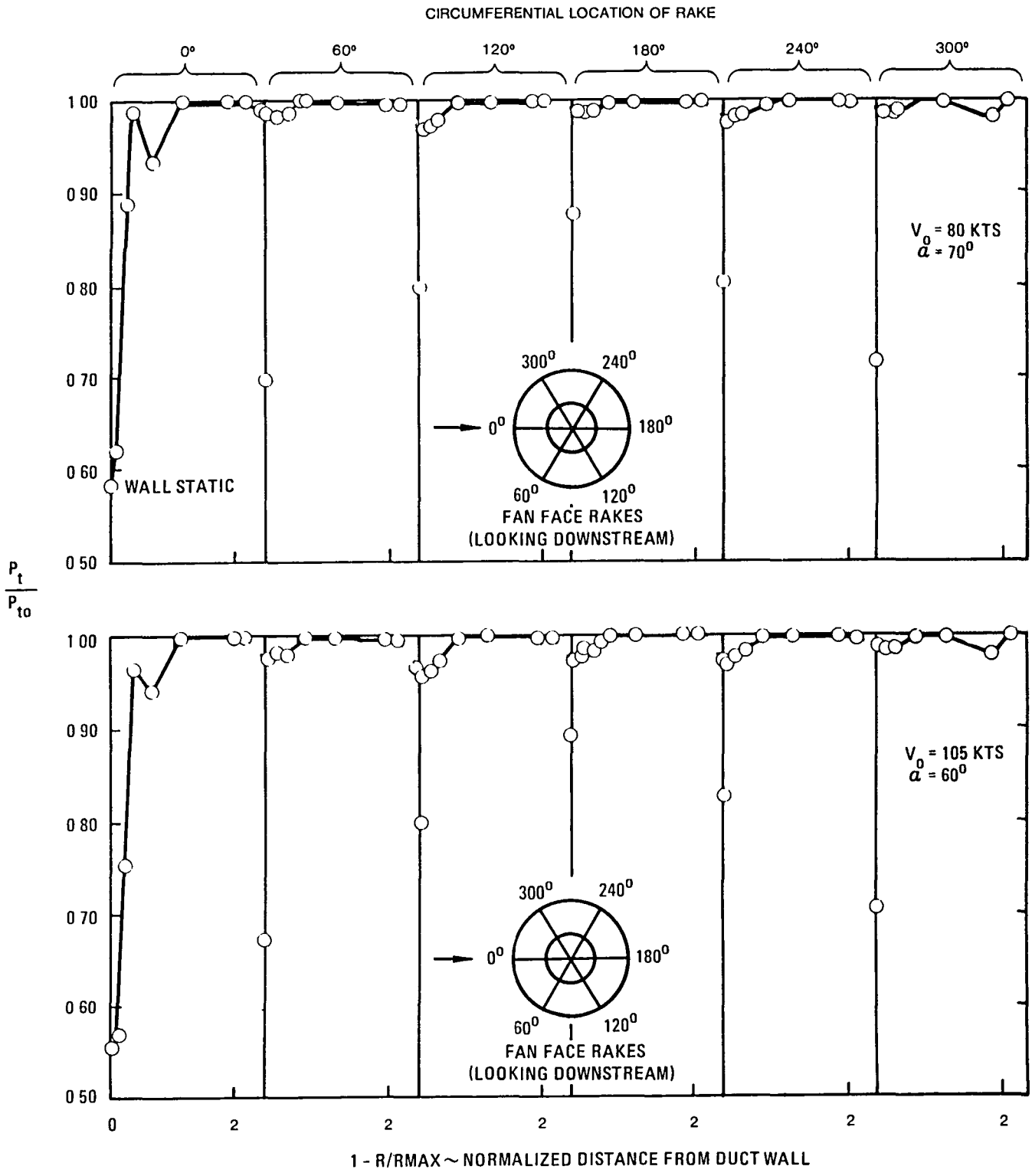

Figure 32. - Fan face total pressure profiles at maximum angles of attack tested, CR = 1.2, 0.51 inch slot gap, no spacer. (Concluded)

At 35 knots/120 degrees/angle of attack, for example, figure 32 shows that the flow on the cowl lip is attached; however, at this high angle the flow over the slat on the windward side experiences pressure losses as evidenced by the loss in recovery at $(1-R/R_{max})$ of 0.065. The surface static pressure distributions are presented in figure 33 for the same inlet and flow conditions as are presented in figure 32. The pressures measured at the last two taps at the trailing edge of the slat at V_o = 35 kts., figure 33(b), are becoming closer as the angle of attack increases. As these two pressures approach being equal, the boundary layer approaches incipient separation with a concomitant thickening of the boundary layer demonstrated in figure 32 at an $\alpha = 120^o$. At the higher tunnel speed of 105 knots and with a 60 degree angle of attack the flow separates from the cowl lip on the windward side, resulting in the total pressure profile of figure 32. This separation is also evidenced by the cowl static pressure distribution of figure 33e, whereby the cowl pressures decrease with increasing angle-of-attack until at 60 degrees a further reduction cannot be sustained and a noticeable change in slope of the adverse pressure gradient occurs. For reference, the slat/cowl circumferential surface static pressure distributions for this condition are presented in figure 34, and, as expected, these pressures become more positive with angular displacement from the critical zero degree windward location. Also, for reference, the slot flow total pressure recovery for high angle of atttack conditions is shown in figure 35.

Effect of Inlet Flow Velocity Distortion on Fan Performance

Flow distortion parameters have been developed by the various engine manufacturers and correlated to fan blade stress levels of particular engines; thereby allowing definition of an operating envelope for the inlet once the distortion levels have been defined. These parameters have generally been based on the total pressure distortion.

Because of the static pressure gradient existing, both radially and circumferentially, at the fan face during high angles of attack, a velocity distortion also exists; causing a change in relative blade angle of attack during rotation. This is illustrated by the typical inlet flow velocity distortion profiles shown in figure 36. Also shown for comparison are the profiles at zero degrees angle of attack. This velocity distortion results in a change in effective blade angle of attack, as shown in figure 37. This blade angle was calculated from the flow velocity (axial) and the blade velocity (tangential) at each probe location. It should be mentioned that crossflows are induced by the fan to attempt to obtain a constant flow through each blade passage and are not considered in the above calculation.

The effect of the velocity distortion on the fan performance, i.e. the total pressure ratio distribution, is shown in figure 38. Comparison of these profiles with the zero degree angle of attack profile shows that the velocity distortion carries through the fan to some extent. However, it is also interesting to note in figure 39 that the average fan total pressure is not affected by the distortion. This result appears consistent with the criteria of using a total pressure distortion parameter to specify engine operating limits, since the total pressure distortion was also very low.

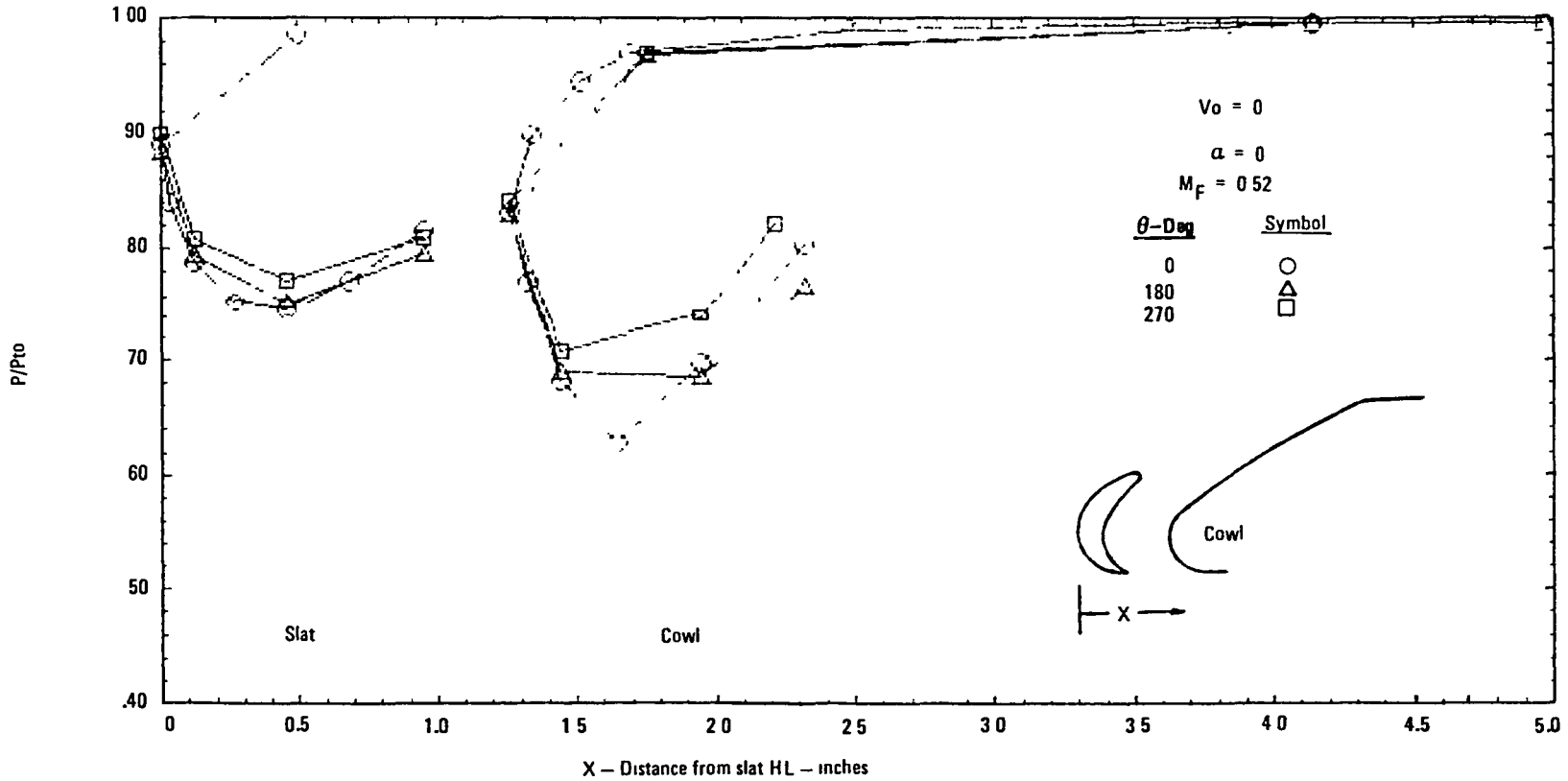

Figure 33(a). - Slot/cowl surface static pressure distribution, CR = 1.2, 0.51 inch slot gap, no spacer.

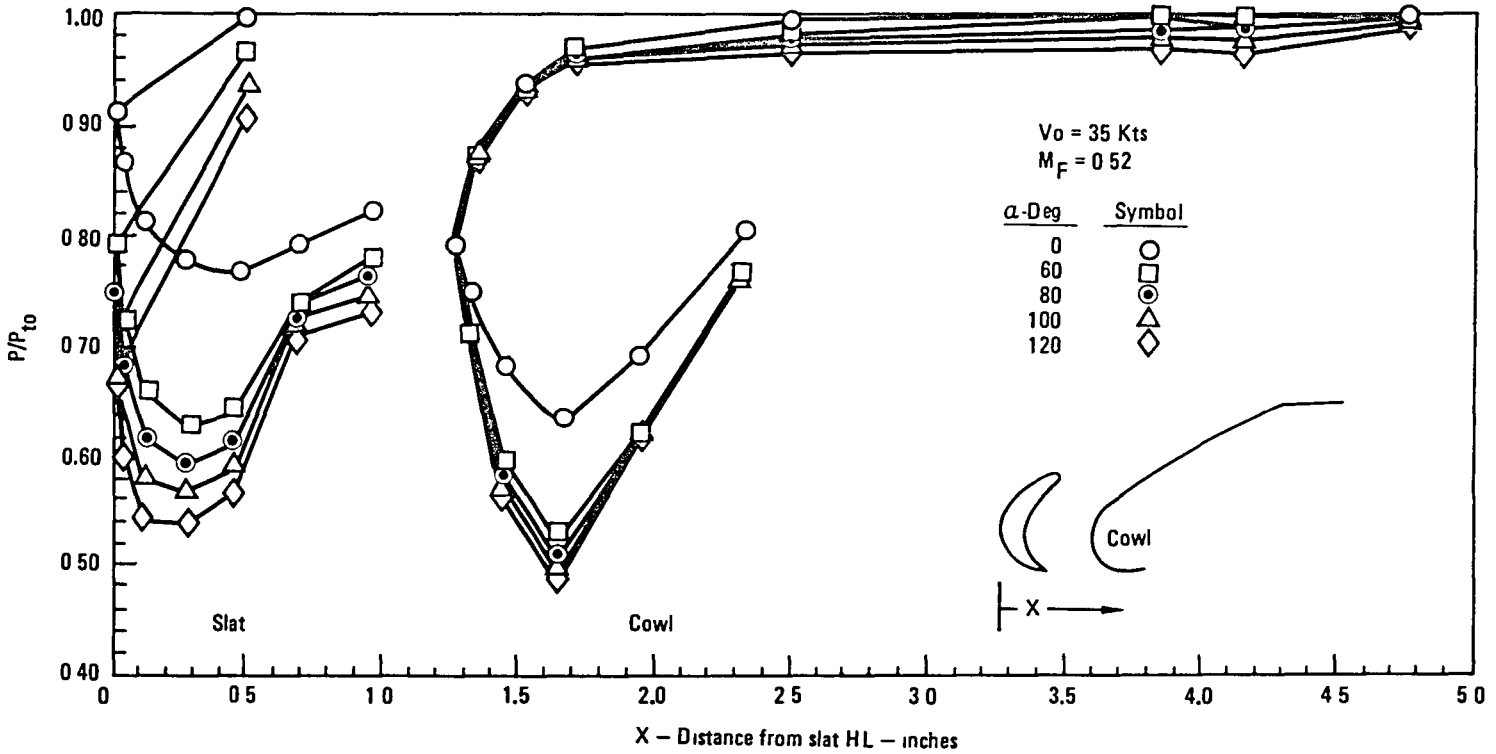

Figure 33(b). - Slat/cowl surface static pressure distribution, CR = 1.2, 0.51 inch slot gap, no spacer.

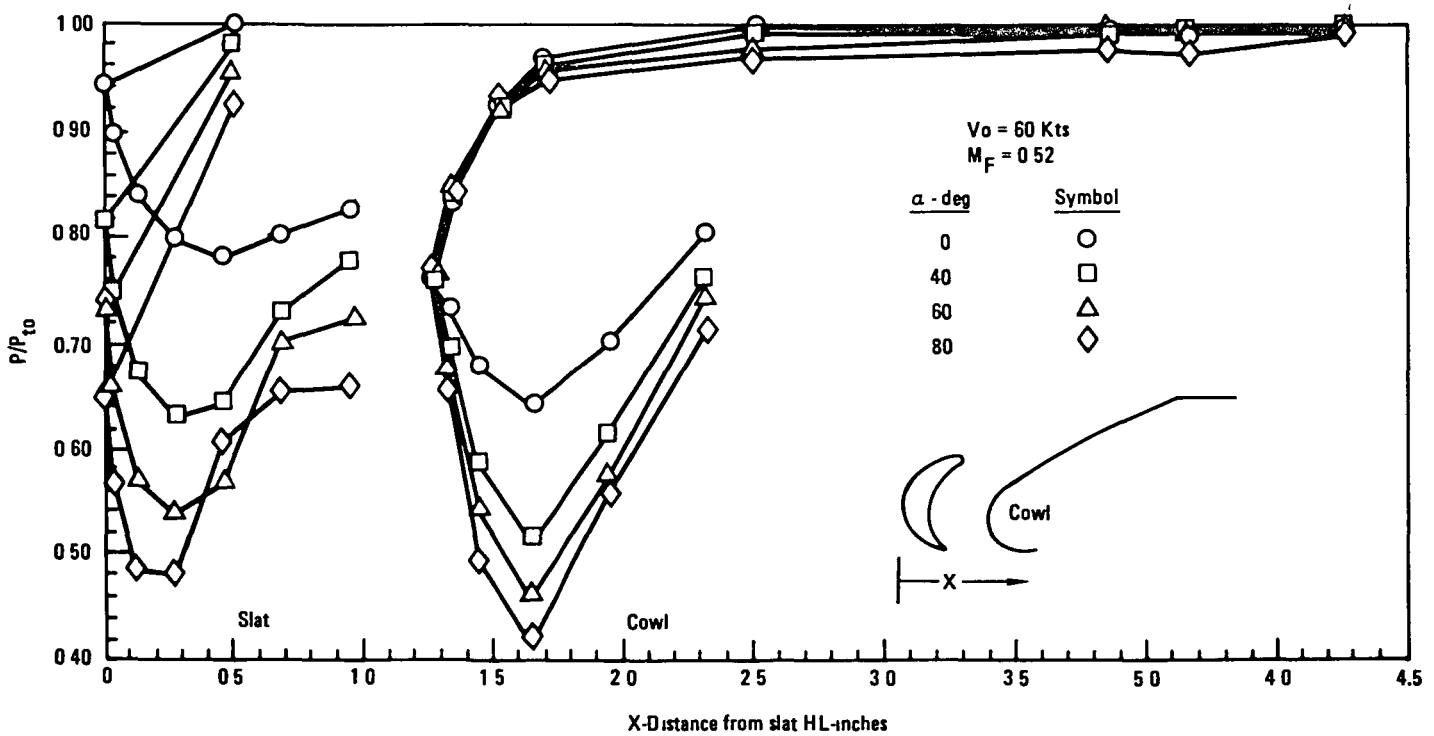

Figure 33(c). - Slat/cowl surface static pressure distribution, CR = 1.2, 0.51 inch slot gap, no spacer.

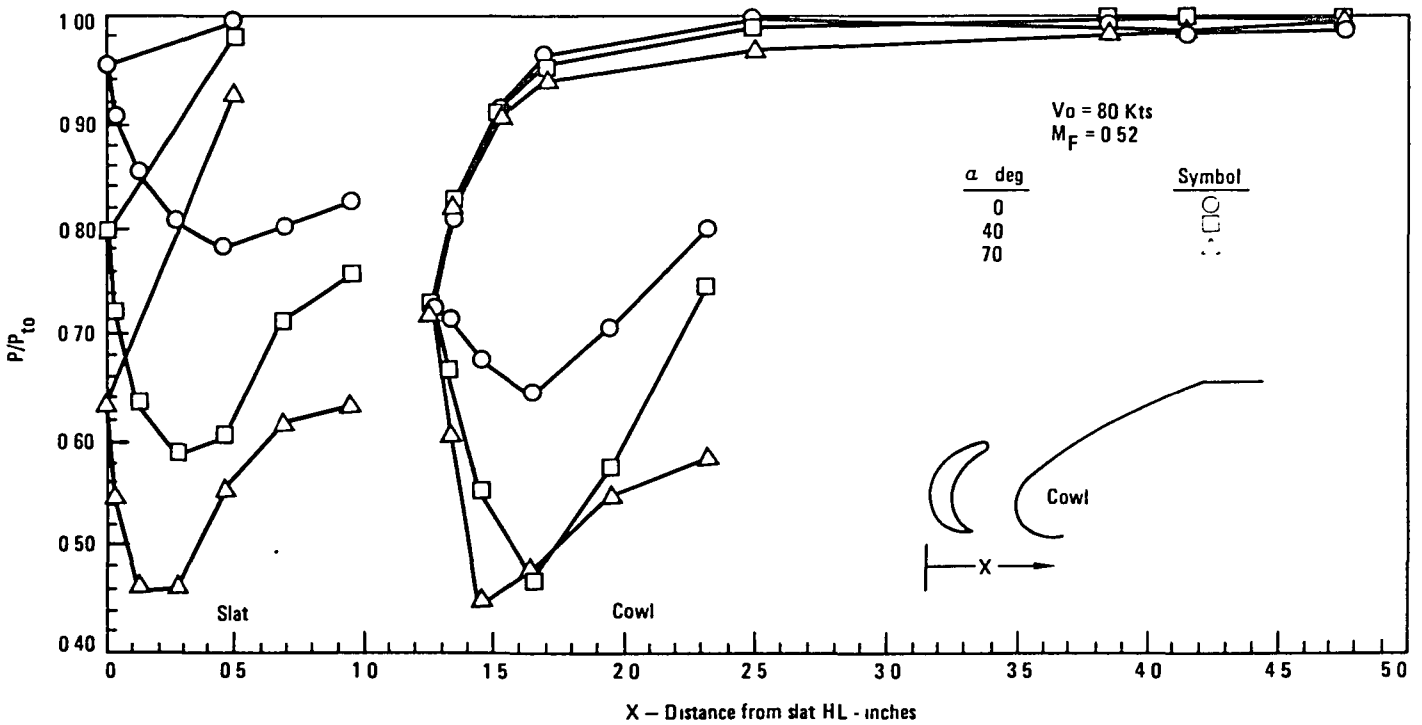

Figure 33(d). - Slat/cowl surface static pressure distribution, CR = 1.2, 0.51 inch slot gap, no spacer.

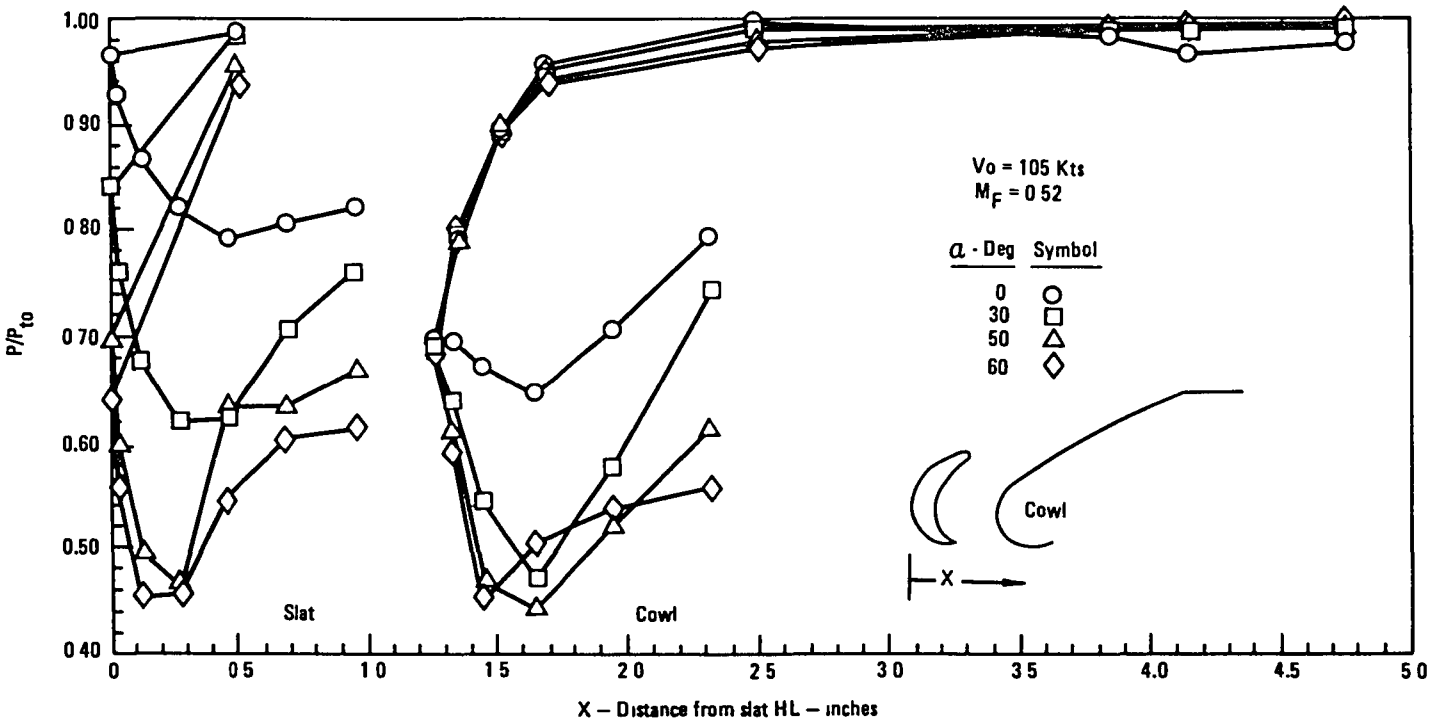

Figure 33(e). - Slat/cowl surface static pressure distribution, CR = 1.2, 0.51 inch slot gap, no spacer.

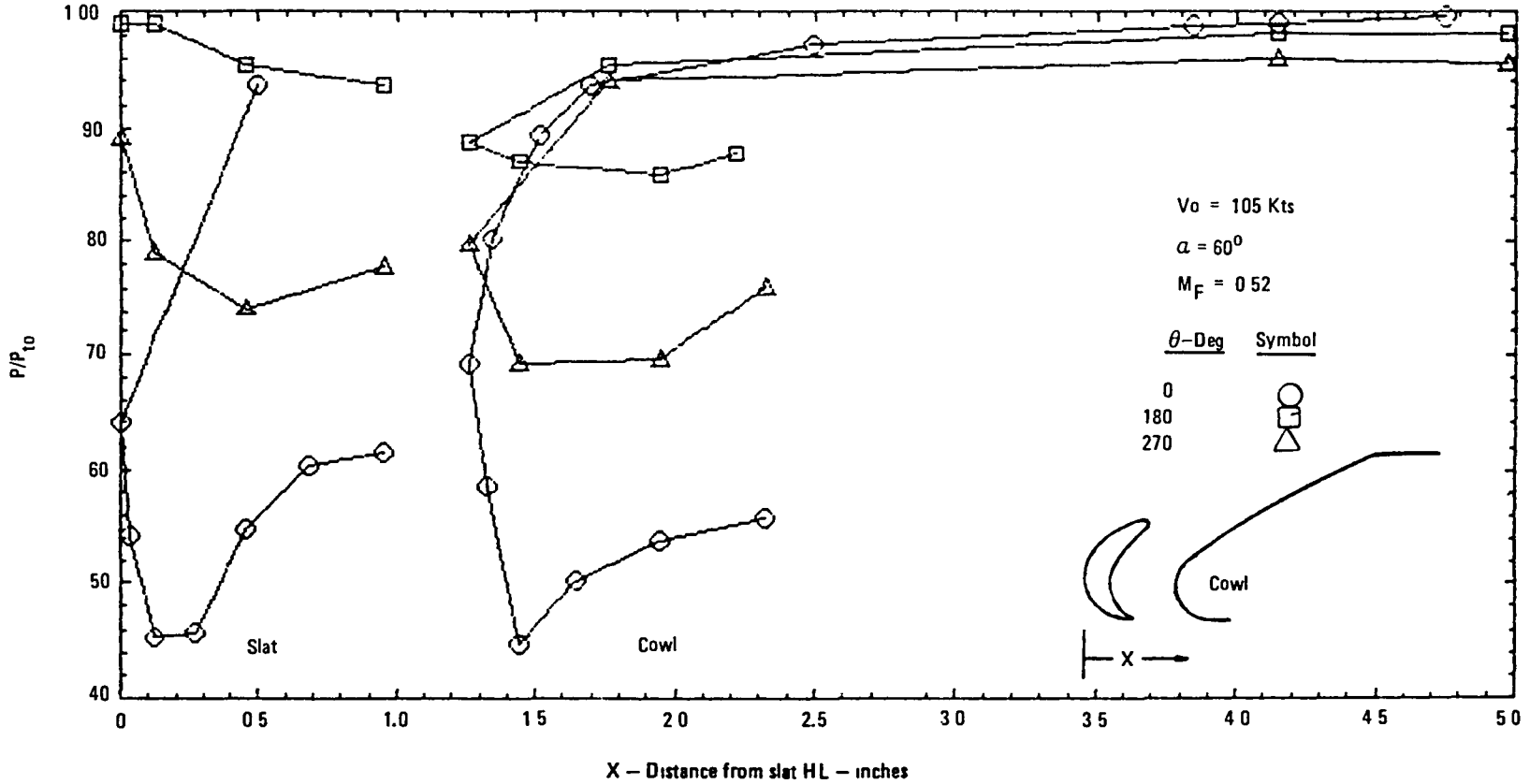

Figure 34. - Slat/cowl circumferential static pressure distribution, max angle of attack 105 kts., CR=1.2, 0.51 inch slot gap, no spacer

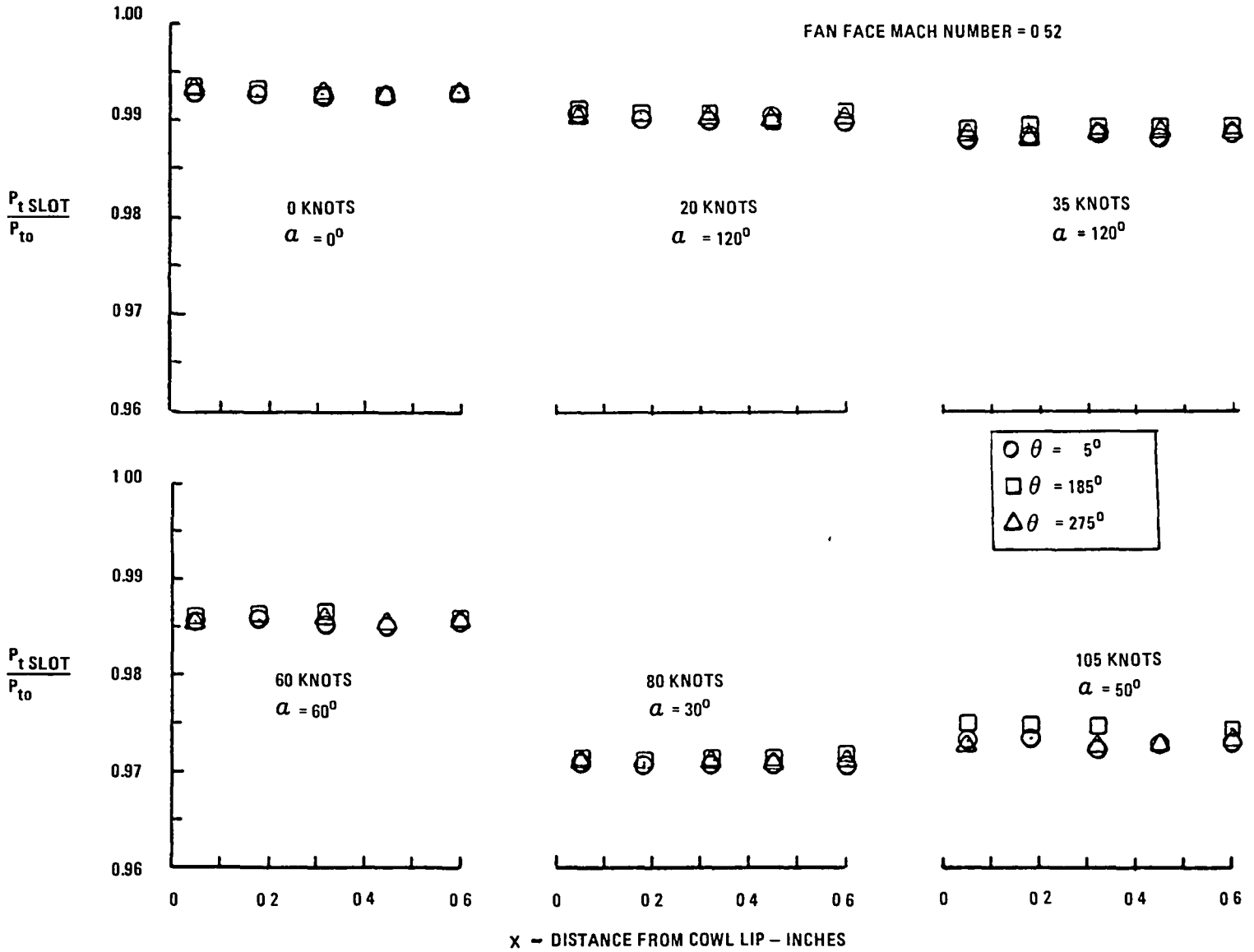

Figure 35. - Slot flow total pressure recovery, CR=1.2, 0.51 inch slot gap, no spacer.

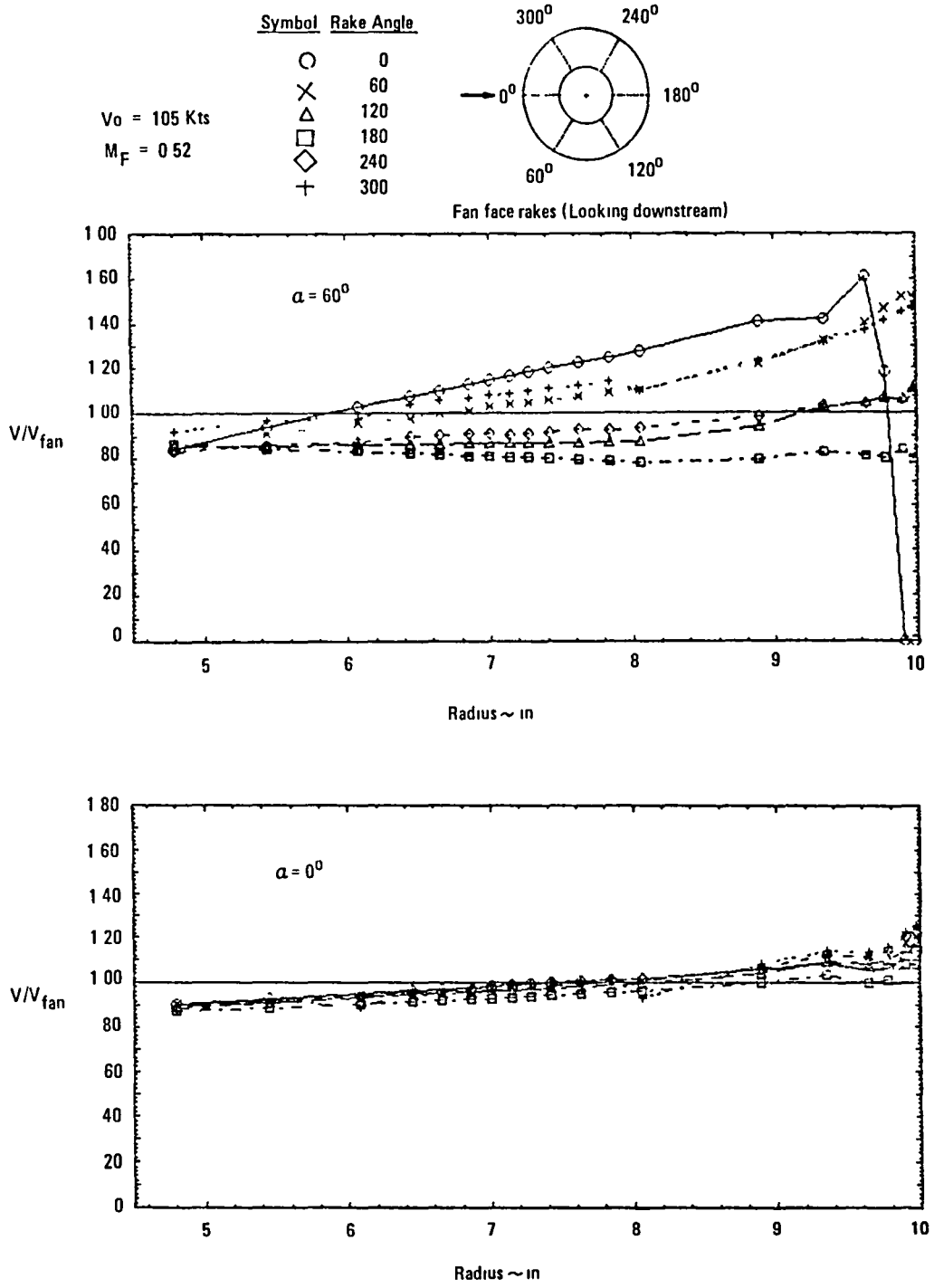

Figure 36. - Effect of angle of attack on fan face velocity distortion radial and circumferential, CR=1.2, 0.51 inch slot gap, no spacer.

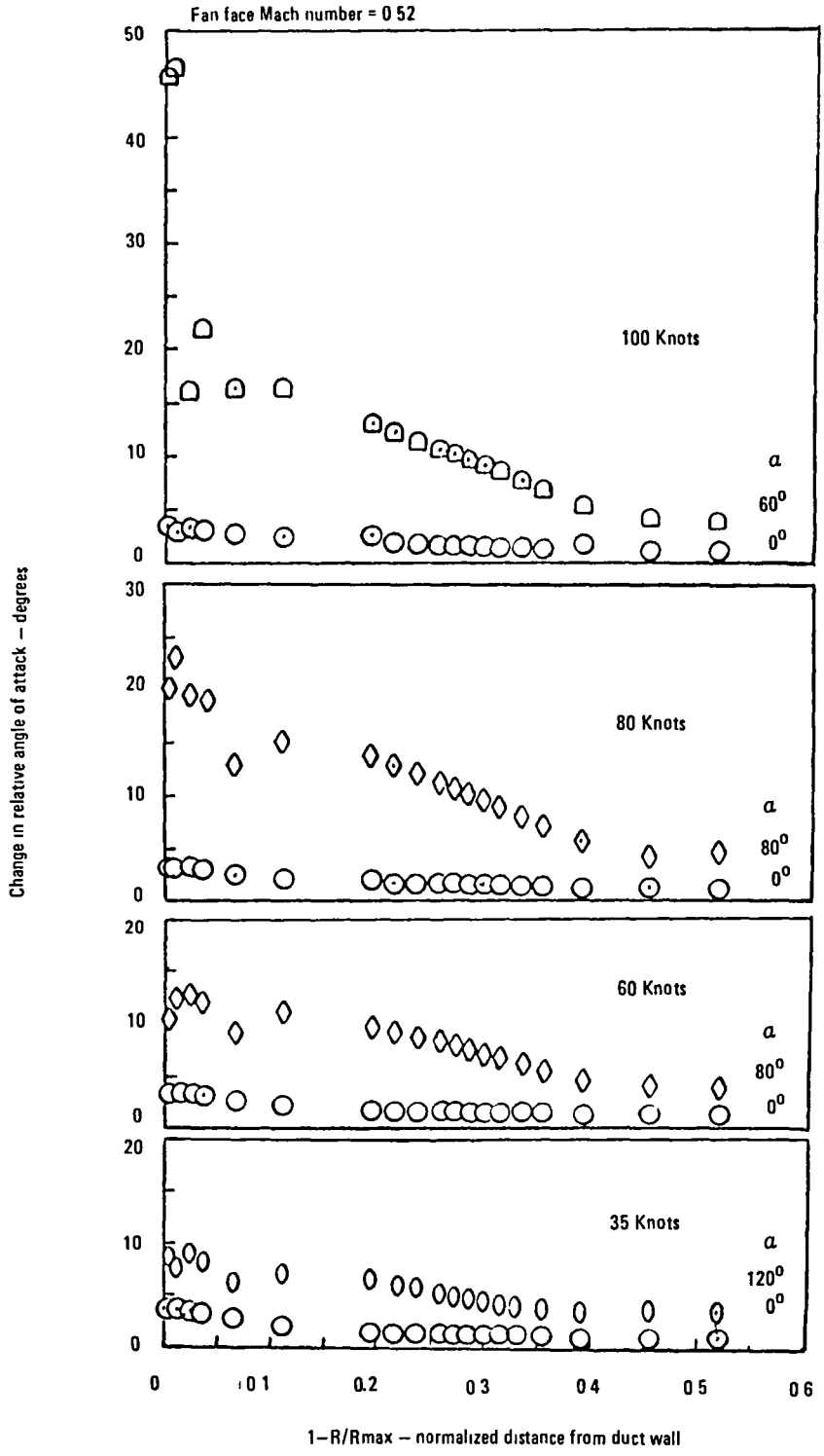

Figure 37. - Change in fan blade relative angle of attack during 1 revolution, CR=1.2, 0.51 inch slot gap, no spacer.

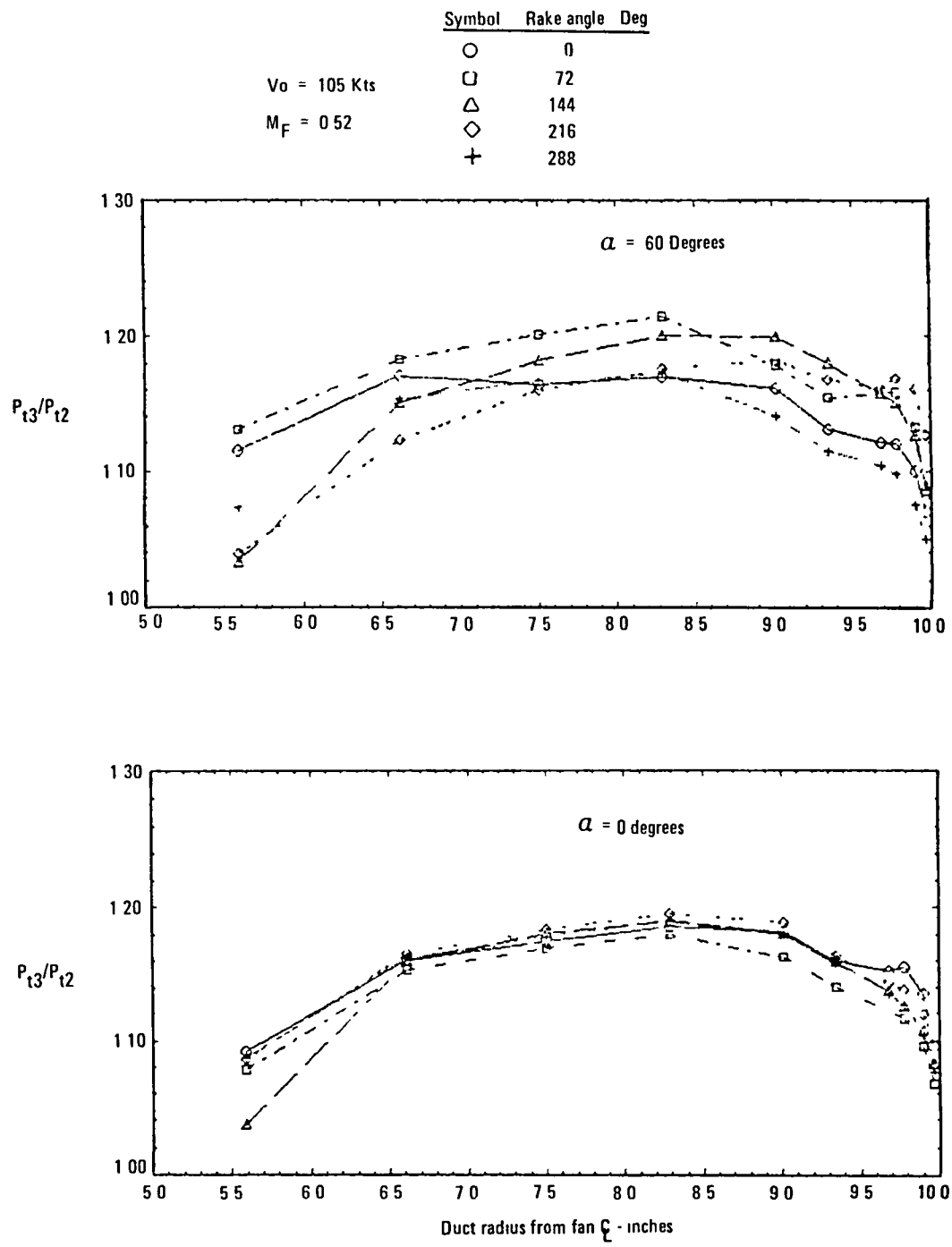

Figure 38. - Effect of inlet flow velocity distortion on fan exit total pressure distribution, CR=1.2, 0.51 inch slot gap, no spacer.

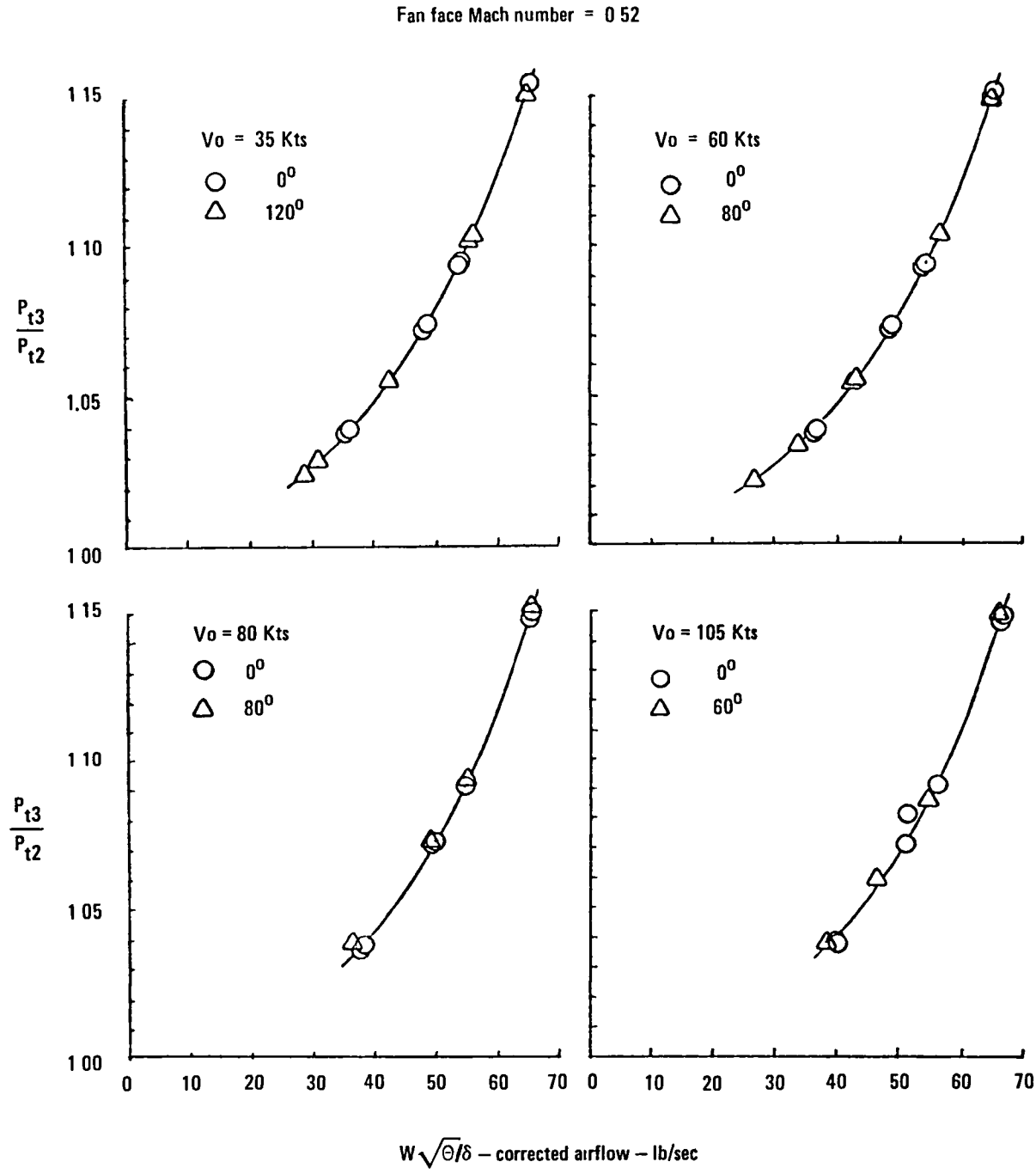

Figure 39. - Effect of model angle of attack on fan pressure ratio, CR=1.2, 0.51 inch slot gap, no spacer.

Effect of Slat Contraction Ratio

The alternate slat configuration tested had a lip contraction ratio of 1.3, resulting in a larger turning radius for the internal flow at the expense of increased external highlight to maximum diameter ratio (for the same maximum area). The measured recoveries for this configuration are shown in figure 40 as a function of inlet airflow ratio and are summarized relative to the estimated V/STOL operating envelope in figure 41 for maximum airflows tested.

Comparing these data with those obtained with the 1.2 contraction ratio slat (figure 42) verifies the expected result of improved total pressure recovery with increased contraction ratio. At forward speeds less than 60 knots, where separation is not evident for either contraction ratio, this improvement is minimal. At the higher speeds, however, higher angles of attack were attained with the 1.3 contraction ratio slat before the onset of flow separation. Conversely, at the same tunnel speed/angle of attack condition a higher recovery was measured. The flow separation envelopes for these configurations are discussed later.

Figure 43 compares the zero degree rake total pressure profiles for the two contraction ratio slats at identical operating conditions. The 1.3 contraction ratio slat results in a higher measured total pressure at a distance from the duct wall of $1-R/R_{MAX} = 0.07$, where the profile reflects the flow conditions over the slat. Also, at a forward speed of 105 knots the total pressures adjacent to the duct wall are higher for the larger contraction ratio slat, indicating a less pronounced separation over the cowl lip compared to that with the smaller contraction ratio slat. This results from the influence of the flow from the slat trailing edge on the flow through the slot. As the flow from the slat trailing edge becomes less axially-directed, through separation effects, the pressure gradient acting to help turn the slot flow aft is reduced and local flow separation on the cowl lip increases. The typical effect of the slat larger turning radius on the surface static pressure distributions is shown in figure 44. For the 1.3 contraction ratio slat, the minimum pressure occurs at the highlight; resulting from the sharper surface curvature employed external to the highlight to maintain the same maximum diameter of the inlet model.

Effect of Slot Gap Width

The model hardware was designed such that the slat could be moved fore and aft to investigate the effect of the slot-gap width on performance. For no gap, as simulated with the 360 degree slot filler blocks, the entire inlet/fan airflow is accommodated by the slat lip. As the slat is moved forward, allowing a portion of the fan flow to pass through the slot, the flow over the slat becomes less susceptible to flow separation since the pressure loading on the slat is reduced. However the flow over the cowl lip becomes more susceptible to flow separation since it becomes more heavily loaded.

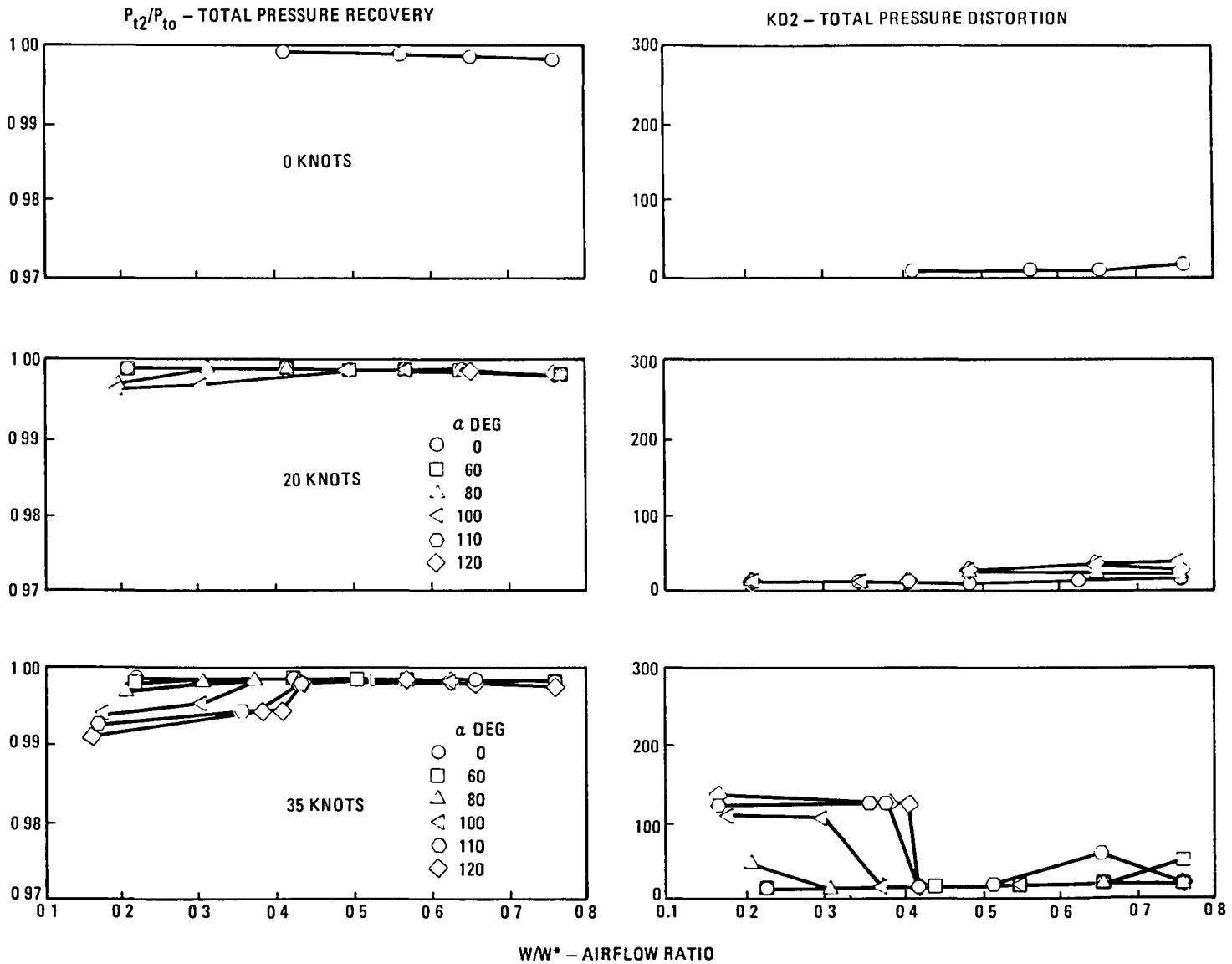

Figure 40. - Inlet total pressure recovery and flow distortion, CR-1.3, 0.51 inch slot gap, no spacer.

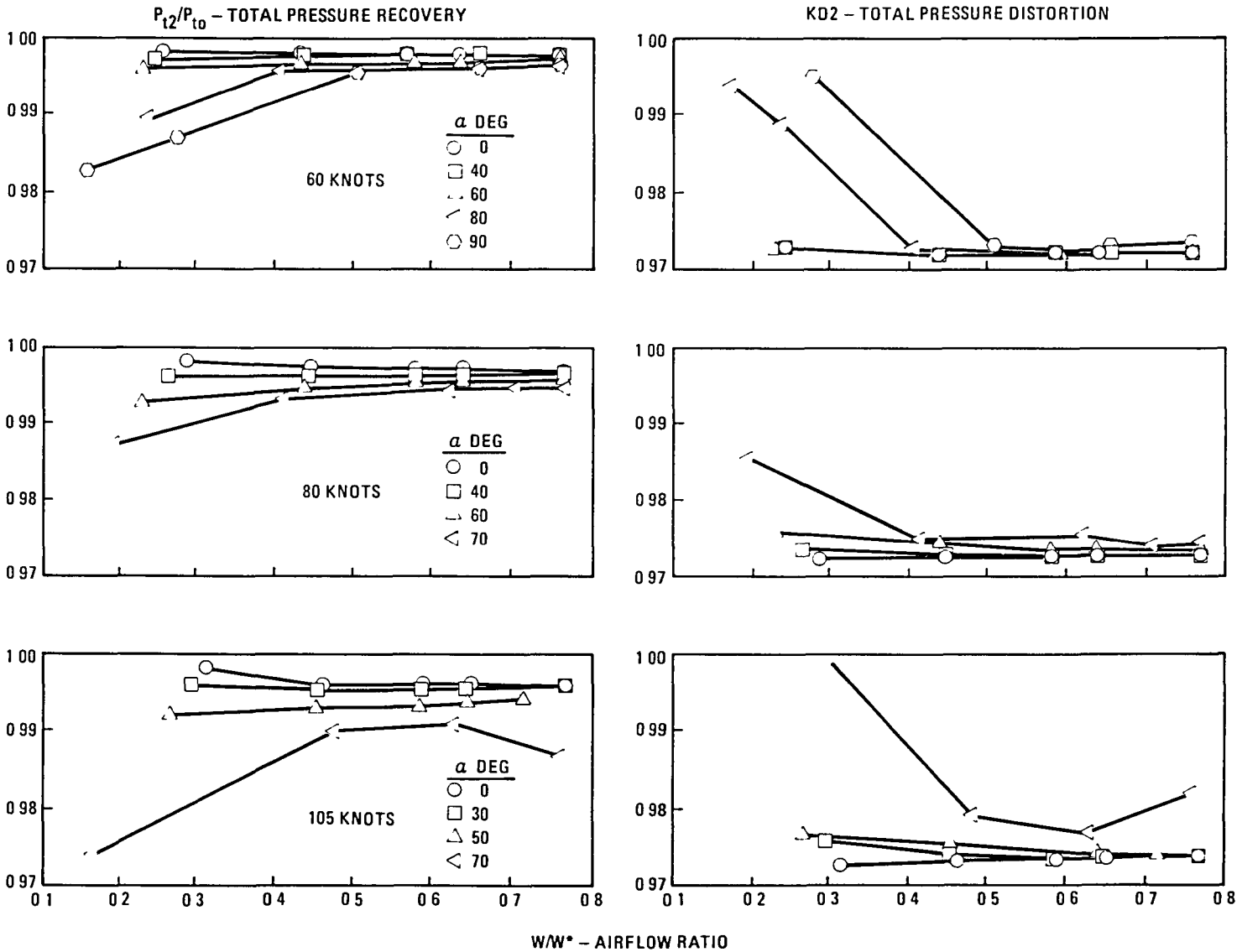

Figure 40. - Inlet total pressure recovery and flow distortion, CR-1.3, 0.51 inch slot gap, no spacer. (Concluded.)

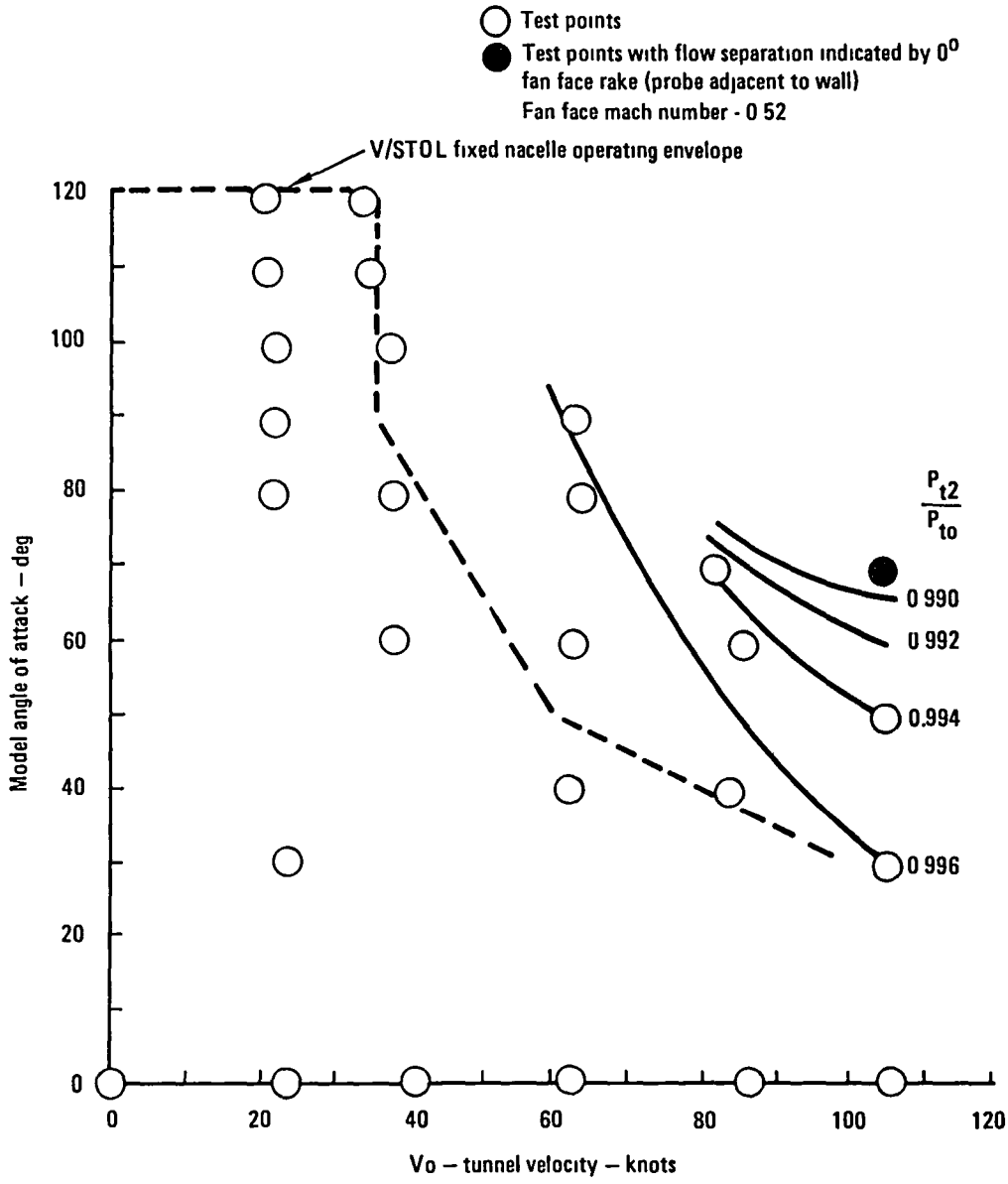

Figure 41. - Total pressure recovery summary over inlet operating envelope, CR=1.3, 0.51 inch slot gap, no spacer.

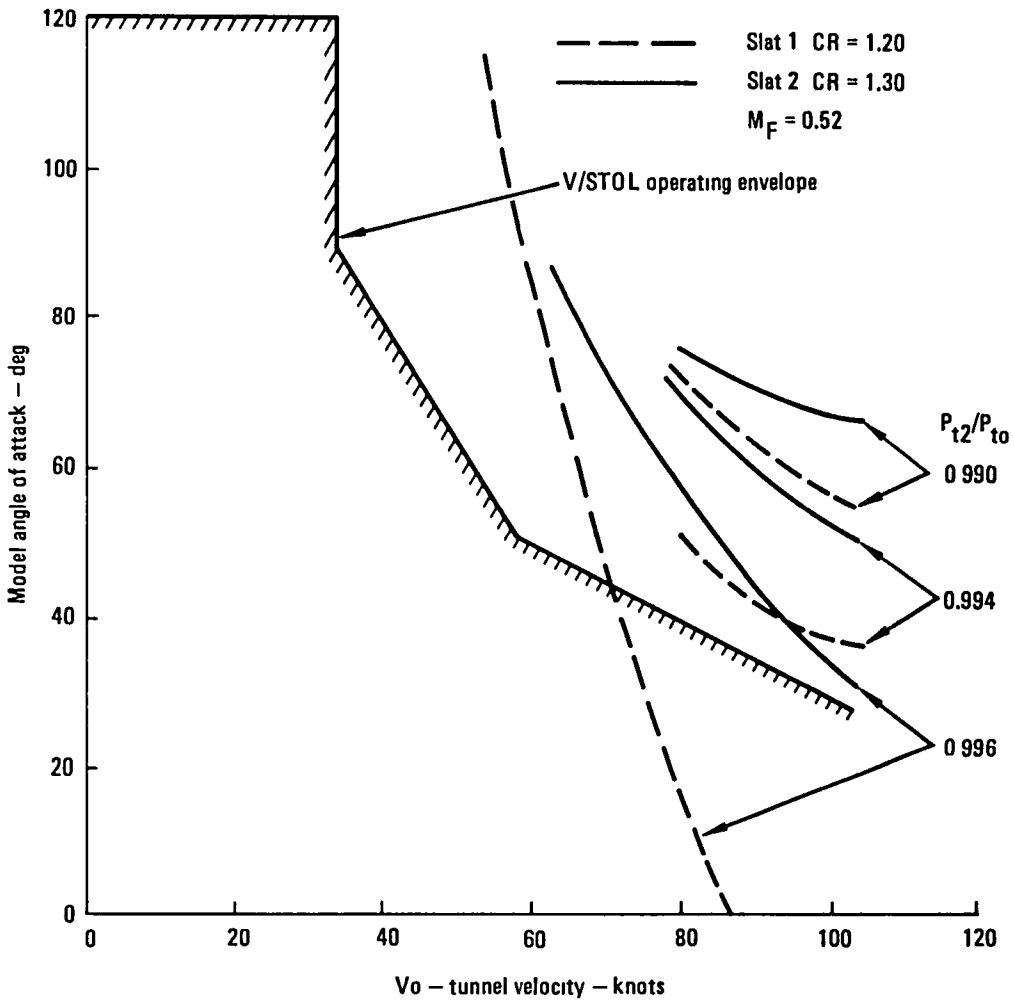

Figure 42. - Effect of slat contraction ratio on total pressure recovery over the inlet operating envelope.

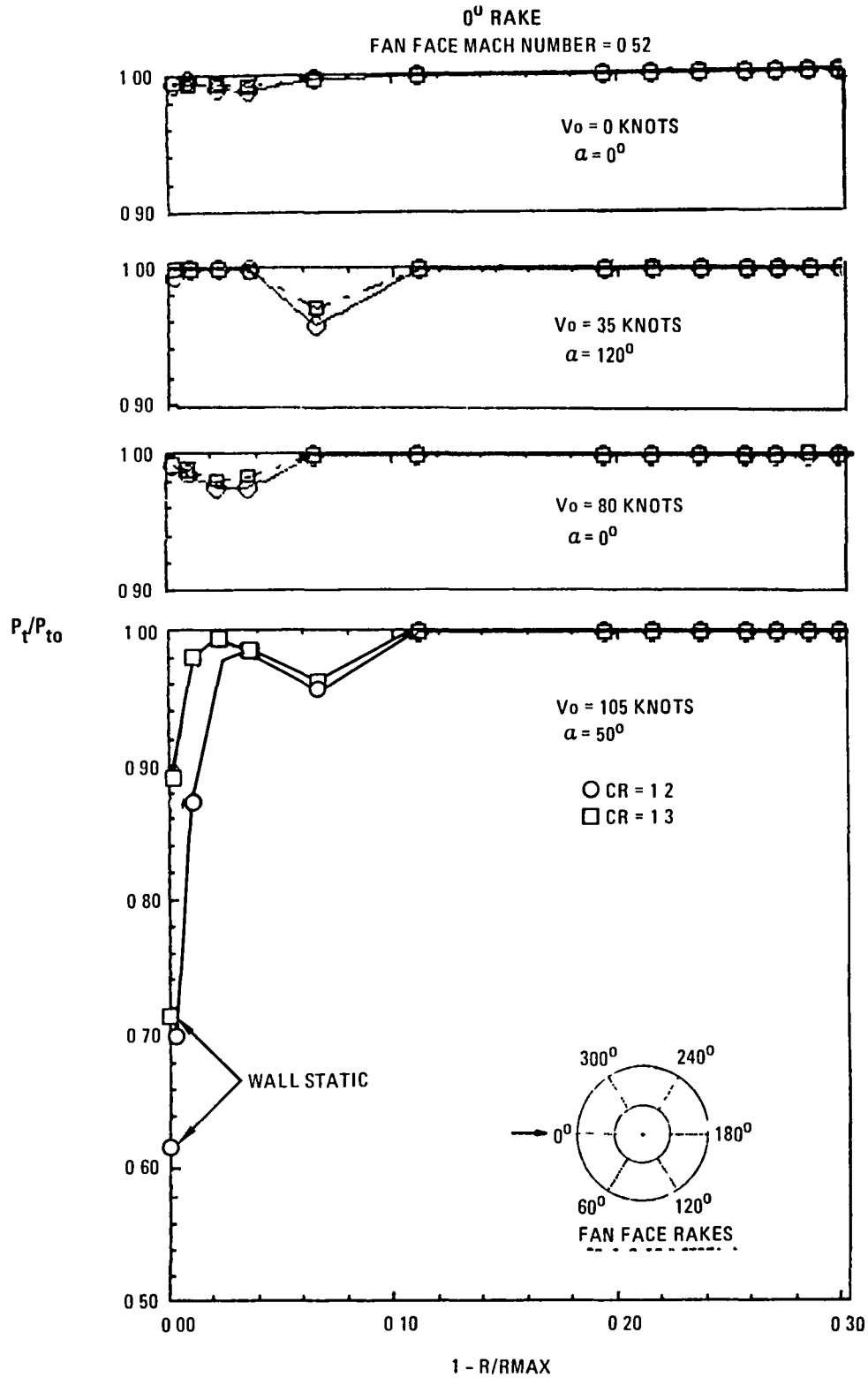

Figure 43. - Comparison of fan face total pressure profile for two contraction ratios, 0.51 inch slot gap, no spacer.

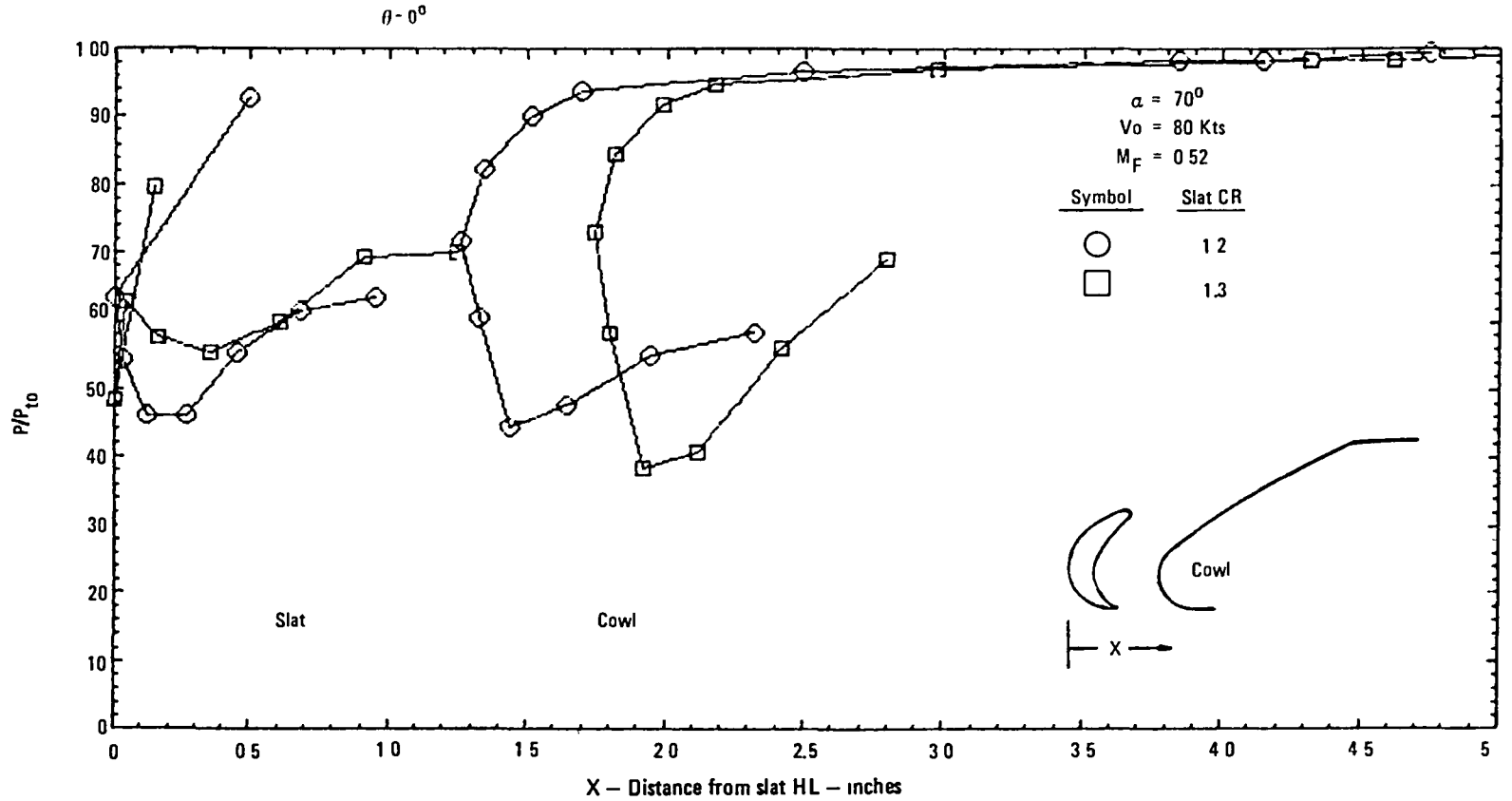

Figure 44. - Effect of slat contraction ratio on slat/cowl surface static pressure distribution.

The effect of slot gap width on total pressure recovery is presented in figure 45 for the 1.2 contraction ratio slat and for each of the tunnel speeds tested. Considering the V/STOL operating envelope, the slot provides the most benefit at the 35 knot/120 degree angle of attack condition; with an optimum slot width at approximately 0.36 inches. As can be noted, the slot improves the total pressure recovery by almost 2 percent over the no-slot configuration. If the angle-of-attack requirement was to increase at the high speeds, this benefit would be more significant because of flow separation effects.

At the higher forward speeds (greater than 60 knots) figure 45 shows that the higher fan face total pressure recovery occurs with a slot gap width of approximately 0.36. The degradation in recovery with increasingly greater gap distances is also verified by the data in figure 46, for which the 4 inch throat/fan spacer was installed, and also for the 1.3 contraction ratio slat in figure 47.

Based on the criteria that flow separation occurs at a fixed value of peak surface velocity or Mach number, the most optimum slot gap width exists where both the slat and cowl lips are equally loaded, i.e., the peak pressures are the same. Figure 48 compares these pressures at the static condition for a variation in gap width with the 4 inch throat/fan spacer installed. It is clearly seen that as the gap width is increased the pressure loading decreases on the slat and increases on the cowl; with equal loading occurring at a gap width of 0.25 inches. At this condition the loading is relatively low, however, resulting in maximum surface Mach numbers of 0.72. Similar data are presented for the high speed/high angle of attack condition in figure 49, along with the zero degree rake total pressure profiles. At increasing gap widths the slat pressure loading is reduced, however unlike the data for the static condition in figure 48 flow separation eventually occurs on the cowl as evidenced by both the total pressure profile and the absence of increasingly lower minimum peak pressures on the surface. Similar data are presented in figures 50 and 51 for each contraction ratio slat with no throat/fan spacer installed. Also shown in figure 52 is the slot flow total pressure recovery for these configurations.

Effect of Fan Throat Spacer

Provisions were made to displace the inlet throat forward of the fan face by installation of 2 and 4 inch length constant area spacers. The effect of these spacers is to reduce the favorable "pumping action" (or upstream influence) of the fan and the effect of the spinner on the lip static pressure distribution, particularly with regard to keeping the flow attached. Also, the spacers provide a duct section forward of the fan face that allows reattachment of locally separated lip flow. These effects can be discerned from the fan face total pressure recovery plots in figures 53 and 54 which show the recovery with and without the spacers installed as a function of fan face Mach number for various operating conditions.

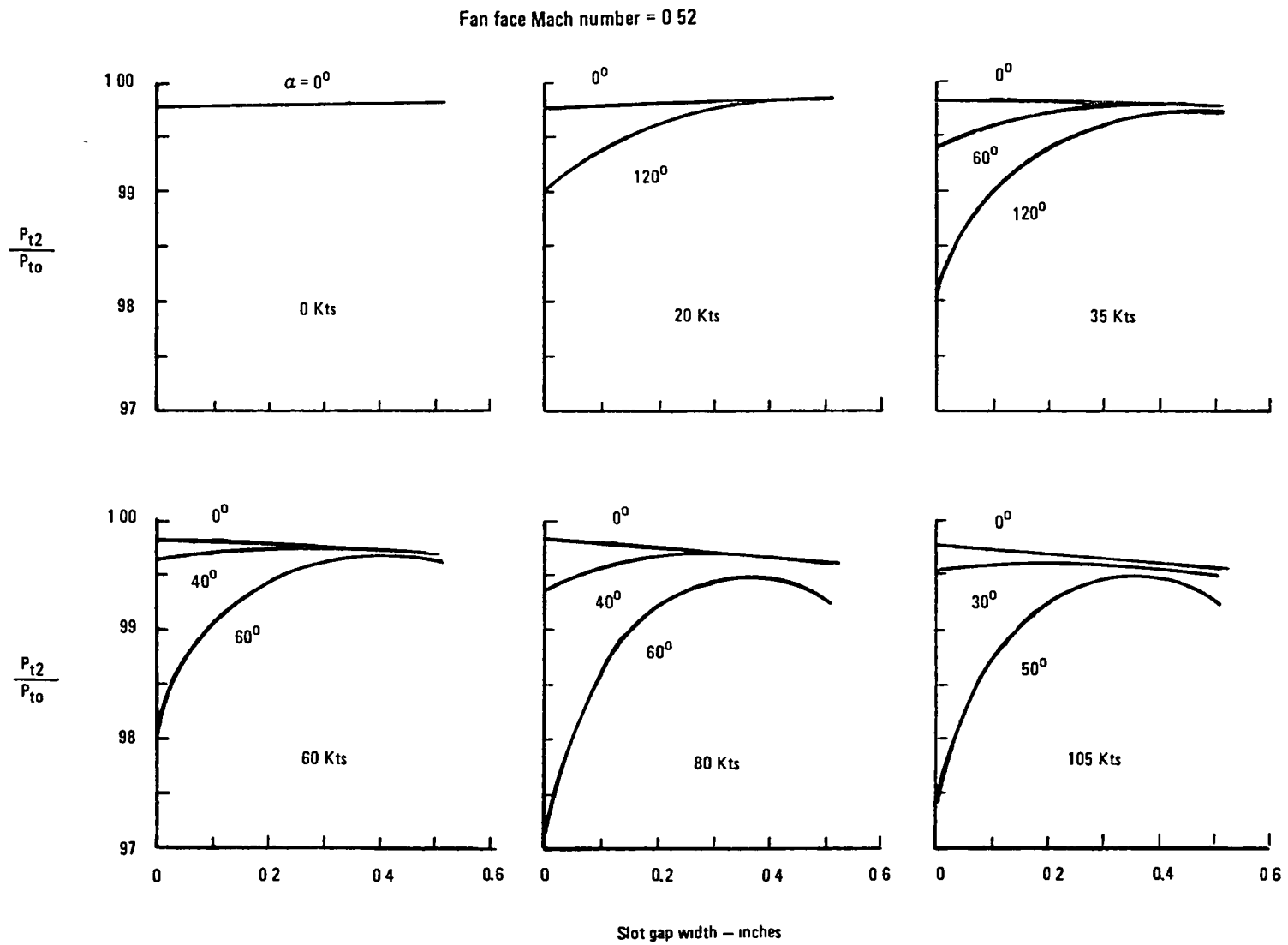

Figure 45. - Effect of slot gap width on total pressure recovery, CR=1.2, no spacer.

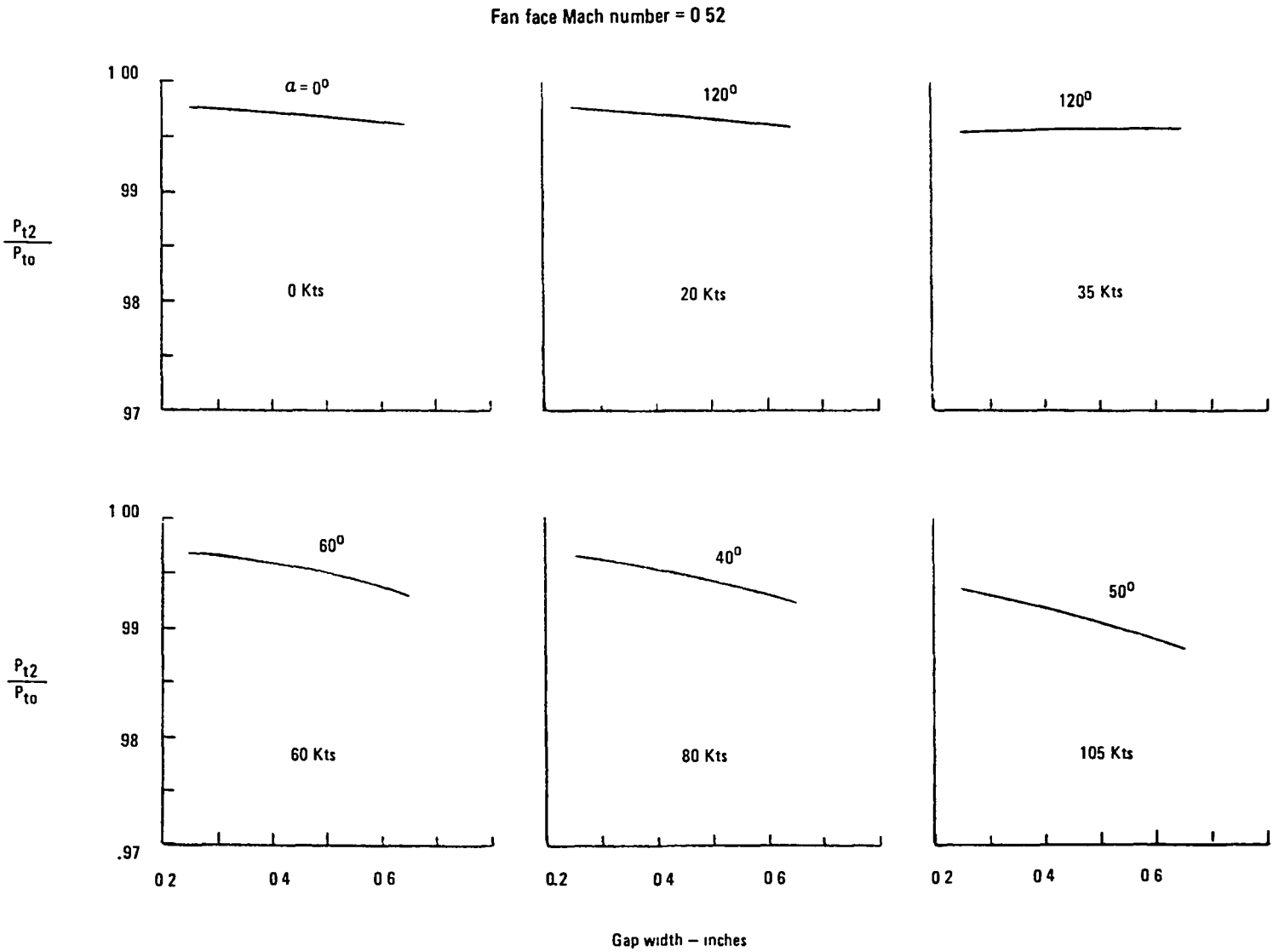

Figure 46. - Effect of slot gap width on total pressure recovery, CR=1.2, 4-inch spacer.

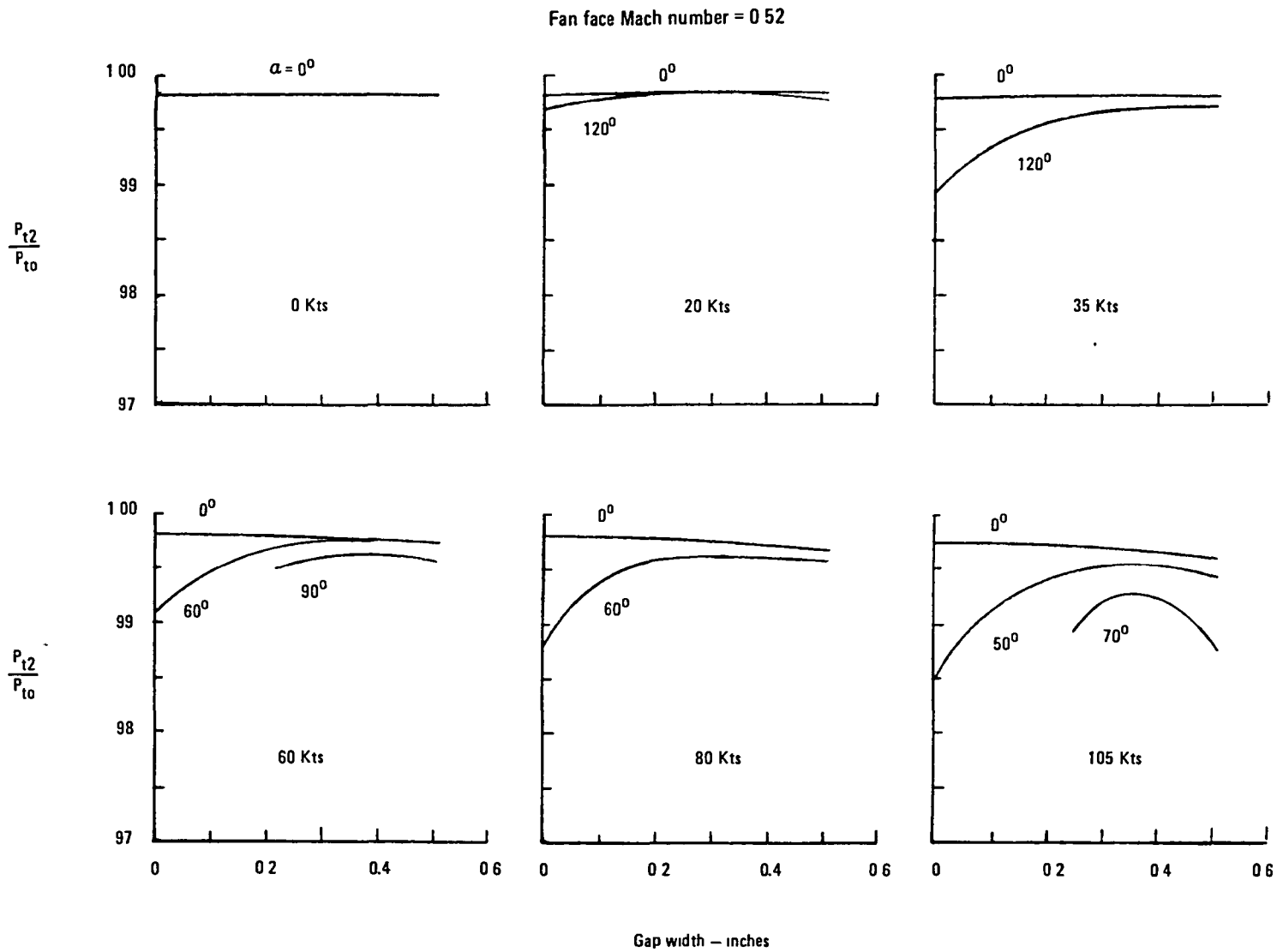

Figure 47. - Effect of slot gap width on total pressure recovery, CR=1.3, no spacer.

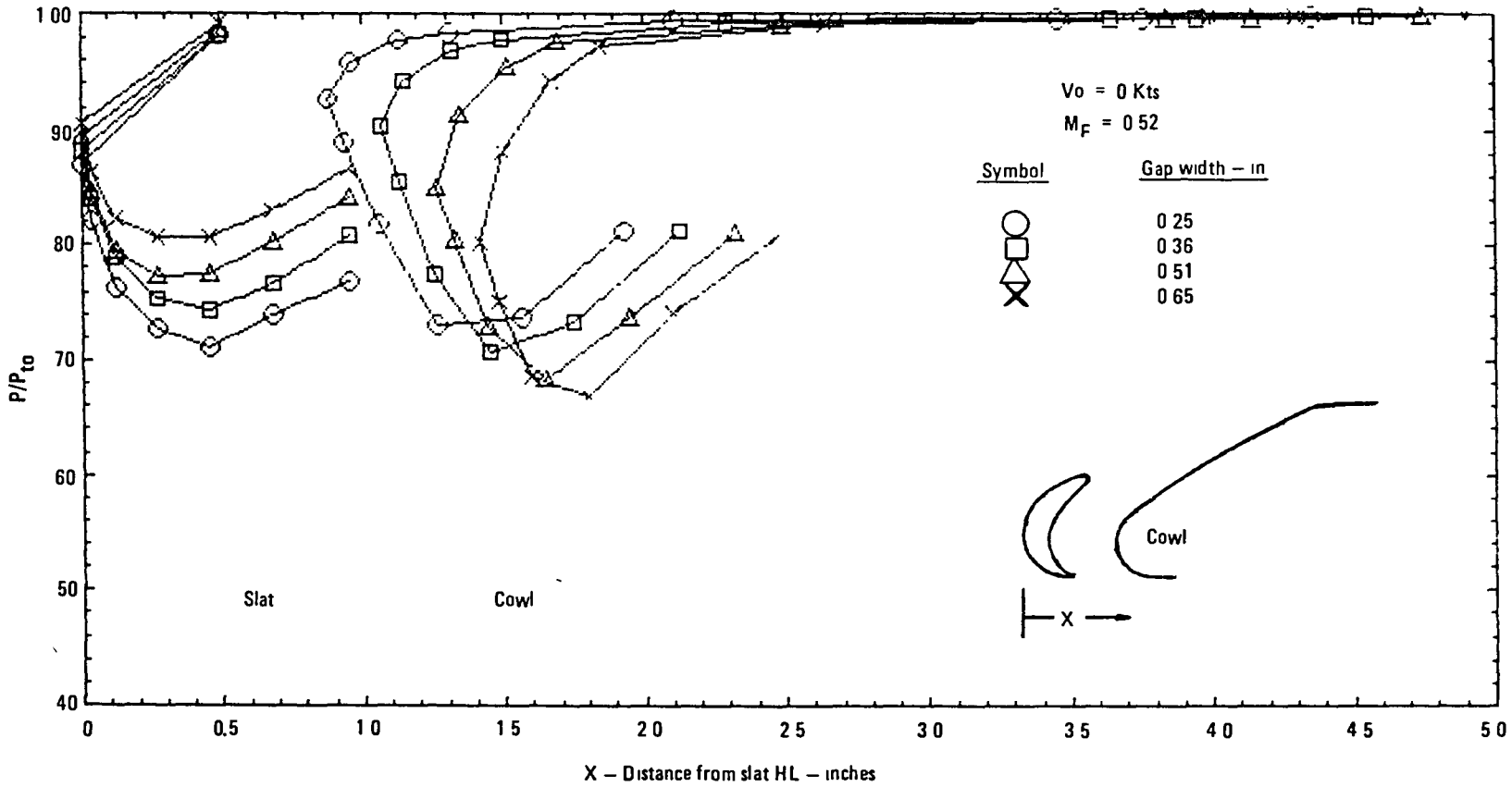

Figure 48. - Effect of slot gap width on fan face total pressure profile and slat/cowl surface static pressures, CR=1.2, 4-inch spacer, static conditions.

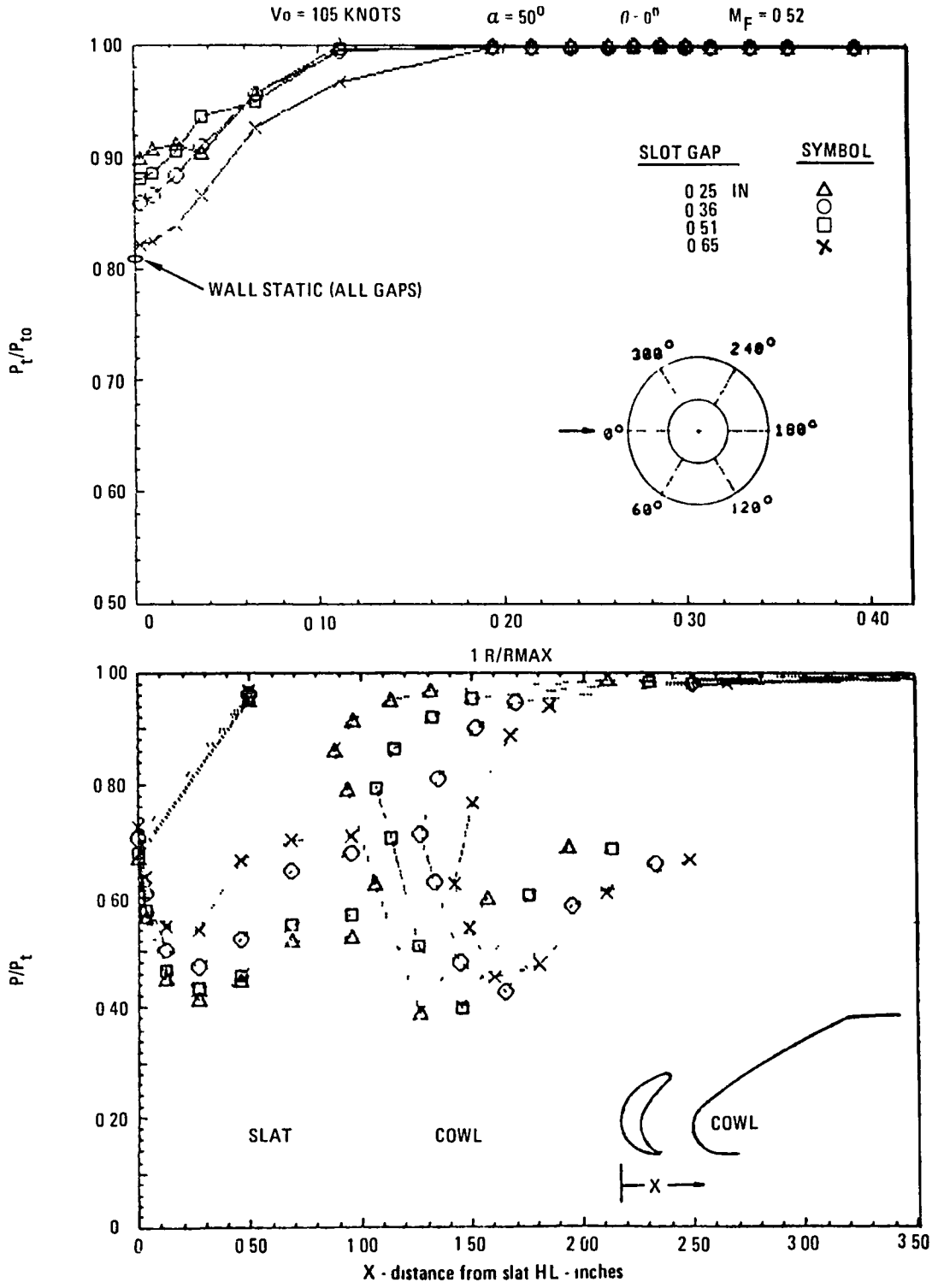

Figure 49. - Effect of slot gap width on fan face total pressure profile and slat/cowl surface static pressures, CR=1.2, 4-inch spacer.

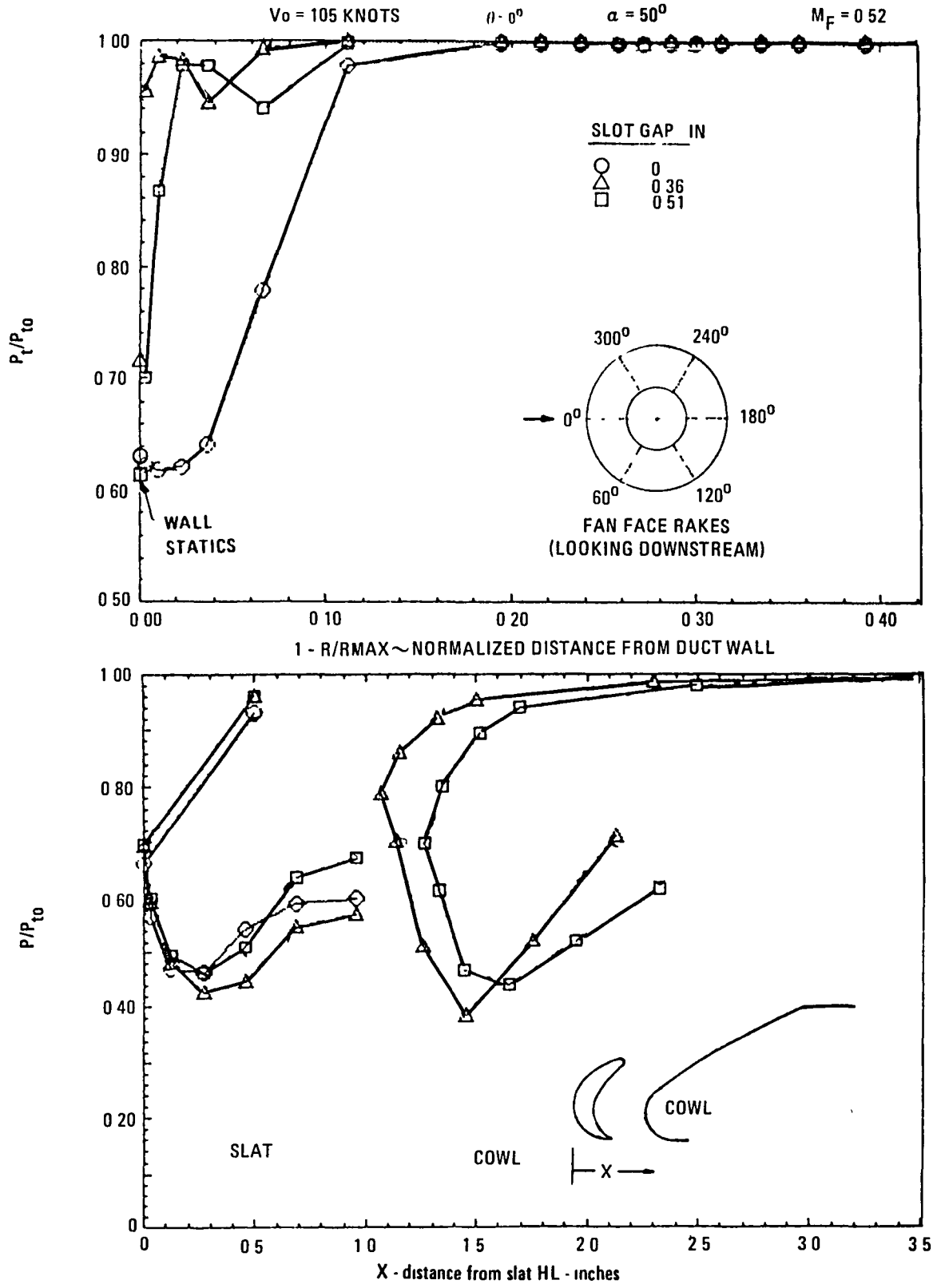

Figure 50. - Effect of slot gap width on fan face total pressure profile and slat/cowl surface static pressures, CR=1.2, no spacer.

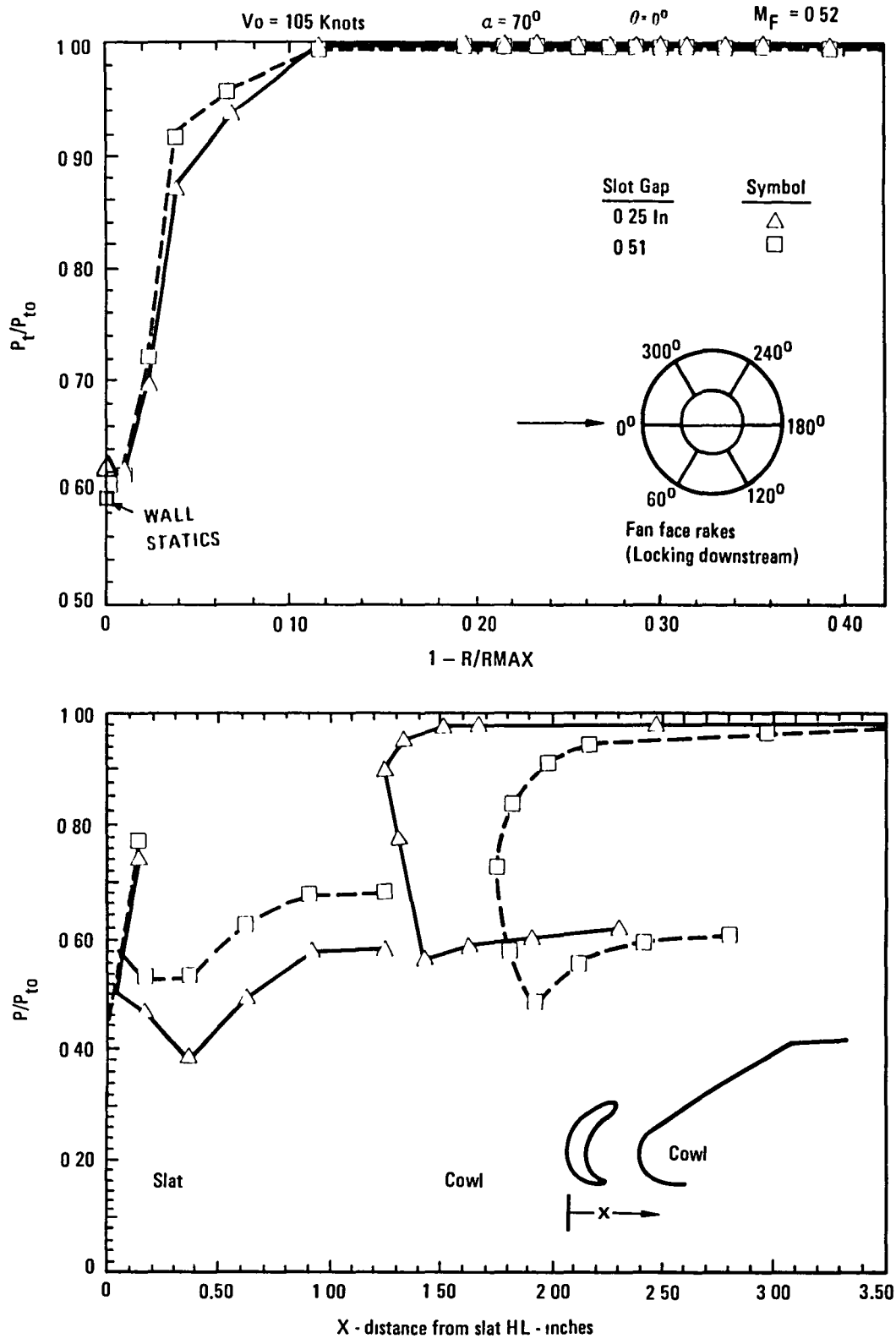

Figure 51. - Effect of slot gap width on fan face total pressure profile and slat/cowl surface static pressures, CR=1.3, no spacer.

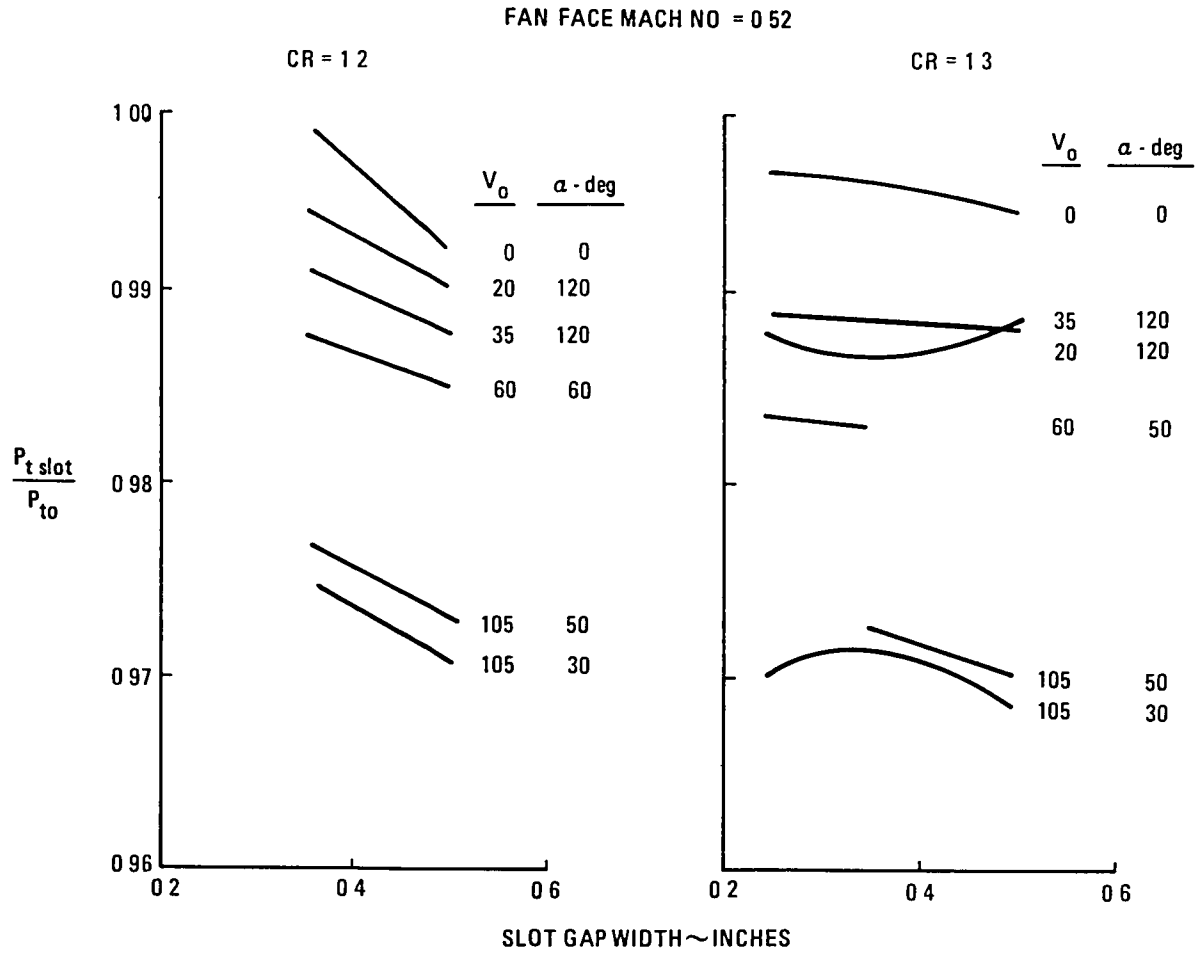

Figure 52. - Effect of slot gap width on slot gap total pressure recovery.

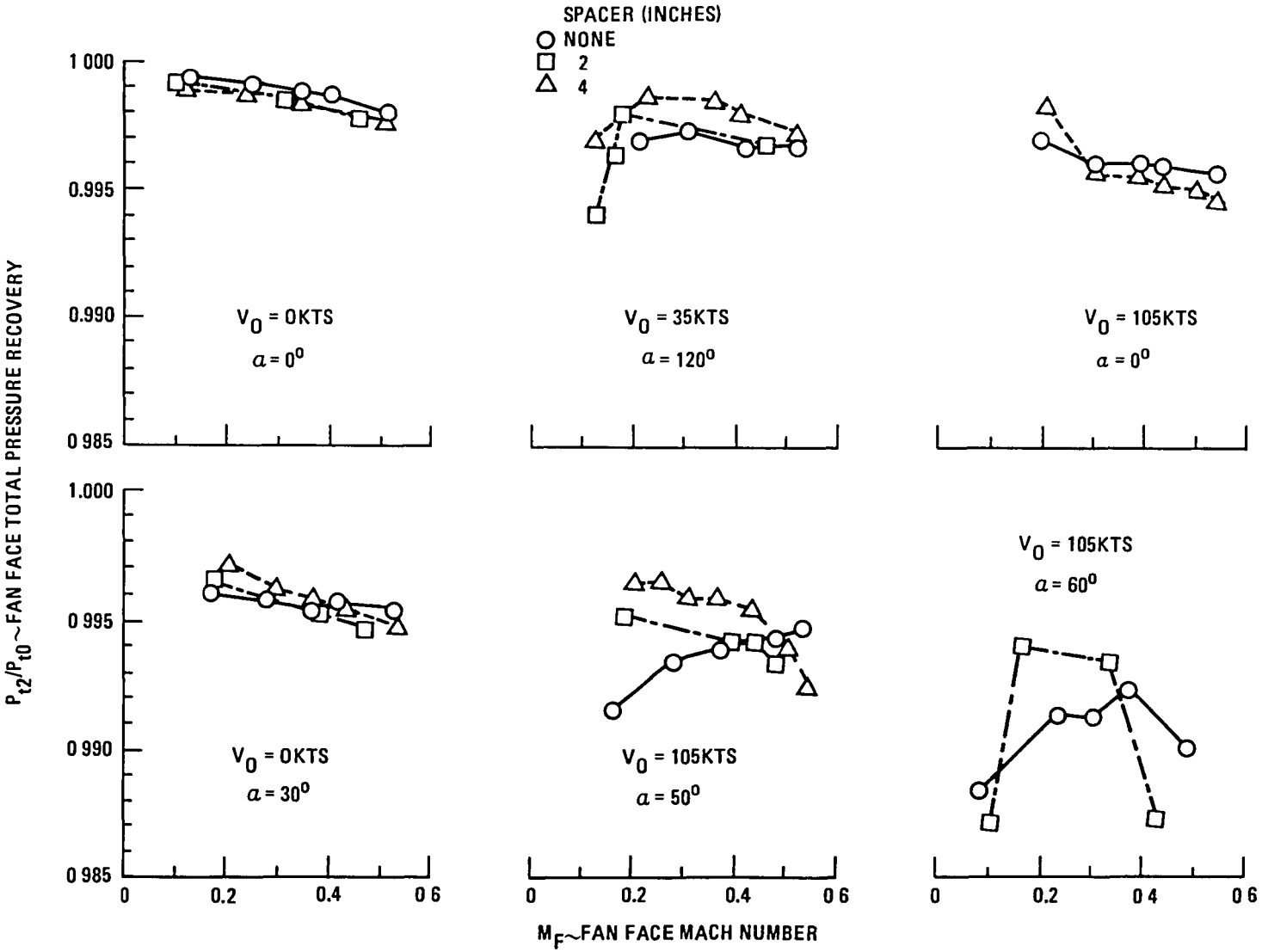

Figure 53. - Effect of fan face Mach number on total pressure recovery with throat/fan face spacers installed, CR=1.2

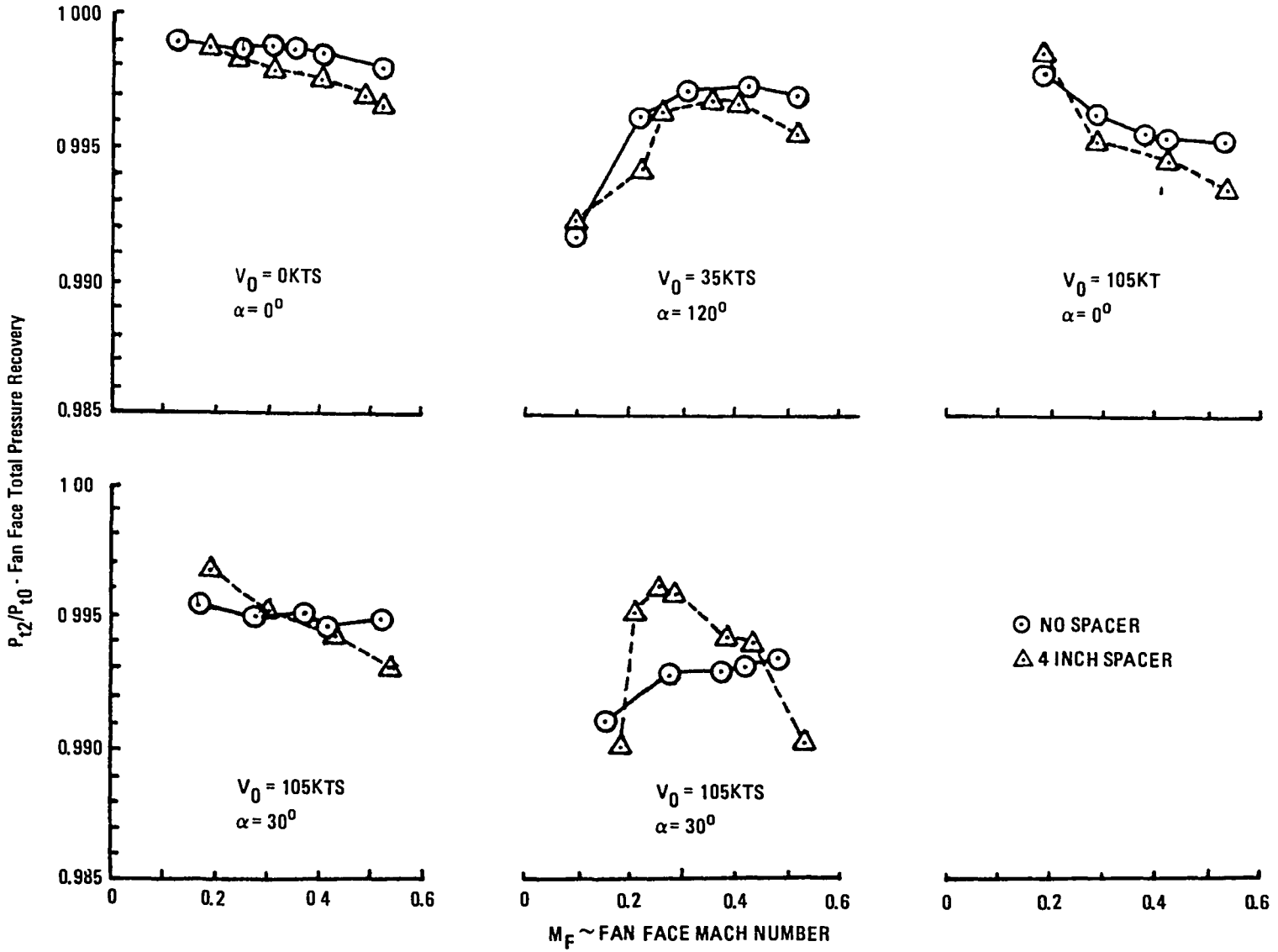

Figure 54. - Effect of fan face Mach number on total pressure recovery with throat/fan face spacer installed, CR=1.3

At combinations of tunnel velocity and model angle of attack where flow separation does not exist (all tunnel velocities at zero angle of attack) the recovery is slightly lower with the spacers installed due to additional wetted surface (friction losses). At higher angles of attack and tunnel speed, however, flow separation occurs on the slat/cowl lip and therefore, the recovery is largely dependent on the strength of the fan pumping action (affected by fan speed and proximity to the inlet throat). With no spacer installed, the data at 105 knots/50 degree angle-of-attack in figure 53 shows a loss in recovery of approximately 1 percent at the low fan speed resulting from flow separation. As the fan speed and inlet airflow increases, the pumping action of the fan located at the throat, reduces the flow separation and roughly halves the recovery loss at the maximum fan speed tested. With the 4 inch spacer installed the trend is exactly opposite. At the low fan speeds the duct length allows re-attachment of the separated flow with a resulting recovery loss of only 0.3 percent. At higher fan speeds, however, the pumping action of the fan is not felt because of the fan face displacement. Also with increased surface velocities, resulting from the increased airflow, flow separation is encountered which increases the recovery loss to approximately 0.8 percent at the maximum fan speed tested. Figure 55 compares the fan face total pressure profiles and slat/cowl surface static pressure distributions with and without the spacers installed, illustrating the above discussion. Also the total pressure recovery at a tunnel speed of 105 knots is presented in figure 56 as a function of spacer length for several fan face Mach numbers. As shown in this figure the inlet throat/fan face spacer has relatively little effect on the fan-face total pressure recovery, especially at low angles of attack. At high angles of attack, where the flow is more likely to separate, the fan face total pressure recovery increases slightly at low fan speeds where the pumping action is small. Evidently, adding length between the throat and fan face allows the flow to reattach ahead of the fan-face which more than compensates for any recovery reduction associated with spinner location.

As discussed previously a significant potential flow velocity distortion occurs at the inlet throat under high angle of attack conditions. The effect of the constant area duct section provided by the spacer is such to reduce this velocity distortion as shown in figure 57. However, as was also discussed earlier this distortion did not affect the fan performance and is expected to have less of an effect on the higher pressure ratio fans being considered for V/STOL applications.

Effect of Slot Gap Fillers on Performance

During the V/STOL aircraft studies at Lockheed twin engine pods were considered for a four engine configuration. The effect of two adjacent nacelles is to essentially block a 90 degree sector over which the slot is effective. To simulate this effect during the program, 90 degree slot fillers were installed and tested. Since the direction of the tunnel flow relative to the

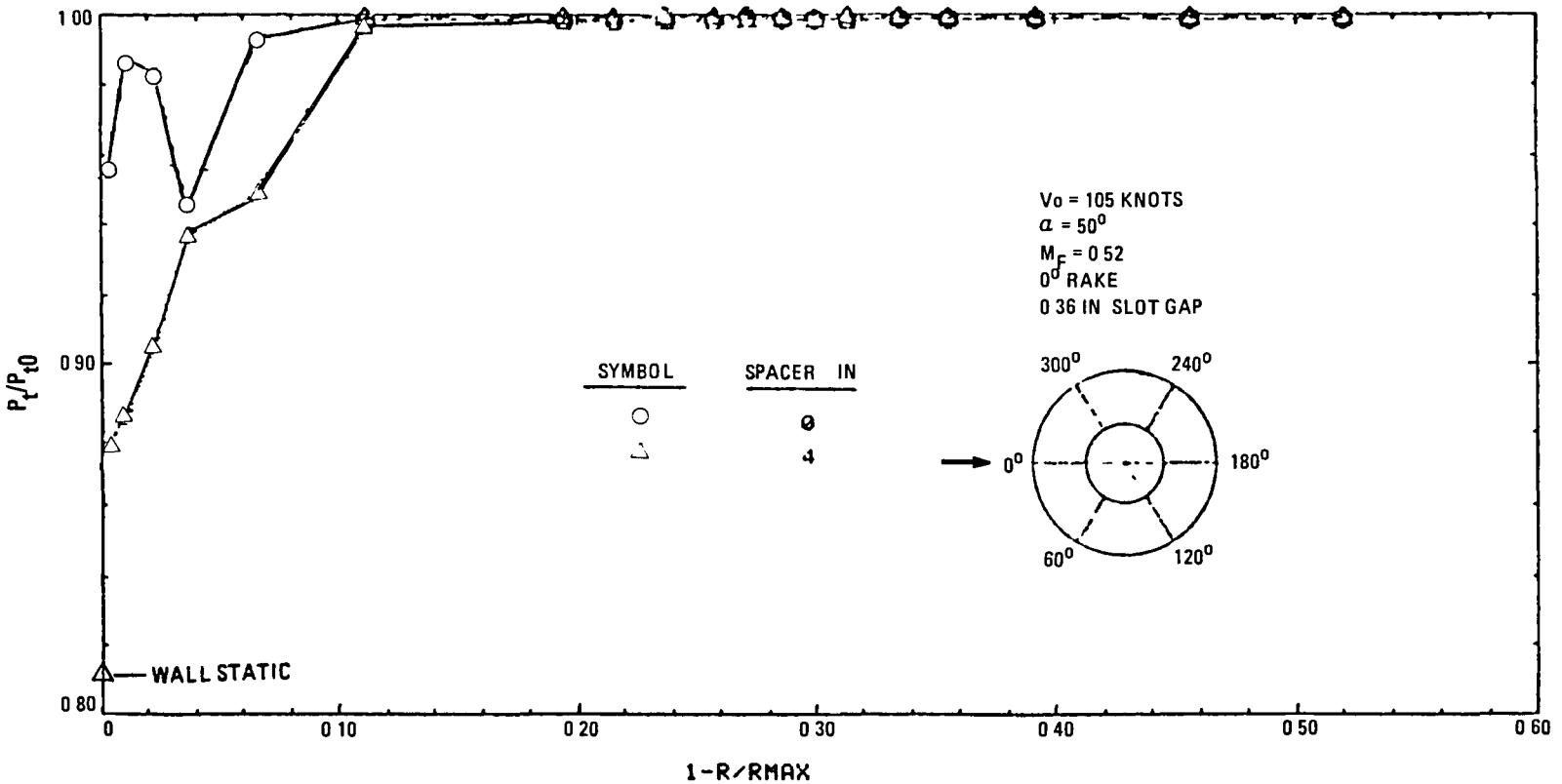

(a) Fan face total pressure profile.

Figure 55. - Effect of throat/fan spacer on fan-inlet performance, CR=1.2, 0.36 inch slot gap.

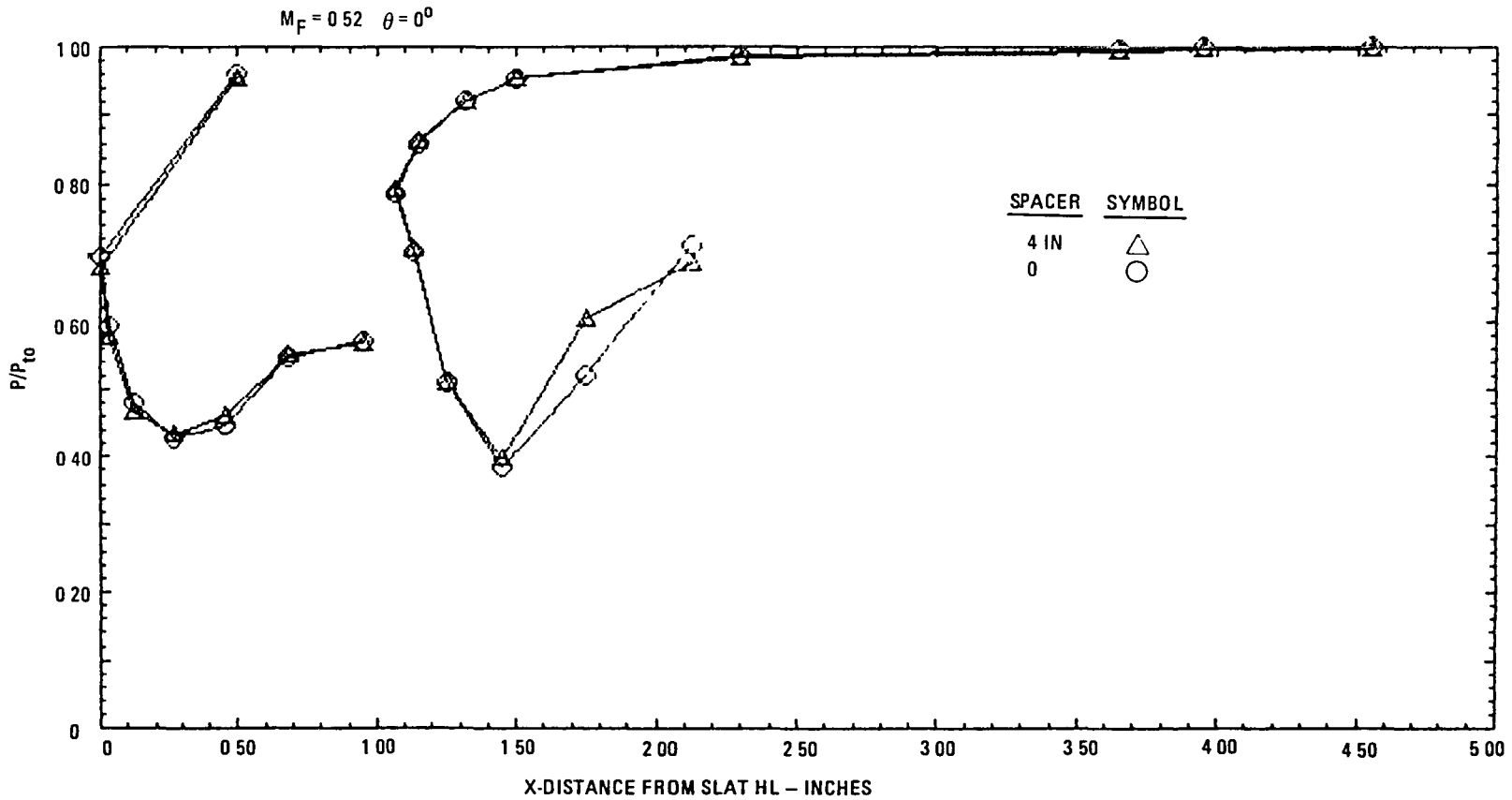

(b) Slot/cowl static pressure distribution.

Figure 55. - Effect of throat/fan spacer on fan-inlet performance CR=1.2, 0.36 inch slot gap. (Concluded.)

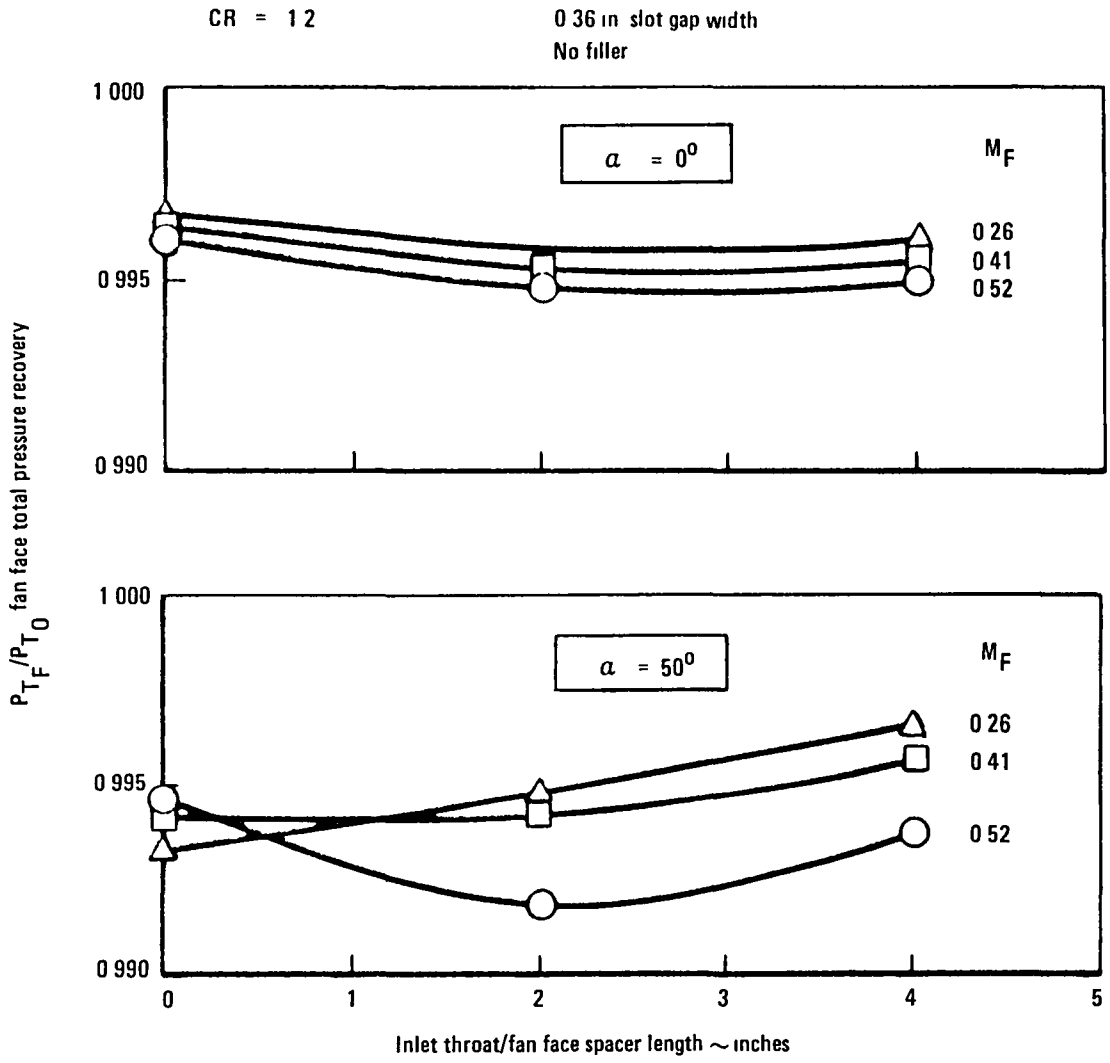

Figure 56. - Effect of inlet throat/fan face spacer on fan face total pressure recovery, CR=1.2, 0.36 inch slot gap, 105 knots.

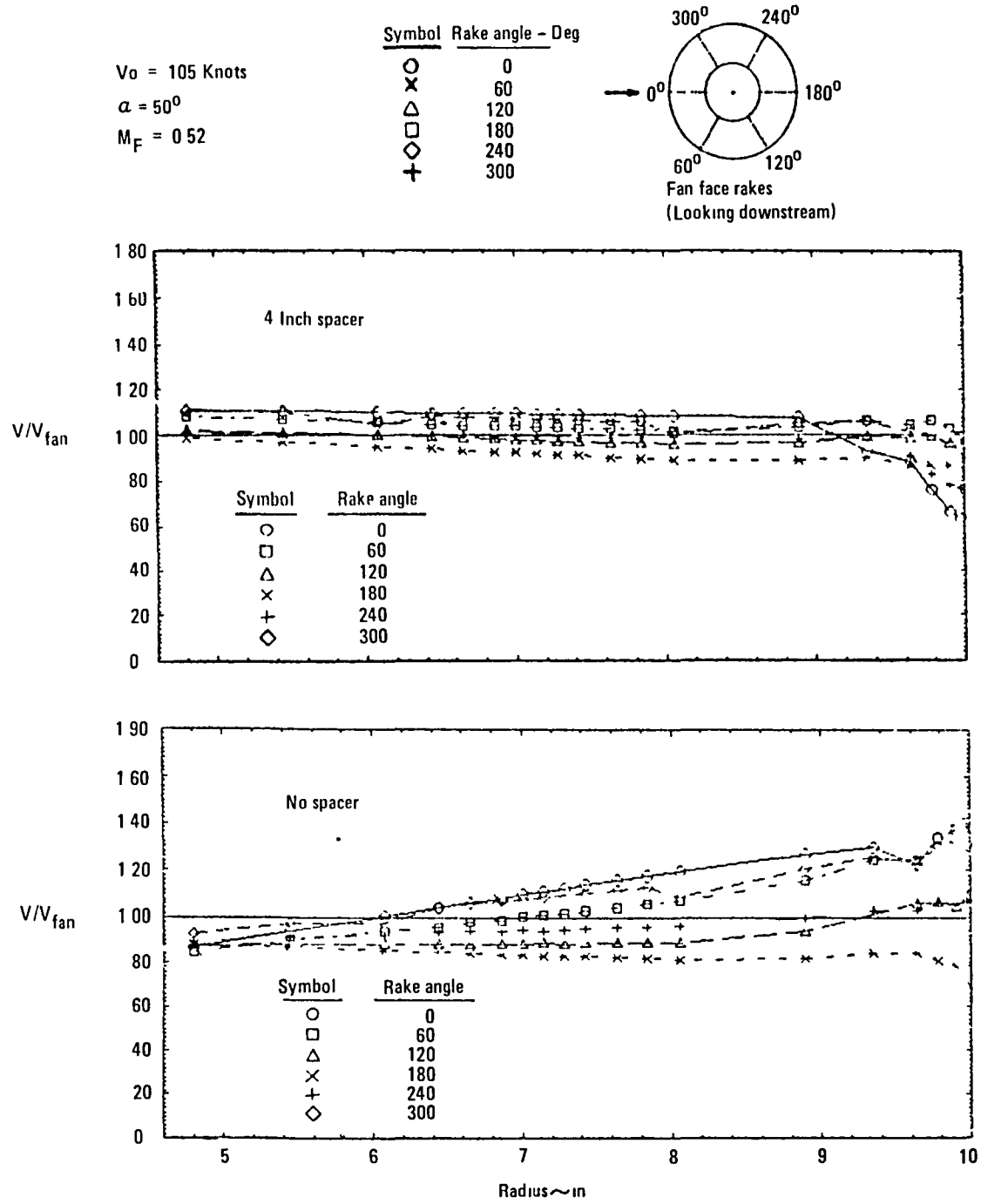

Figure 57. - Effect of throat/fan spacer on fan face flow velocity distortion, CR=1.2, 0.51 inch slot gap, no spacer.

model was fixed, the fillers were installed in two separate locations. The first location was at the bottom of the inlet with the filler extending circumferentially from 45 degrees to 135 degrees and relative to the tunnel flow represented an angle of attack condition of the aircraft. The second location was at 180 degrees, directly opposite the tunnel flow direction and extending from 135 degrees to 225 degrees and represented a crosswind condition of the aircraft.

Eliminating a 90 degree sector of the slot in the locations described above has essentially no effect on the fan face total pressure recovery as shown in figures 58 and 59. With the filler in the 45-135 degree location the slat/cowl surface static pressures are only slightly reduced as shown typically in figure 60 for the 80 knot/40 degree angle of attack condition. For the filler installed in the 135-225 degree location, however, the static pressures on the slat are more significantly reduced compared to the no-filler configuration as shown in figure 61. For reference, the fan face rake total pressure profiles are shown with and without each of the fillers installed in figures 62 through 65.

Flow Separation and Inlet Operating Limits

Flow separation occurs from the inlet surface under conditions of adverse pressure gradient/high local surface velocities (or Mach number). As the inlet airflow or fan face Mach number increases there is a proportional increase in the local surface Mach number (potential flow). Also, as the angle of the flow into the inlet increases from the forward direction (resulting from model angle of attack), the reduced static pressures on the internal lip surface on the windward side of the nacelle increase the local Mach number further.

For the zero-length, slotted-lip inlet tested, flow separation was observed, as discussed previously, at maximum fan airflow for various combinations of tunnel velocity and model angle of attack. For the baseline configuration these separation points have been identified in figure 20.

The onset of flow separation was determined using the total pressure profiles as measured by the fan face rakes and, in particular, the critical zero degree rake. Separation was interpreted to affect inlet and fan performance when the total pressure measurement adjacent to the duct wall reached the wall static pressure measurement or when the total pressure profile exhibited a significant reversal in shape. Since the flow in this region is basically from the slot passage, the definition reflects separation from the cowl lip. It has been observed, however, that when the flow separates from the slat and remains attached to the cowl lip (such as shown by the total pressure profile in figure 32 and the corresponding static pressure distribution in figure 33b) the flow at the fan face wall remains attached. Because of the slot flow the separation of flow off the slat is confined to a small

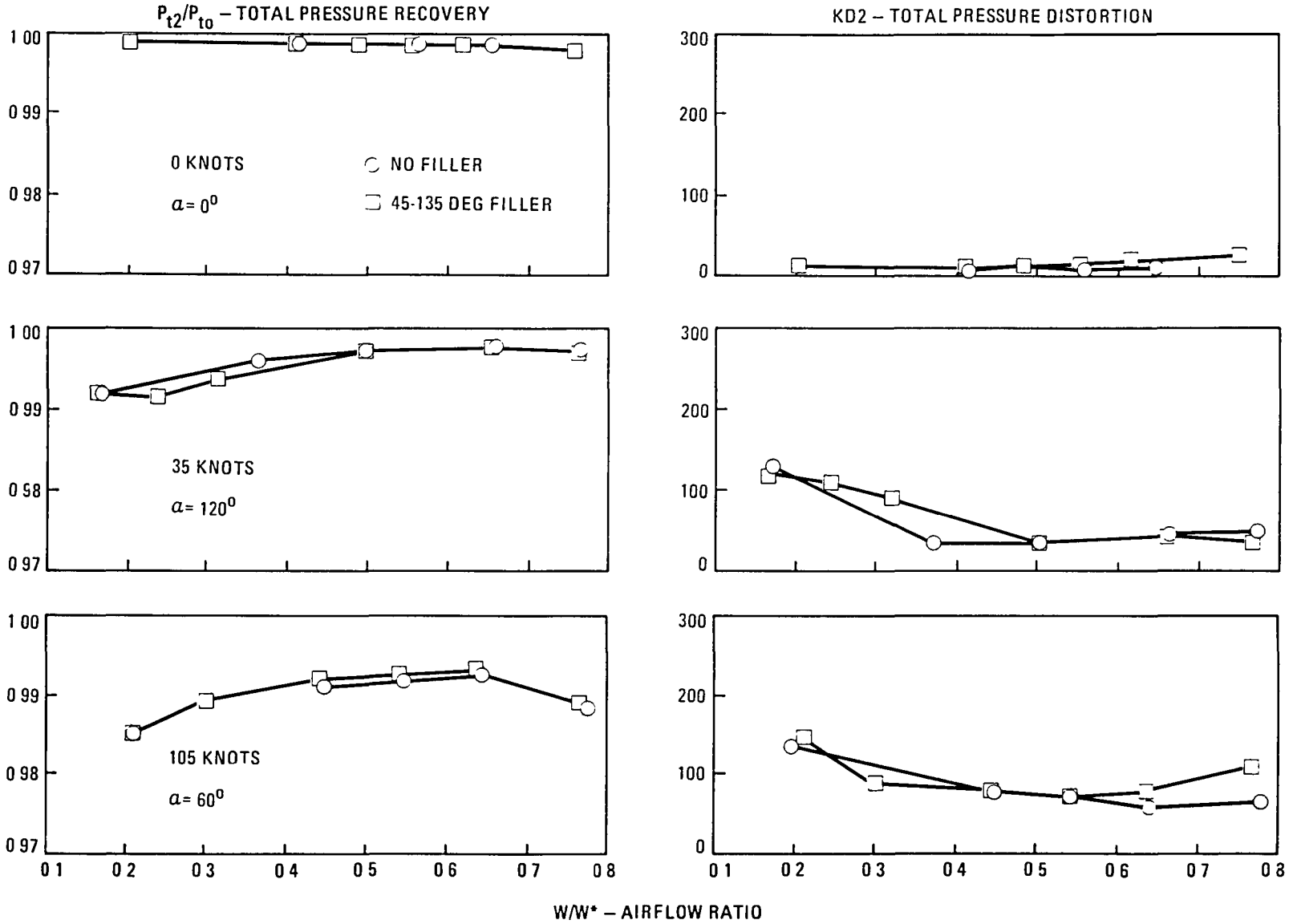

Figure 58. - Effect of 45-135 degree slot filler on total pressure recovery, CR = 1.2, 0.51 inch slot gap, no spacer.

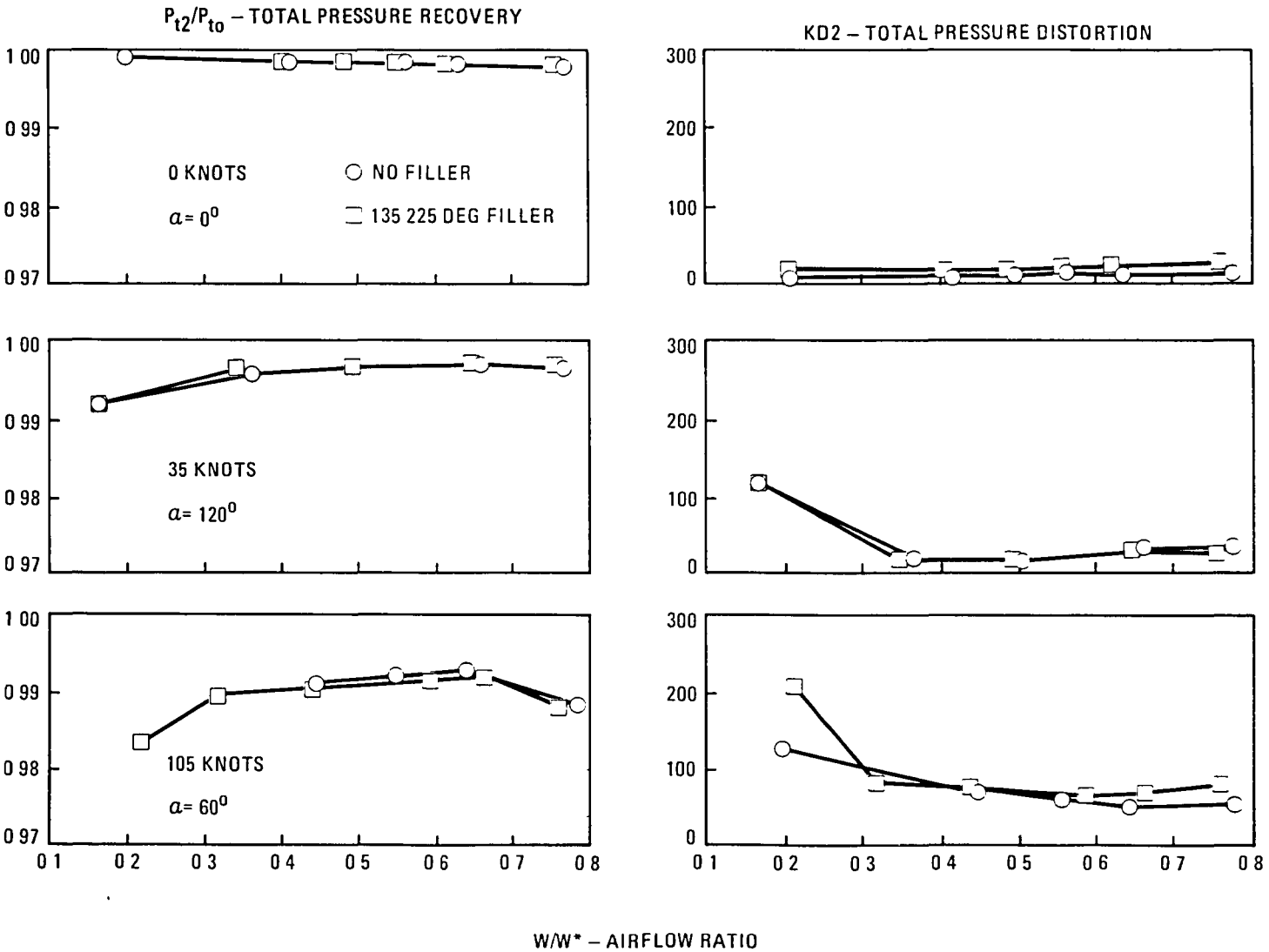

Figure 59. - Effect of 135-225 degree slot filler on total pressure recovery, CR = 1.2, 0.51 inch slot gap, no spacer.

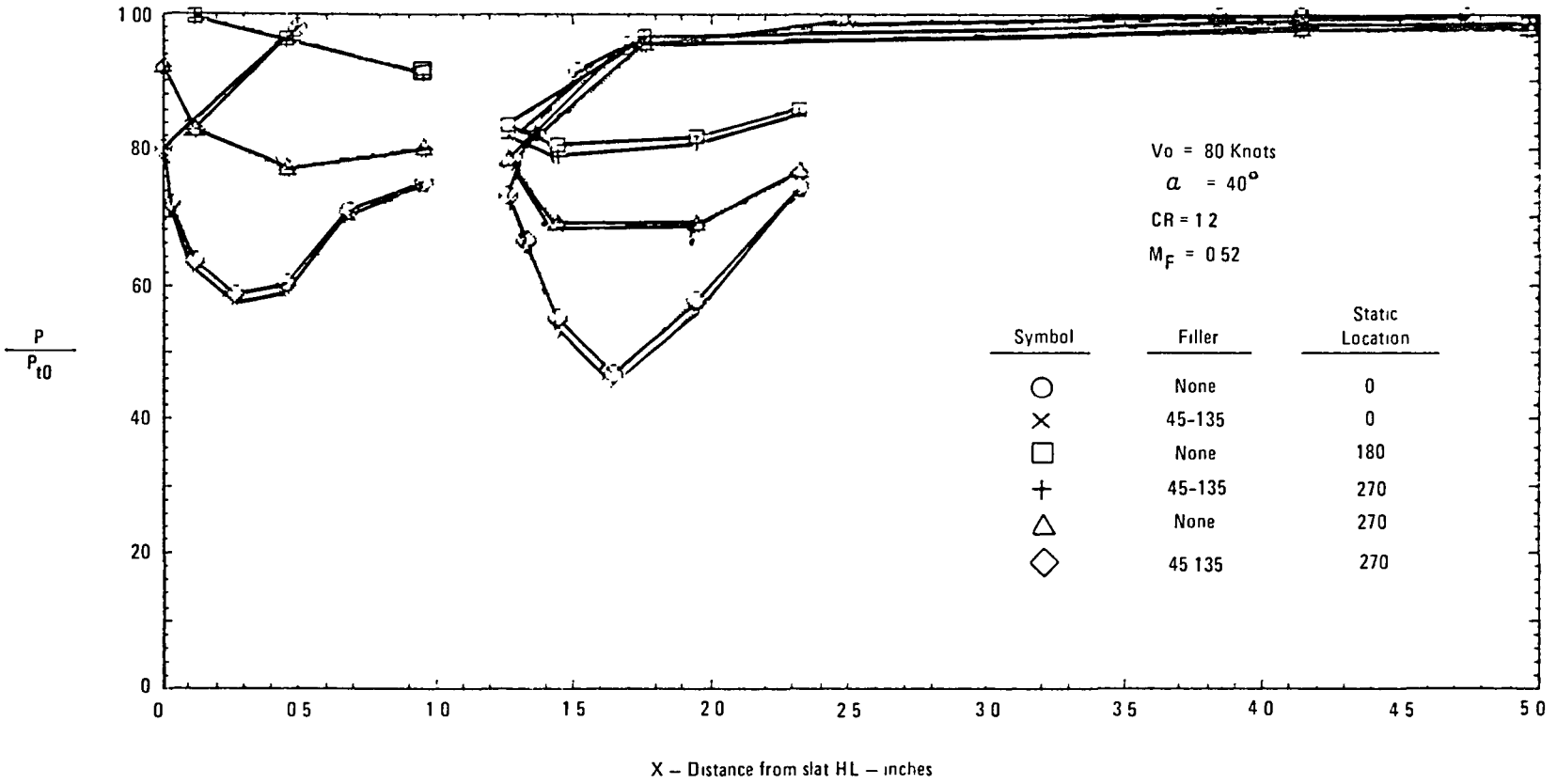

Figure 60. - Effect of 45-135 degree slot filler on slat/cowl static pressure, CR=1.2, 0.51 inch slot gap, no spacer.

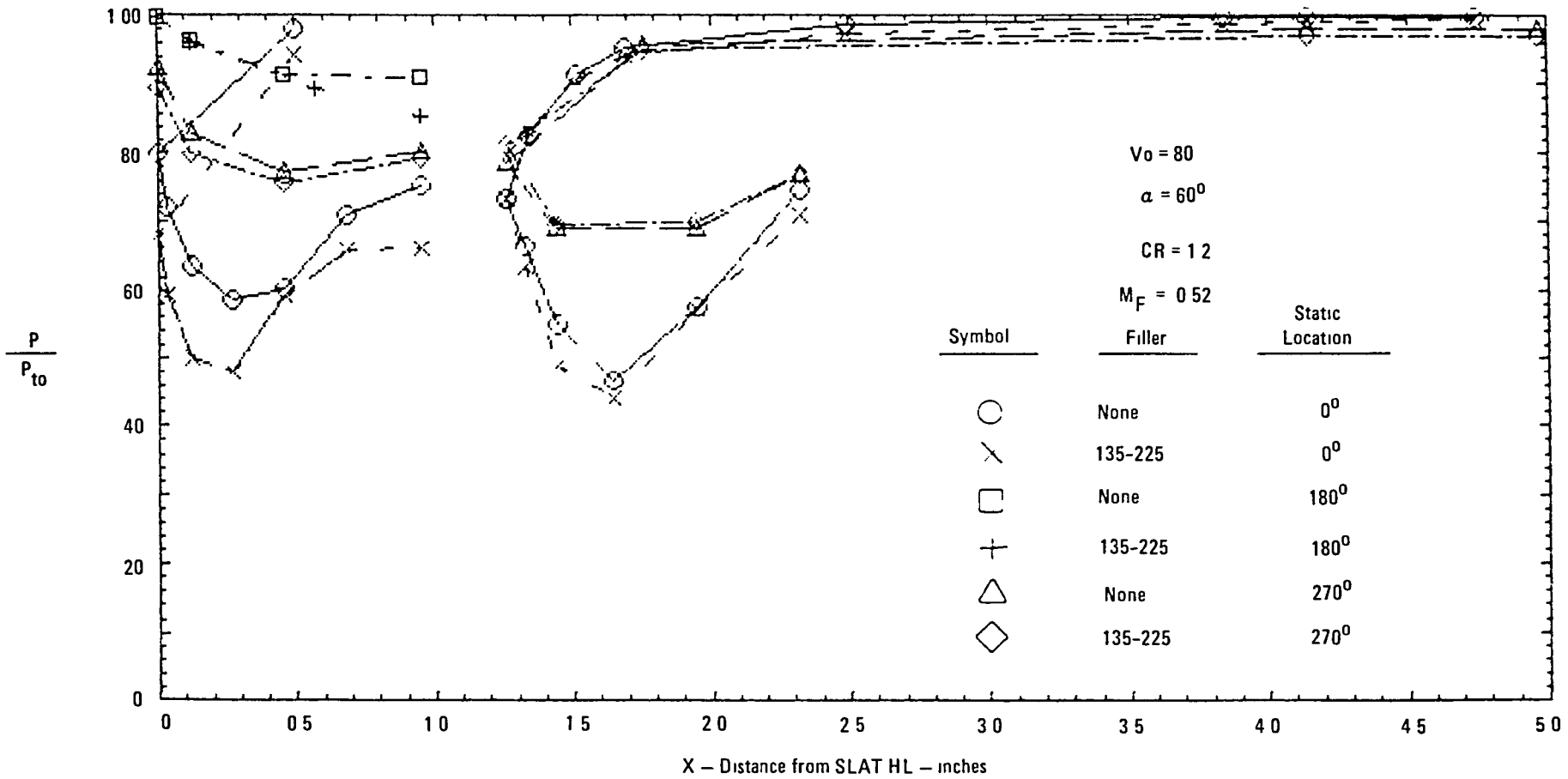

Figure 61. - Effect of 135-225 degree slot filler on slat/cowl static pressure, CR=1.2, 0.51 inch slot gap, no spacer.

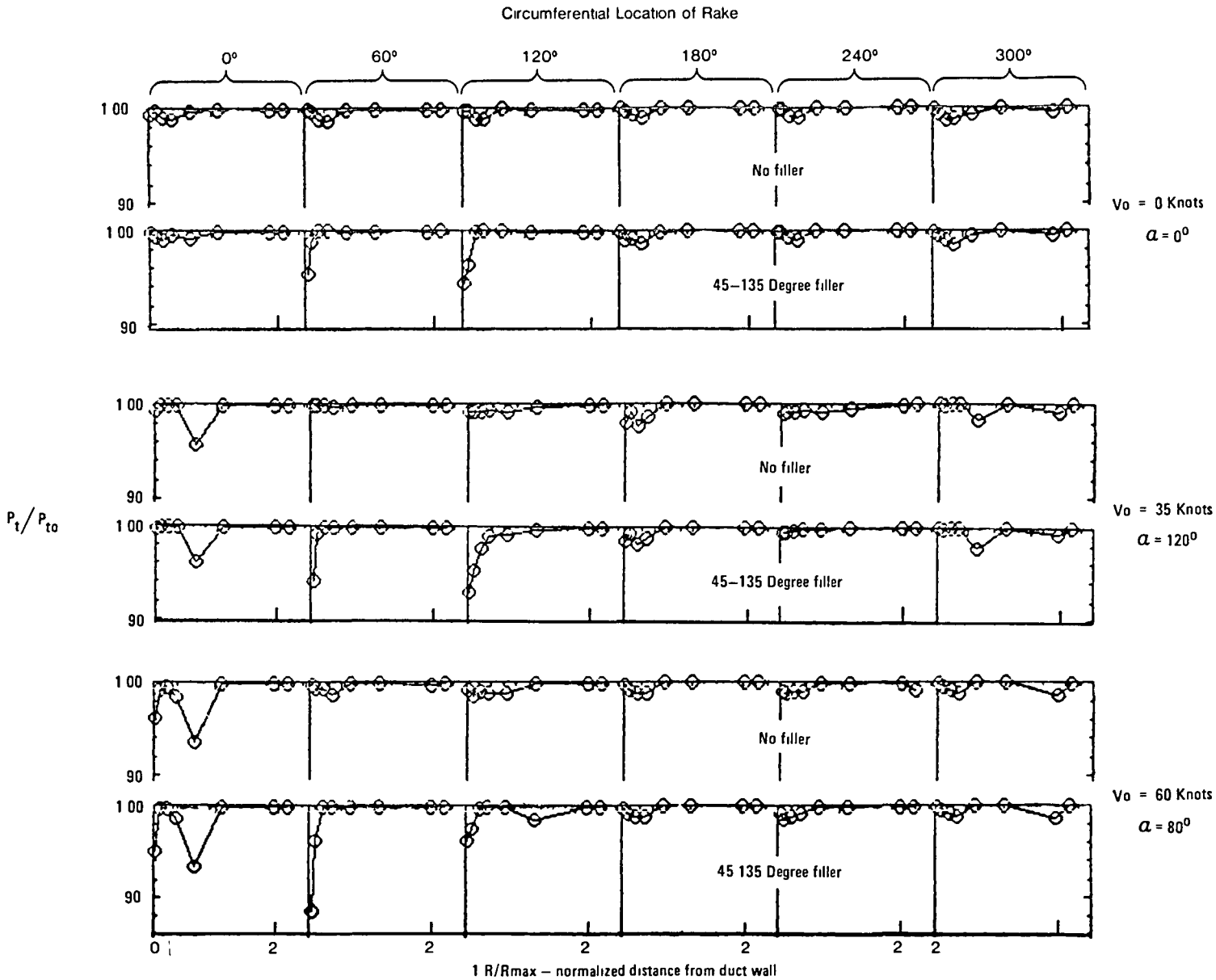

Figure 62. - Effect of 45-135 degree slot filler on total pressure profiles, CR=1.2, 0.51 inch slot gap, no spacer.

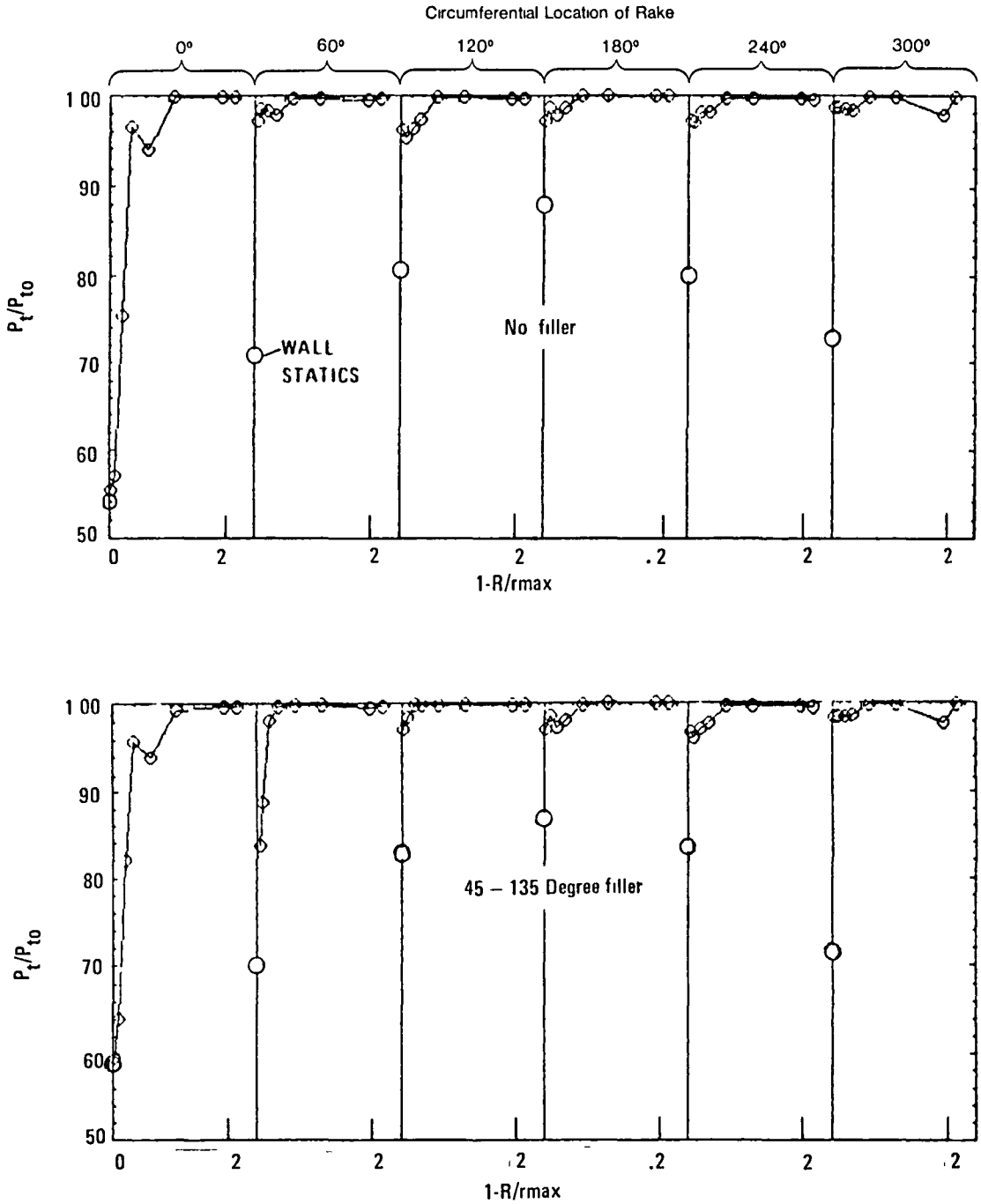

Figure 63. - Effect of 45-135 degree slot filler on total pressure profiles max velocity, CR=1.2, 0.51 inch slot gap, no spacer, Vo=105 Knots, α =60°, M_F=0.52.

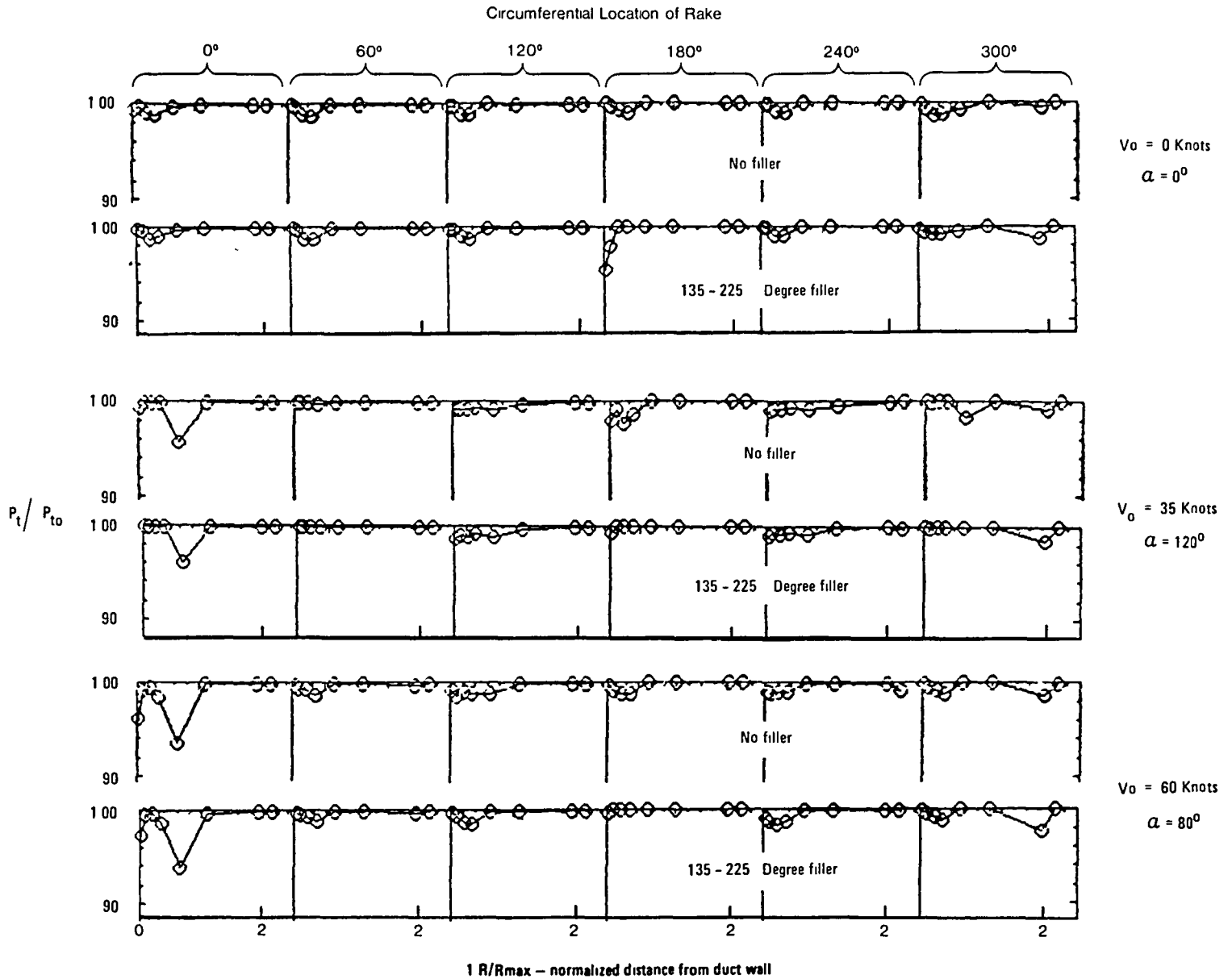

Figure 64. - Effect of 135-225 degree slot filler on total pressure profiles, CR=1.2, 0.51 inch slot gap, no spacer.

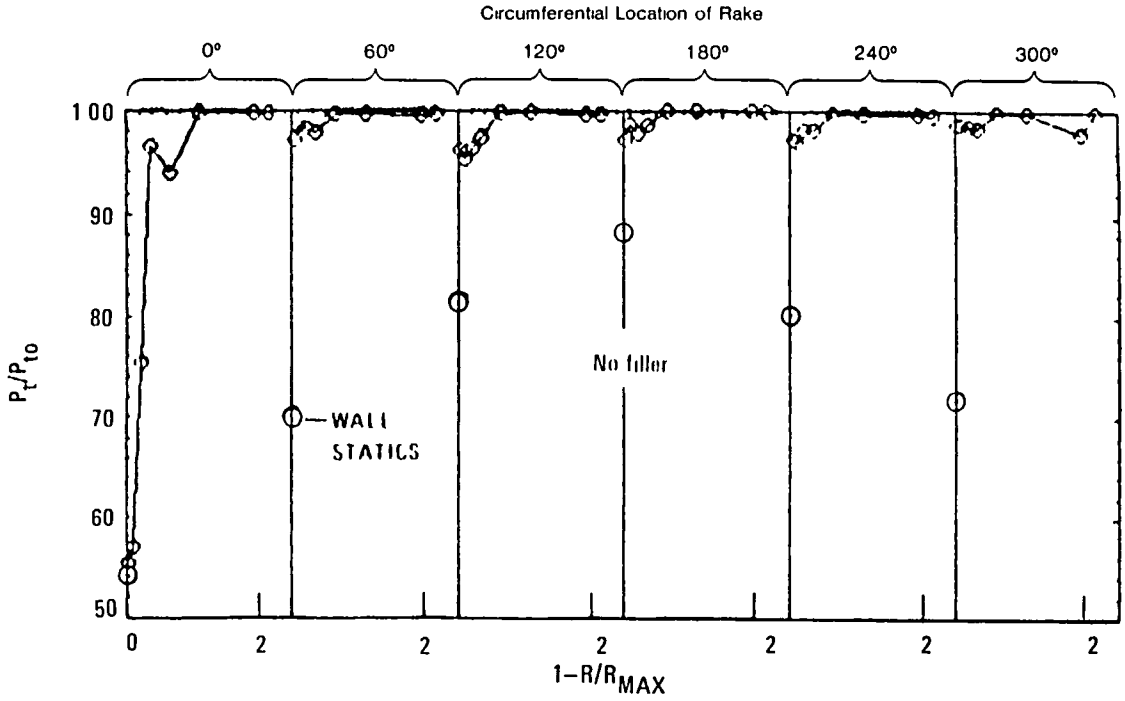

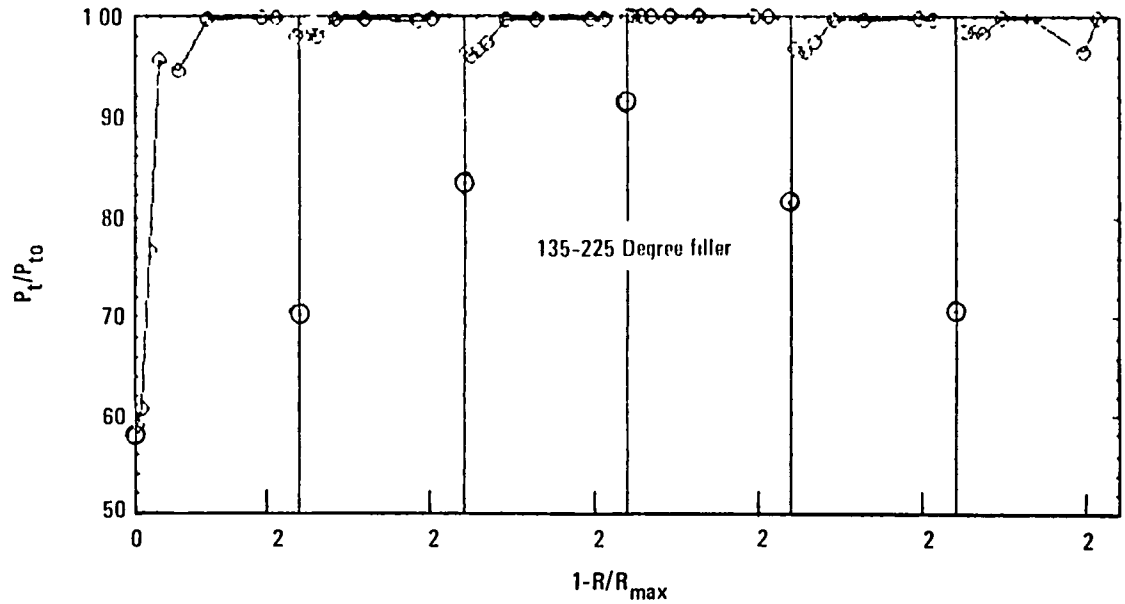

Figure 65. - Effect of 135-225 degree slot filler on total pressure profiles, maximum velocity, CR=1.2, 0.51 inch slot gap, no spacer, Vo=105 Knots, $\alpha=60^{o}$, $M_F=0.52$.

area at the fan face. The low energy flow associated with the separation is energized rapidly because of the mixing that takes place on each side of the region.

Inlet operating limits, velocity/angle of attack, can be established based on the onset of flow separation. These limits will be somewhat conservative compared to limits based on fan blade stress levels. However, once flow separation has been initiated, it is considered that only small increases in speed/angle of attack are sufficient to reach the limit stress levels. Furthermore, some margin is desirous to insure satisfactory operation at the required design point.

During the test, angles of attack have been identified where flow separation is observed. Since discrete angles were tested, however, the angle for actual onset of separation is somewhat less than those identified. It has been shown in reference 2 that the maximum surface Mach number can be used as criteria for the onset of lip separation. Curves showing the maximum surface Mach numbers obtained on the model have been plotted, as shown typically in figure 66 for the baseline configuration. Since the static pressure taps were located at discrete intervals on the surface, higher local values of Mach number may have occurred between the measurements. Referring to figure 66, as the angle of attack increases for each tunnel speed the maximum surface Mach number increases until flow separation occurs, noted by the abrupt change in slope of the curve.

To establish limit angles for each tunnel speed, the segment of the Mach number curves prior to a change in slope (attached flow) were extrapolated, as shown in figure 66 to a maximum value consistent with not exceeding those angles of attack identified with separation from the total pressure profiles. This maximum value of Mach number was then used as a limiting value to determine the maximum angle for each tunnel speed. For the baseline configuration, for example, a maximum surface Mach number of 1.3 was selected as shown in figure 66. The intersection of this value and the extrapolated curves result in angles that do not exceed those for which separation has been identified in figure 28. Similar procedures were used for the other slot-gap settings and the resulting limiting envelope curves presented in figures 67 and 68 for the 1.2 and 1.3 contraction ratio lips, respectively.

It should be mentioned that this procedure is not entirely rigorous but does provide a conservative estimate of the speed/angle of attack limitation for the inlet based on the test data. It should also be re-iterated that the limits are based on observed separation at the fan face rake, whereas localized separation on the slat/cowl exists at less stringent conditions.

In addition to obtaining flow separation at high speeds and high angles of attack (just described) this phenomenon also occurred to some extent at the very low engine airflows (associated with idle powers) and with very high model angles of attack. At low airflows (low fan speeds) the fan does not provide a favorable pumping effect on the inlet lip and flow separation ensues. As the

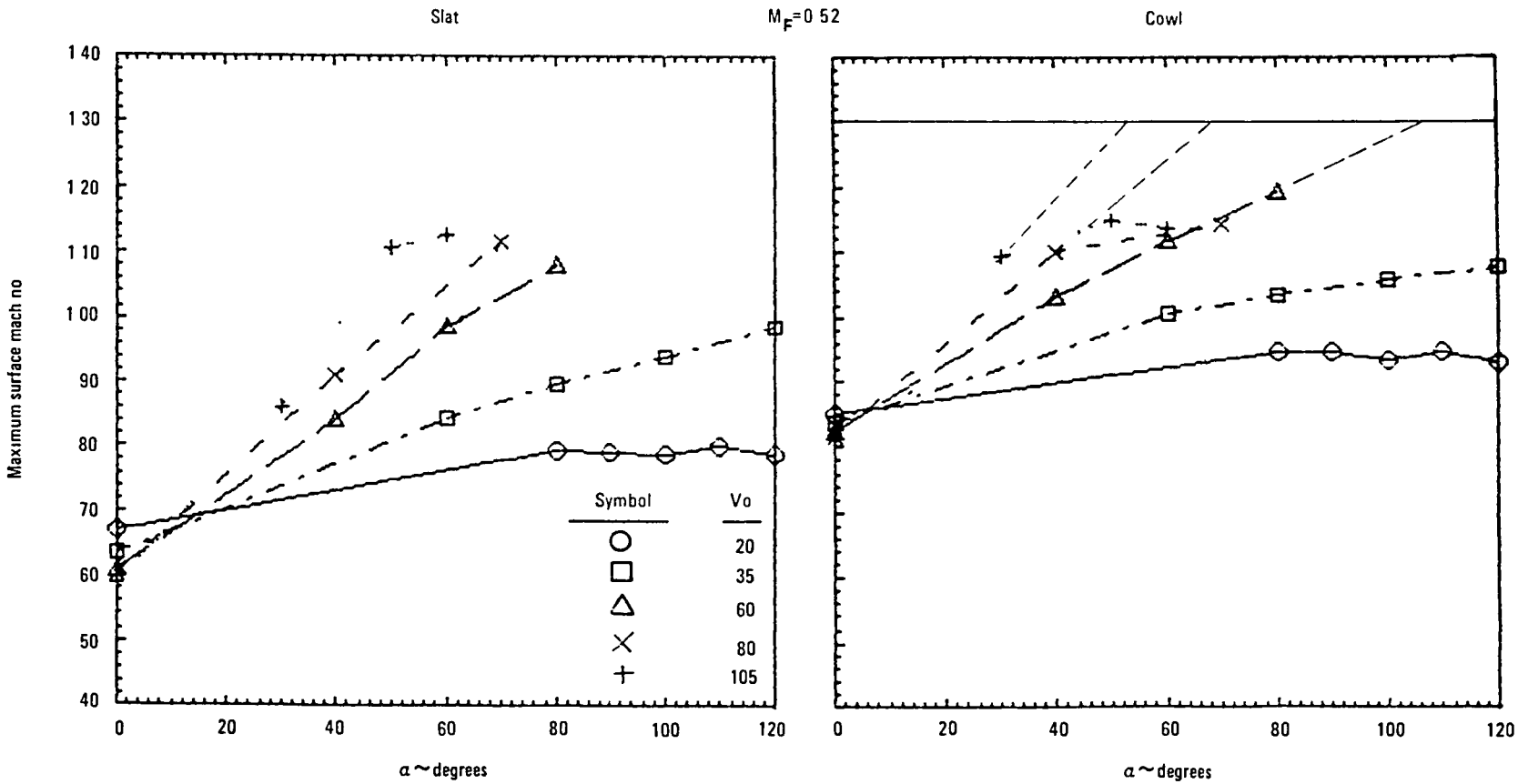

Figure 66. - Maximum slat/cowl surface mach no. calculated from measured static pressures, CR=1.2, 0.51 inch slot gap, no spacer.

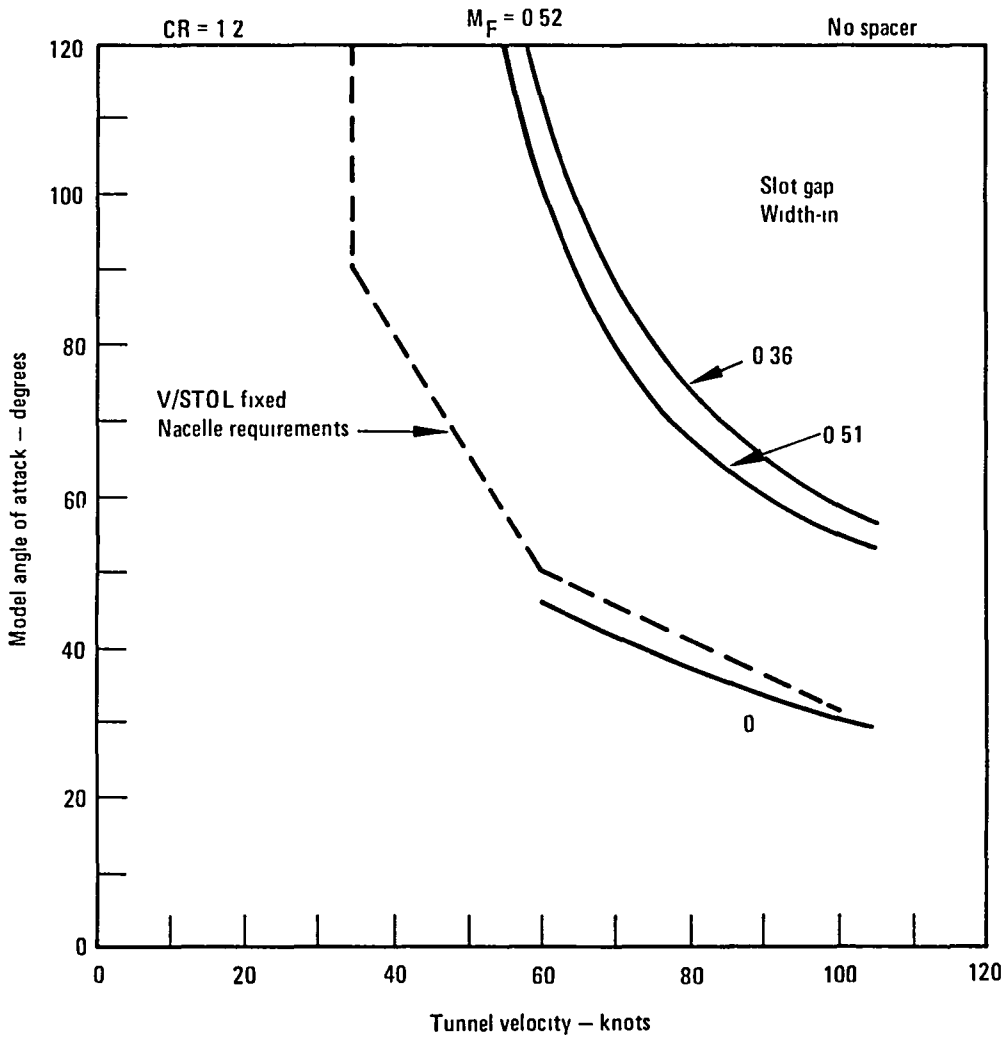

Figure 67. - Inlet angle of attack for flow separation, CR=1.2.

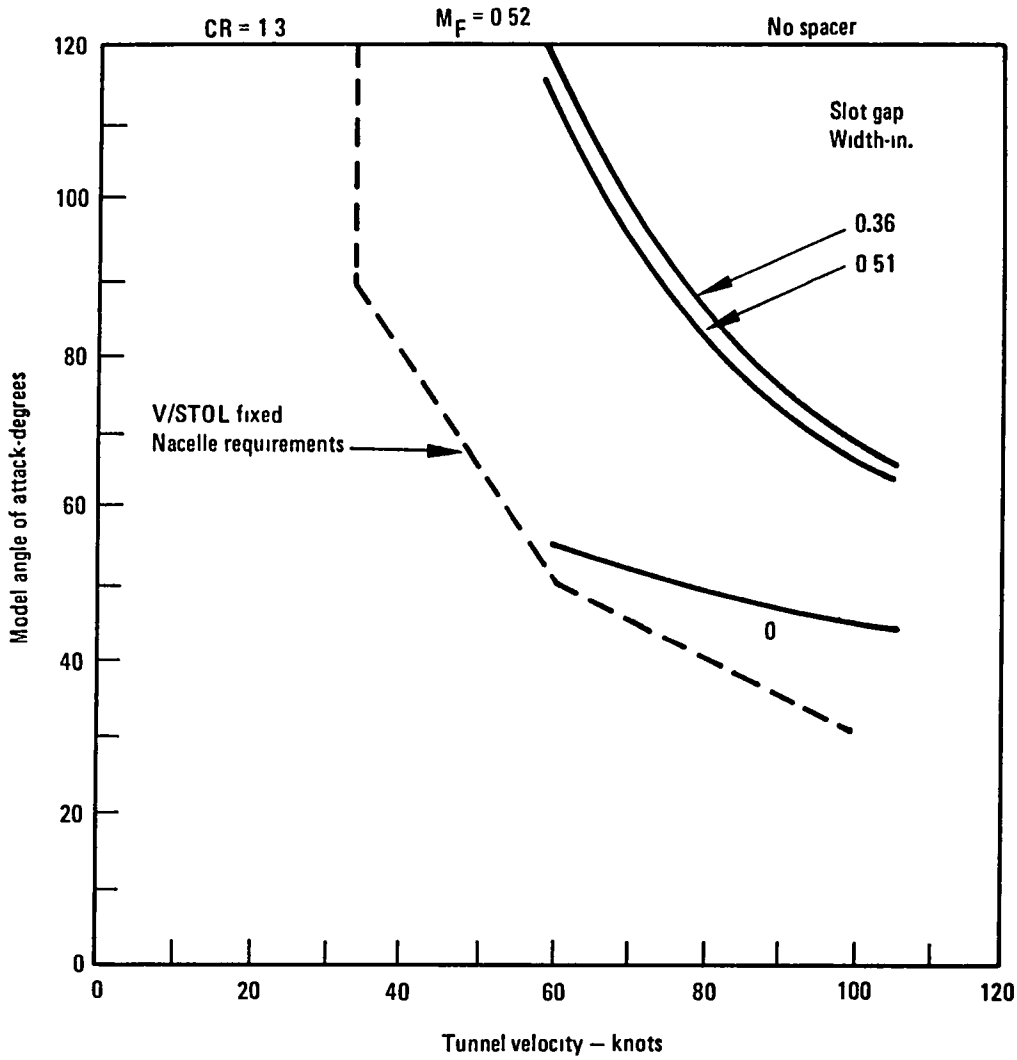

Figure 68. - Inlet angle of attack for flow separation, CR=1.3.

fan speed and pumping effect increase, the separation is reduced and an improvement in recovery is obtained. The fan face total pressure profile and surface static pressure distributions in figure 69 illustrate the low airflow separation as well as the re-attachment as the flow is increased. At these conditions the measured blade stress levels were very low as would be expected with the low fan speeds. Also, as mentioned previously, these operating conditions are not primarily of interest for the V/STOL application.

When discussing experimental inlet performance, it is convenient to present the data in figure 67 in the form of the angle of attack limit of the inlet as a function of the fan face Mach number for a given value of free-stream velocity as in figure 70. There are two regions presented. One of these is the fan operating region. The upper boundary of the fan operating region represents the inlet angle of attack requirement for a fixed nacelle configuration represented by the dotted curve in figure 20. For comparison, figure 70 is annotated with inlet angle of attack requirements for a tilt nacelle and tilt nacelle with nozzle vanes. The side boundaries of the fan operating region are determined by the operating range of the fan jet engine, that is, from full to part throttle as shown. The inlet must provide a steady supply of air to the fan at high pressure recovery and low distortion. For the inlet to achieve these high performance goals the flow must not separate.

The second region is bounded by the separation bound of the inlet with a 1.2 contraction ratio slat represented by the solid and dashed curve in figure 70. The area of the figure that lies below the inlet curve represents conditions for attached flow; the area above the curve represents conditions for separated flow. The inlet flow is fully attached between the two data points. This configuration was not tested at 90° angle of attack. If the flow separates off the walls of the main cowl where the surface is wetted by air ingested into the inlet and to a lesser extent off the slat surfaces, the pressure recovery decreases and this would in turn reduce thrust; concomitantly the accompanying distortion increases would increase fan blade stresses. The inlet must be designed with the idea of preventing boundary layer separation. This is done by keeping the surface velocities as low as possible. It can be seen from the figure that the inlet meets the requirements of a fixed nacelle at 80 kts but does not meet the requirements of a simple tilt nacelle during full throttle operation. At part throttle conditions there is no difficulty with fan operation. Further testing would be required to determine if the 1.2 contraction ratio slat would satisfy the fan requirements of the tilt nacelle with a nozzle vane.

There are different phenomena responsible for the inlet separation of each branch of the inlet curve. The boundary layer separation on the branch of the curve to the left is caused by adverse pressure gradients due to decelerating the local surface velocity. This cause of separation has been labeled "diffusion-limit separation." The boundary layer separation on the right branch of the inlet curve is caused by standing shock waves located at the inlet wall surface. As the surface Mach number becomes supersonic and a certain limit is reached, a shock is formed that separates the boundary layer. This limit has been labeled the "Mach number limit." The right side of the

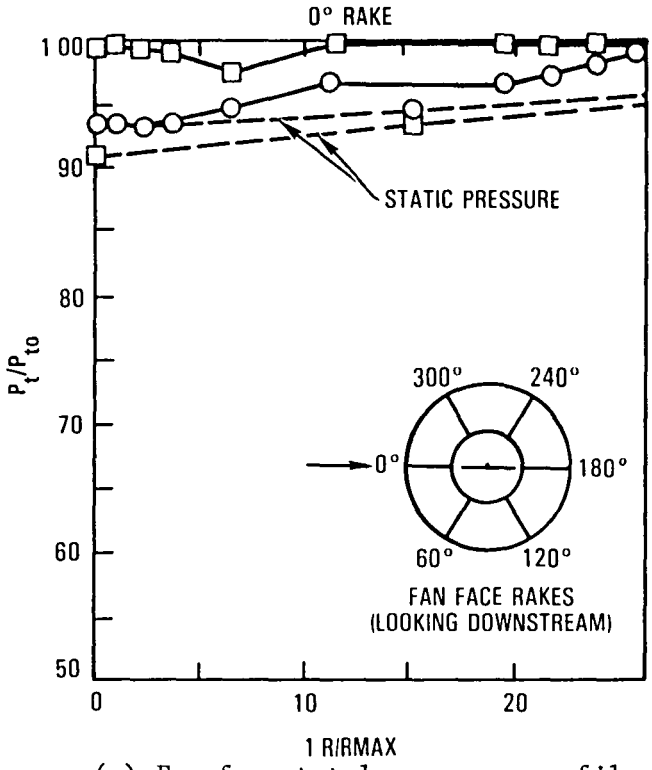

(a) Fan face total pressure profile.

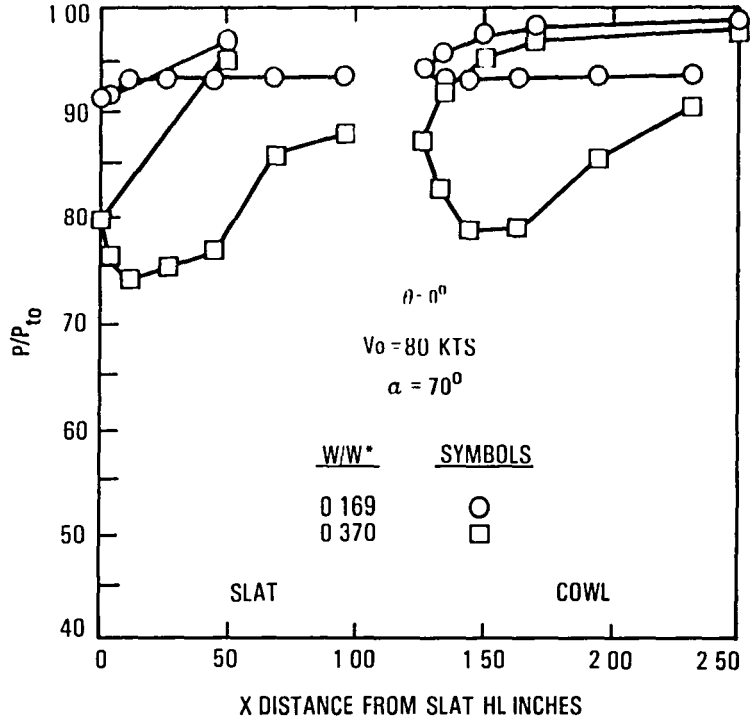

(b) Slat/cowl surface static pressure distribution.

Figure 69. - Pressure measurements illustrating flow separation at low fan speed, CR=1.2, 0.51 inch slot gap, no spacer.

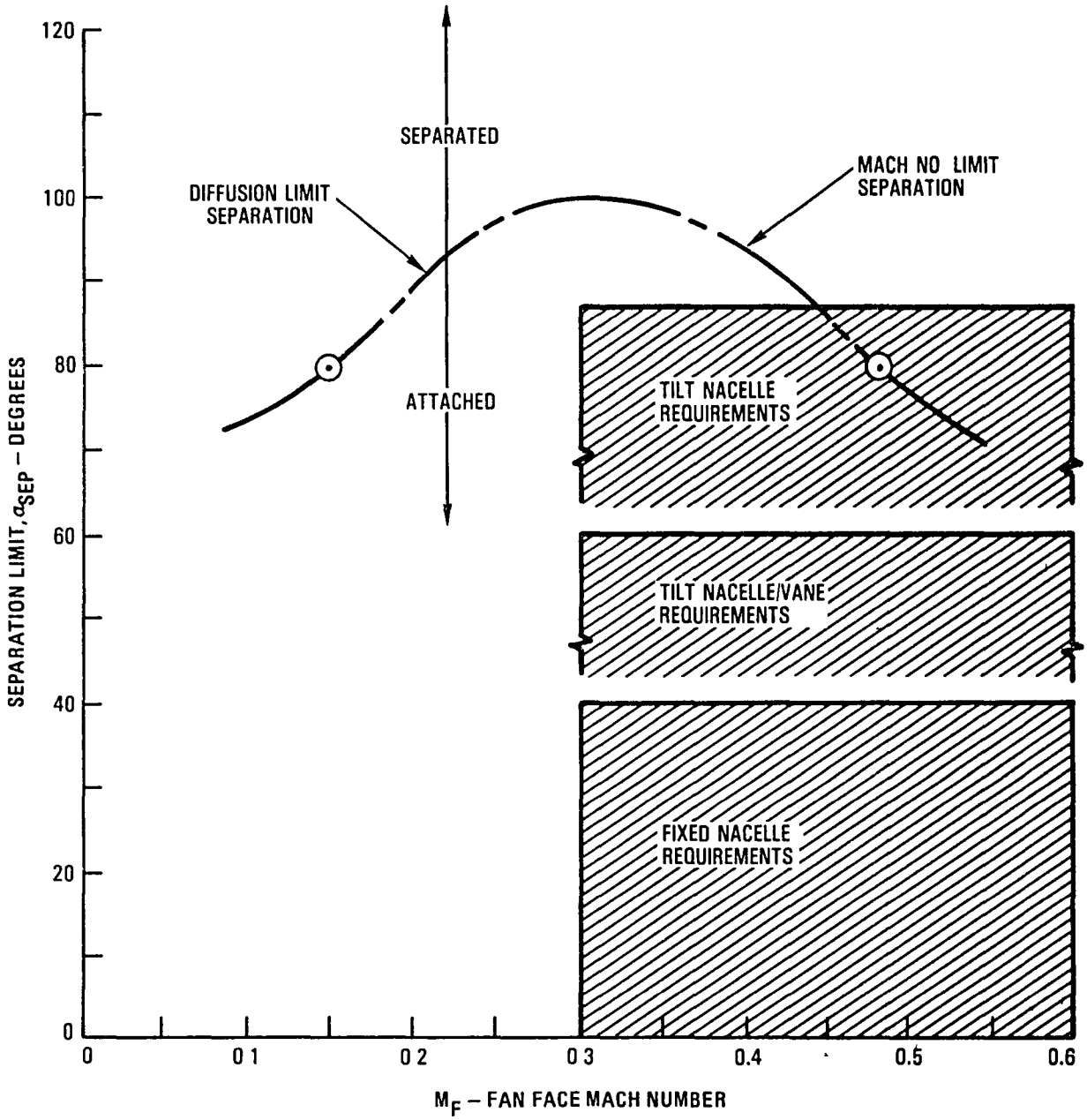

Figure 70. - Estimated angle-of-attack separation bounds, CR=1.2, 80 knots, 0.36 inch slot gap, no spacer.

inlet separation bounds curve or Mach number limit boundary does not satisfy the fan requirements for a tilt nacelle configuration. This suggests the use of a higher contraction ratio slat.

The flow separation boundary curve for the 1.3 contraction ratio is presented in figure 71 where the separation bounds has changed to a higher angle of attack. It appears that the 1.3 contraction ratio slat would (1) marginally satisfy the tilt nacelle fan requirements and (2) easily satisfy the tilt nacelle with nozzle vane fan requirements even up to 100% fan speed.

Comparison of Surface Velocity Distributions with Potential Flow

During the model configuration development phase of the program, potential flow solutions for the slat/cowl surface velocity distributions were obtained by NASA-LeRC for several configuration variables (contraction ratio, slot gap width, etc). The velocity distributions calculated by the measured static pressures during the test are compared to these predictions in figures 72 and 73 at static operating conditions. Excellent agreement between these data are obtained on the cowl surface. On the slat surface agreement is good, however, below the highlight the predicted velocities are slightly higher than those calculated from the test data. During the test, however, it was noted that because of the fan/turbine exhaust flow an ejector type pumping action induced some tunnel flow velocity (approximately 27 ft/sec), and therefore the true static condition was not simulated. Subsequently, additional potential flow solutions were generated using the freestream velocity measured during the test. These results, shown as the dashed lines in figure 73 indicate the effect of tunnel speed to only slightly better approximate the test data.

CONCLUSIONS

The following conclusions regarding the application of zero-length, slotted-lip inlets to subsonic military aircraft were derived from the test data of this program.

Zero-length, slotted-lip inlets are suitable for most subsonic military aircraft where the minimum inlet length is not constrained by acoustic treatment considerations. The inlet is particularly well suited for V/STOL aircraft where large inlet lip contraction ratios are required. For a tilt nacelle type V/STOL aircraft, the reduction in inlet lip contraction ratio in going from a long conventional axisymmetric inlet to a zero-length, slotted-lip inlet is sufficient not only to compensate for an increase in throat area but also to allow for a reduction in maximum cowl radius. Even for a fixed nacelle type V/STOL aircraft, a sizable reduction in inlet length can be obtained without adversely affecting the maximum cowl radius.

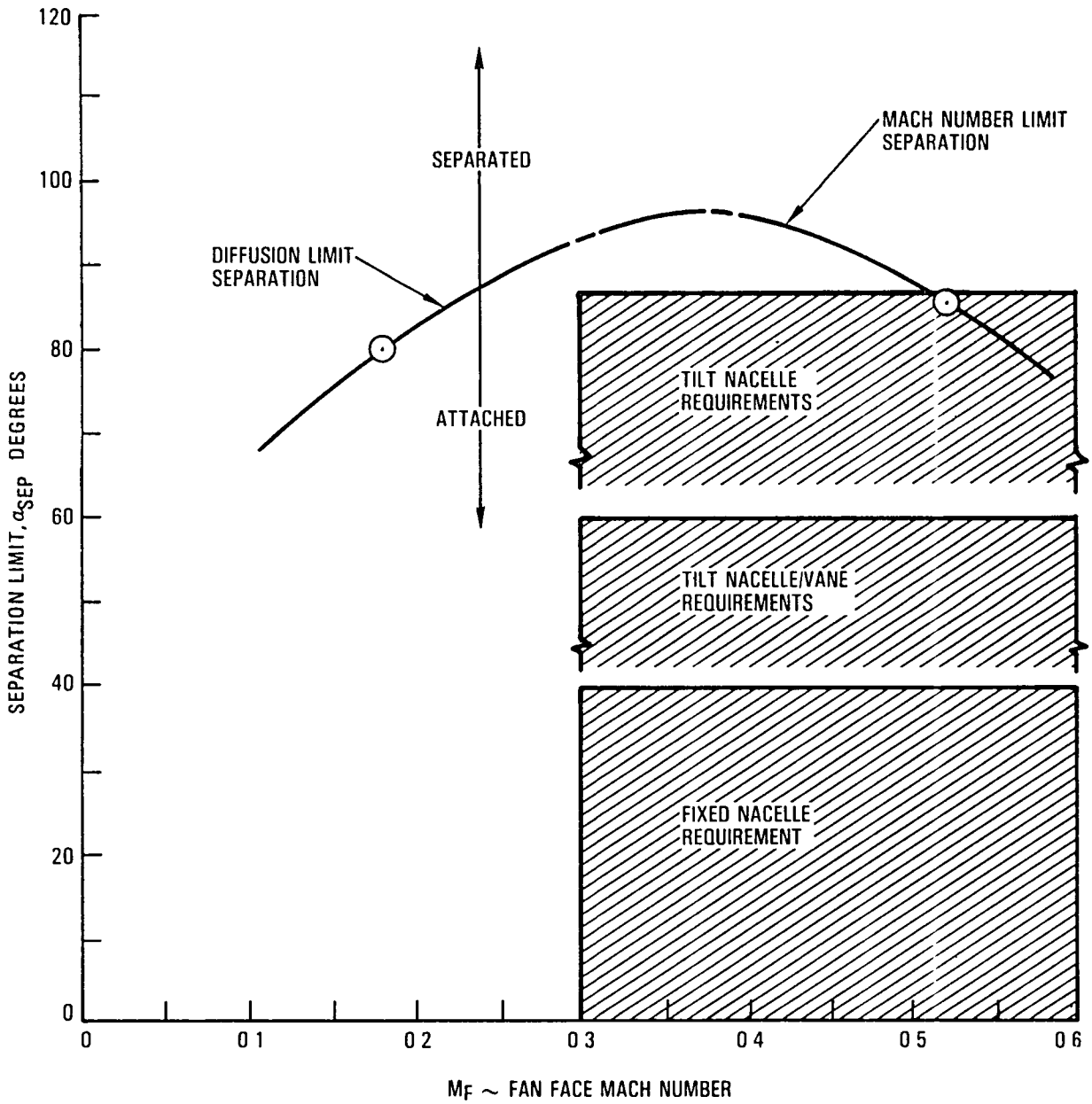

Figure 71. - Estimated angle-of-attack separation bounds, CR=1.3, 80 knots, 0.36 inch slot gap, no spacer.

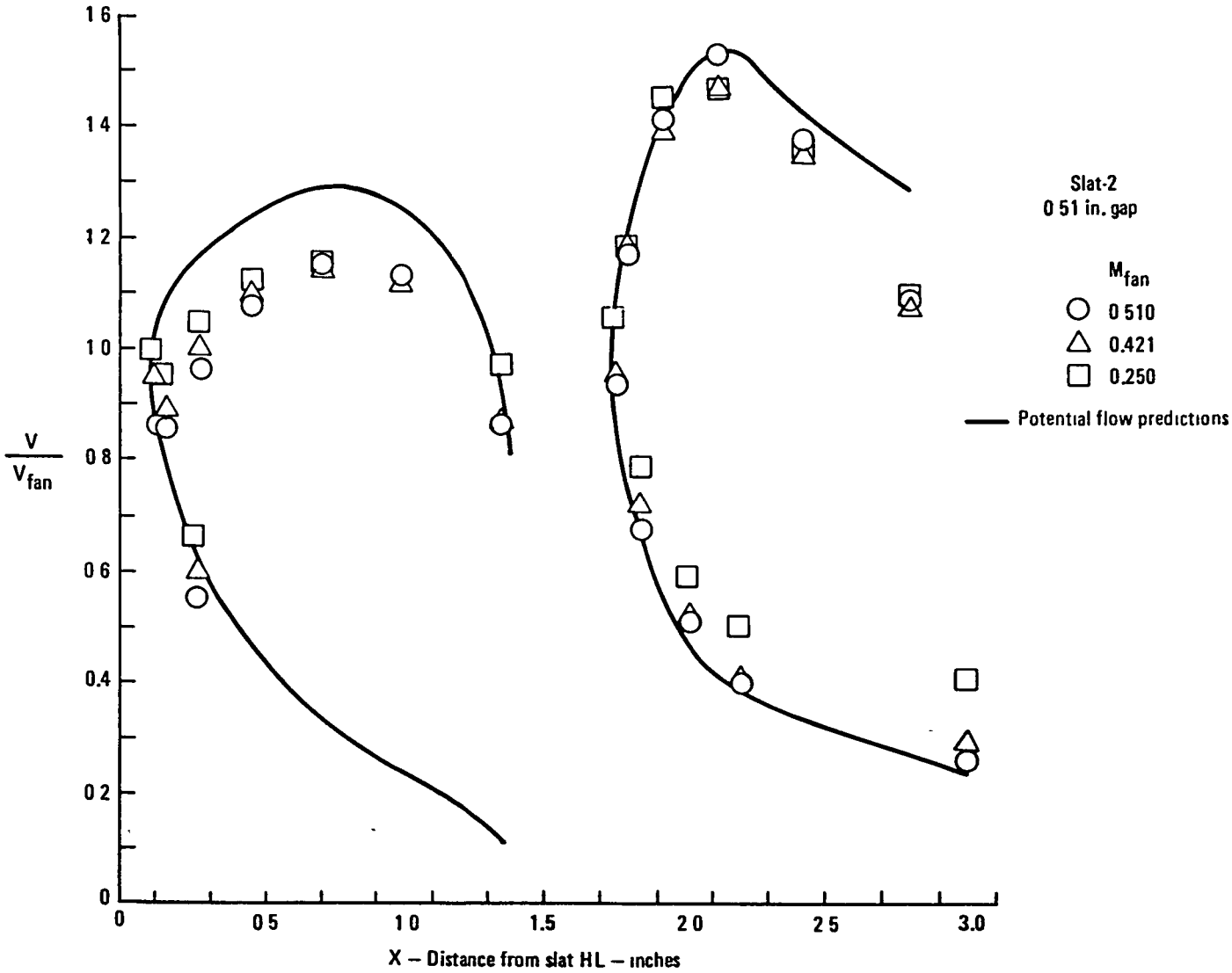

Figure 72. - Comparison of slat/cowl measured surface static pressures with potential flow predictions, CR=1.3.

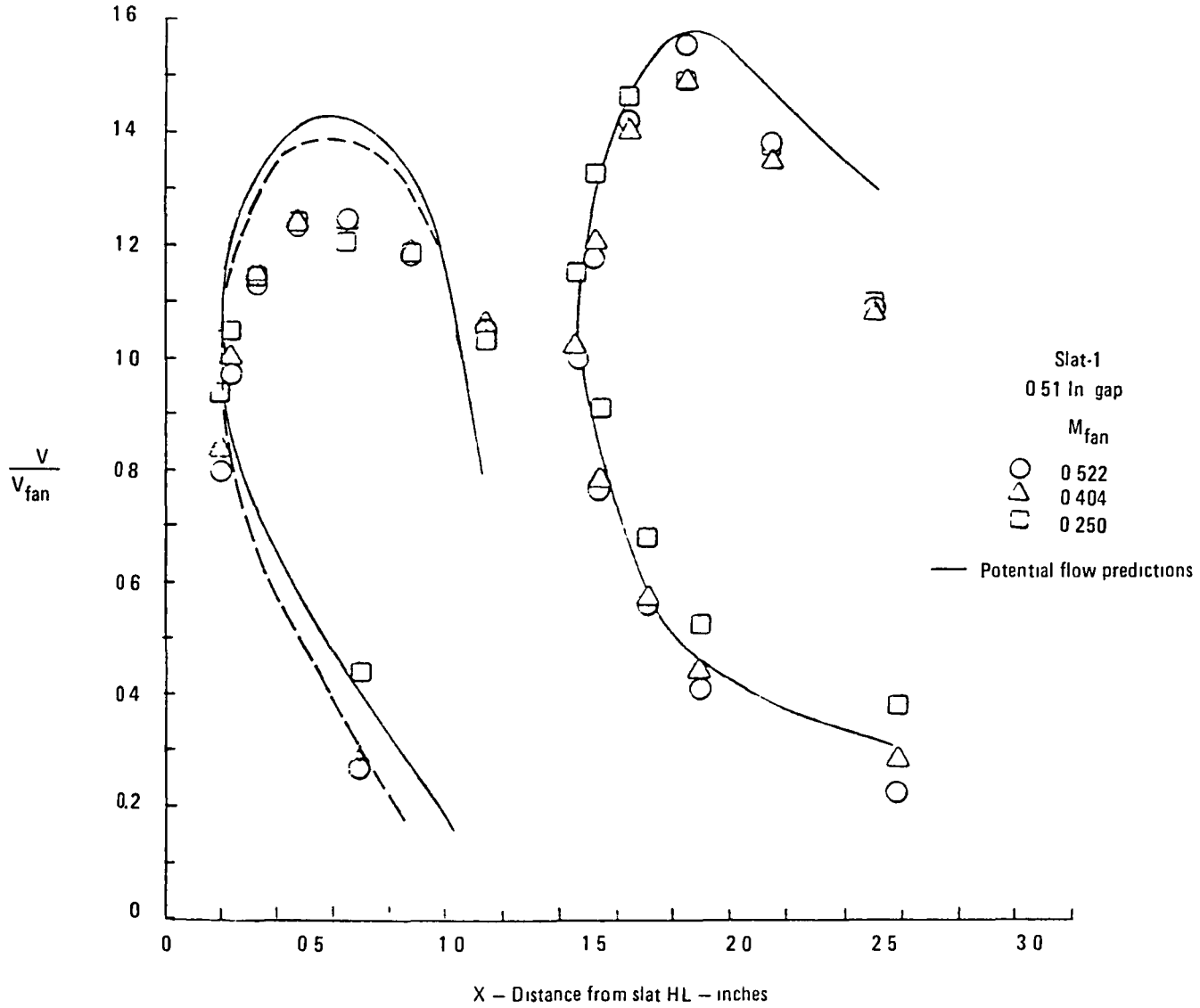

Figure 73. - Comparison of slat/cowl measured surface static pressures with potential flow predictions, CR=1.2.

The model tests in the NASA-LeRC 9-by 15-foot low speed tunnel indicate that zero length, slotted-lip inlets having 1.2 and 1.3 contraction ratio slats satisfy all critical low-speed inlet operating requirements for V/STOL aircraft with fixed nacelles and tilt nacelles with nozzle vanes, respectively. The fan face total pressure distortions and fan blade vibratory stresses were extremely low for both types of V/STOL aircraft, and the maximum total pressure recovery loss for all conditions within the operating envelopes was less than one percent.

The inlet performance measured during the test was dependent on slot gap width and relatively independent of inlet throat/fan face spacer length and slot flow blockage created by 90 degree slot fillers. Optimum performance was obtained at a slot gap width of 0.36 inches. The spacers were effective in reducing potential flow distortion, although this type of distortion did not have an adverse effect on the fan simulator. The negligible effect of the slot fillers on inlet performance indicates that good inlet performance could also be obtained for a Siamese inlet arrangement.

REFERENCES

1. Lewis, G.W. Jr., and Tysl, E.R., "Overall and Blade-Element Performance of a 1.20-Pressure Ratio Fan Stage at Design Blade Angle Setting," NASA TMX-3101, September 1974.

2. Boles, M.A., Luidens, R.W., and Stockman, N.O., "Theoretical Flow Characteristics of Inlets for Tilting-Nacelle VTOL Aircraft," NASA TP-1205.

3. General Electric Company, "TF 34-GE-2 Engine Model Specification E1130C," Amendment 1, 1 May 1973.

4. King, R.W., Schuerman, J.A., and Muller, R.G., "Analysis of Distortion Data from TF 30-P-3 Mixed Compression Inlet Test," NASA CR-2686.

1 Report No NASA TM-82939	2 Government Accession No	3 Recipient's Catalog No
4 Title and Subtitle WIND TUNNEL TESTS OF A ZERO-LENGTH, SLOTTED-LIP ENGINE AIR INLET FOR A FIXED NACELLE V/STOL AIRCRAFT		5 Report Date August 1982 6 Performing Organization Code 505-43-02
7 Author(s) R. R. Woollett, W. E. Beck, Jr., and E. R. Glasgow		8 Performing Organization Report No E-1338 10 Work Unit No
9 Performing Organization Name and Address National Aeronautics and Space Administration Lewis Research Center Cleveland, Ohio 44135		11 Contract or Grant No 13 Type of Report and Period Covered Technical Memorandum
12 Sponsoring Agency Name and Address National Aeronautics and Space Administration Washington, D. C. 20546		14 Sponsoring Agency Code

15 Supplementary Notes
R. R. Woollett, NASA Lewis Research Center; W. E. Beck, Jr. and E. R. Glasgow, Lockheed-California Company, P.O. Box 551, Burbank, California 91520.

16 Abstract

Zero-length, slotted-lip inlet performance and associated fan blade stresses were determined during model tests using a 20-inch diameter fan simulator in the NASA-LeRC 9- by 15-foot low-speed wind tunnel. The model configuration variables consisted of inlet contraction ratio, slot width, circumferential extent of slot fillers, and length of a constant area section between the inlet throat and fan face. The inlet performance was dependent on slot gap width and relatively independent of inlet throat/fan face spacer length and slot flow blockage created by 90-degree slot fillers. Optimum performance was obtained at a slot gap width of 0.36 inch. The zero-length, slotted-lip inlet satisfied all critical low-speed inlet operating requirements for fixed horizontal nacelles subsonic V/STOL aircraft.

17 Key Words (Suggested by Author(s)) V/STOL Inlets Slots Separation	18 Distribution Statement Unclassified - unlimited STAR Category 02		
19 Security Classif (of this report) Unclassified	20 Security Classif (of this page) Unclassified	21 No of Pages	22 Price*

* For sale by the National Technical Information Service, Springfield, Virginia 22161

End of Document